

UNIVERSIDADE DE SÃO PAULO

TAYNARA OLIVEIRA SILVA

**Estudo da eletrossíntese de peróxido de hidrogênio em reatores eletroquímicos
utilizando eletrodo de difusão gasosa de carbono amorfo com benzofenona**

São Carlos

2023

UNIVERSIDADE DE SÃO PAULO
INSTITUTO DE QUÍMICA DE SÃO CARLOS

TAYNARA OLIVEIRA SILVA

**Estudo da eletrossíntese de peróxido de hidrogênio em reatores eletroquímicos
utilizando eletrodo de difusão gasosa de carbono amorfo com benzofenona**

Tese apresentada ao Instituto de Química de São
Carlos da Universidade de São Paulo como parte
dos requisitos para obtenção do título de Doutora
em Ciências

Área de concentração: Físico – Química

Orientador: Prof. Dr. Marcos Roberto de
Vasconcelos Lanza

Exemplar revisado

O exemplar original encontra-se em
acervo reservado na Biblioteca do IQSC-USP

São Carlos

2023

Autorizo a reprodução e divulgação total ou parcial deste trabalho, por qualquer meio convencional ou eletrônico para fins de estudo e pesquisa, desde que citada a fonte.

Assinatura:

Data:



Documento assinado digitalmente

TAYNARA OLIVEIRA SILVA

Data: 30/10/2023 20:50:38-0300

Verifique em <https://validar.iti.gov.br>

Ficha Catalográfica elaborada pela Seção de Referência e Atendimento ao Usuário do SBI/IQSC

Silva, Taynara Oliveira

Estudo da eletrossíntese de peróxido de hidrogênio em reatores eletroquímicos utilizando eletrodo de difusão gasosa de carbono amorfo com benzofenona / Taynara Oliveira Silva. — São Carlos, 2023.

159 f.

Tese (Doutorado em Físico-Química) — Instituto de Química de São Carlos / Universidade de São Paulo, 2023.

Edição revisada

Orientador: Prof. Dr. Marcos Roberto de Vasconcelos Lanza

1. Eletrocatalisador. 2. Peróxido de hidrogênio. 3. Eletrodo de difusão de gasosa. 4. Processos oxidativos avançados. I. Título.



*Eu dedico esta tese a todos que lutam pela ciência,
pela pesquisa e pela educação.*

AGRADECIMENTOS

O presente trabalho foi financiado pela Fundação de Amparo à Pesquisa do Estado de São Paulo (FAPESP - processo nº 2019/08701-4; 2017/10118-0; 2022/07227-0).

Primeiramente, gostaria de agradecer ao meu orientador Dr. Marcos Roberto de Vasconcelos Lanza, por todo apoio e ajuda no desenvolvimento dessa tese e também pelo meu desenvolvimento profissional como pesquisadora.

Dr. Manuel Andrés Rodrigo, *agradezco por lo aprendido y ayuda durante mi estadía en Ciudad Real (España), lo que fue fundamental para la conclusión de la tesis y una gran oportunidad científica.*

Agradeço imensamente aos meus amigos Paulo Jorge Marques Cordeiro Junior, Robson Souto, Fausto Eduardo Bimbi Júnior, Guilherme Vilalba Fortunato, Mateus Schiavon Kronka, Leticia Mira, Michell de Oliveira Almeida, Laís Gimenes Vernasqui, Aline Resende Dória, em especial agradeço a Lorena Athie Goulart, Isaac José Sánchez Montes e Gêssica de Oliveira Santiago Santos, sem vocês eu não seria a pesquisadora que sou hoje, o cuidado de vocês para comigo foi essencial nos meus momentos mais necessários.

Agradeço a todos do meu grupo de pesquisa GPEA- Grupo de Processos Eletroquímicos Ambientais, e agradeço também aos técnicos José Augusto Fragale Baio e Benedito Manoel dos Santos.

Agradeço por todo suporte e colaboração para minha trajetória acadêmica, a minha família, meu irmão Taynan Oliveira Silva, meu pai Vander Alves da Silva, minha avó Maria de Lurdes Bernardini Oliveira e a meu avô João dos Santos Oliveira, e em especial minha mãe Vania Aparecida de Oliveira Silva por ter sido minha fonte de canalizar o ânimo e esperança, e você ter me suprido com todo amor.

Agradeço a todos meus amigos: Carmen Elena Barragán Ruiz, Carolina Machado, Luana Portela, Larissa Carvalho Gersanti, Rafael Silva, Thamires Mariano, Bianca Ferreira, Ana Laura Azevedo, Pilar Castro, Raira Castro, Paula Salazar Nogales, Sabrina Valeria Bueno, Agustina de Oliveira, Giovanna Pellechia do Amaral, Raíza Fonseca Xavier Lima, Rayne Araujo, Maria Clara Brandaglia e a todos meus amigos que me acompanharam na minha trajetória. Em especial gostaria de agradecer a Lorrana Bichoff por ter me dado todo incentivo e palavras de apoio antes mesmo de ingressar na Pós-graduação, não me recordo de um momento da minha vida que você não estivesse; Agradeço imensamente a Nayra Taveira Rodrigues por ter sido um pontinho de luz na minha vida desde a graduação até o Doutorado, obrigada por colorir minha vida nos momentos que precisei; Agradeço a minha amiga Virginia

Giangrossi por ter sido meu ponto de apoio em tantos momentos, se eu dia for preciso retribuir o quão bem você me faz eu não saberia por onde começar.

Agradeço ao meu girassol Mariana Miguel, por estar sempre ao meu lado, nas minhas conquistas e derrotas, poder partilhar minha vida com você é o maior privilégio que já tive.

Agradeço a todos os professores que passaram na minha vida, Professores do SESI-Tambaú, Professores da Universidade Federal do Triângulo Mineiro - Uberaba, Professores da Universidade de São Paulo – São Carlos.

Agradeço genuinamente às secretárias do programa de pós-graduação, pelo trabalho impecável e atencioso delas para com os alunos.

Agradeço ao meu time de flag São Carlos Bulldogs, pelos bons momentos.

Por fim, agradeço genuinamente a todos e todas que fizeram de alguma forma parte na minha caminhada Universitária, Acadêmica e Científica.

“Realmente, é de admirar que eu não tenha desistido de todos os meus ideais, tão absurdos e impossíveis eles são de se realizar. Conservo-os, no entanto, porque apesar de tudo ainda acredito que as pessoas, no fundo, são realmente boas.”

Anne Marie Frank

RESUMO

A busca por novas tecnologias e catalisadores mais eficientes para a eletrossíntese de peróxido de hidrogênio (H_2O_2) a partir da reação de redução de oxigênio (RRO) por meio da transferência de 2 elétrons despertou o interesse de muitos pesquisadores devido à ampla gama de aplicações industriais do H_2O_2 . As dificuldades na produção de H_2O_2 a partir da RRO estão relacionadas com o desenvolvimento de catalisadores eficazes e de baixo custo, bem como de um reator eletroquímico que otimize a produção de H_2O_2 em larga escala. O primeiro capítulo dessa tese explorou o material amorfo carbono Printex L6 (PL6C) modificado com composto orgânico benzofenona-3,3',4,4'-tetracarboxílico (BTDA) para ser usado como matriz catódica para a RRO via síntese de H_2O_2 , análises eletroquímicas mostraram que o material modificado atingiu valor satisfatório de seletividade de 97,7%, isso devido ao aumento de sítios ativos do material devido ao acréscimo de grupos oxigenados em sua estrutura. O material modificado PL6C/BTDA 2% foi então utilizado para a fabricação de eletrodo de difusão de gás (EDG) e sua performance foi examinada no Capítulo 2, ao empregá-lo para a geração de H_2O_2 *in situ* foram atingidos valores de 275 mg L^{-1} a 25 mA cm^{-2} , ao aplicar essa condição para a remoção do interferente endócrino Ciprofloxacina via Processos Eletroquímicos Oxidativos Avançados (PEOA), o objetivo foi atingido em 20 min com completa degradação do poluente. No Capítulo 3, estudou-se a otimização do processo e da célula eletroquímica utilizada, sugerindo um reator com design novo para a geração de H_2O_2 e também seu aumento de escala, a disposição de célula dívida colabora para uma maior geração de H_2O_2 ; a nova proposta de reator com célula dívidada atingiu valores de eficiência faradaica de ~ 90% com EDG PL6C e valores muito satisfatórios de 99,99% com EDG PL6C/BTDA 2%. O Capítulo 4 apresenta uma possibilidade, até então não explorada, onde o H_2O_2 foi gerado *in situ* e acumulado nos primeiros 10 min, atingindo valores de $\sim 112 \text{ mg L}^{-1}$ em 25 mA cm^{-2} , o que foi suficiente para, subsequentemente, ser ativado com UVC e utilizado na degradação do composto Norfloxacin via PEOA, que se sucedeu por completo em 10 min. As conquistas discutidas nesta tese com relação à eletrossíntese de H_2O_2 a partir materiais catalisadores para degradação de contaminantes orgânicos tem potencial para contribuir com novos estudos visando o desenvolvimento de sistemas de produção de H_2O_2 e de catalisadores ainda mais eficientes para serem utilizados na degradação de contaminantes.

Palavras-chave: Eletrocatalisador; Peróxido de hidrogênio; Eletrodo de difusão de gasosa; Processos oxidativos avançados.

Study of hydrogen peroxide electrosynthesis in electrochemical reactors using amorphous carbon and benzophenone gas diffusion electrode

ABSTRACT

The search for new technologies and more efficient catalysts for the electrosynthesis of hydrogen peroxide (H_2O_2) from the oxygen reduction reaction (ORR) via 2-electron transfer has aroused the interest of numerous researchers, due to the wide range of industrial applications of H_2O_2 . Difficulties in the production of H_2O_2 from ORR are related to the creation of an effective and low-cost catalyst as well as an electrochemical reactor that optimizes the production of H_2O_2 on a large scale. The Chapter 1 explored the material of amorphous Printex L6 carbon (PL6C) modified with benzophenone-3,3',4,4'-tetracarboxylic dianhydride (BTDA) to be used as cathode matrix for ORR via H_2O_2 synthesis, electrochemical analyses showed that the modified material reached a satisfactory selectivity value of 97.7%, due to the increase of active sites of the material due to the addition of oxygenated groups in its structure. The modified material PL6C/BTDA 2% was used in the fabrication of gas diffusion electrode (GDE), to employ for the *in situ* generation of H_2O_2 and its performance was examined in the Chapter 2, when employing it for the *in situ* generation of H_2O_2 values of 275 mg L^{-1} at 25 mA cm^{-2} were achieved, when applying this condition for the removal of the endocrine interferent Ciprofloxacin via electrochemical advanced oxidative processes (EOAP), the objective was reached in 20 min with complete degradation of the pollutant. Chapter 3 the optimization of the process and the electrochemical cell used was studied, suggesting a reactor with a new design for the H_2O_2 generation and also its increase in scale, the arrangement of divided cell collaborated for a greater H_2O_2 generation; the new proposal of reactor with divided cell reached values of Faradaic efficiency of $\sim 90\%$ with EDG PL6C and very satisfactory values of 99.99% with EDG PL6C/BTDA 2%. Chapter 4 presents a possibility, hitherto unexplored, where the *in situ* H_2O_2 generated was accumulated in the first 10 min, reaching values of $\sim 112 \text{ mg L}^{-1}$ at 25 mA cm^{-2} , which was sufficient to subsequently, be activated with UVC and used in the degradation of the compound Norfloxacin via EOAP, which took place completely in 10 min.. The achievements discussed in this thesis regarding the electrosynthesis of H_2O_2 using materials catalysts are likely to contribute to the development of even more efficient H_2O_2 production systems for degradation of pollutants.

Keywords: Electrocatalyst; Hydrogen peroxide; Gas diffusion electrode; Advanced oxidative processes.

LISTA DE FIGURAS

INTRODUÇÃO

- Fig. 1** – Principais métodos de obtenção de H_2O_2 e suas principais aplicações.....25
- Fig. 2** – Vantagens do processo de eletrogeração *in situ* do H_2O_2 comparado com a geração via antraquinona.....27
- Fig. 3** – Diagrama dos possíveis mecanismos da reação de redução do oxigênio.....32
- Fig. 4** – Representação da tripla interface do EDG.....33

CHAPTER 1.

- Fig. 1.1** – Depicts the mechanism involving the ORR stages on the active sites present on the surface of carbon-based materials for 4 and 2 electrons.....40
- Fig. 1.2** – Illustrates the functional groups present in carbon material surface.....42
- Fig. 1.3**- Molecular structure of BTDA.....43
- Fig. 1.4** – Schematic diagram of the electrochemical cell of the RRDE.....45
- Fig. 1.5** – Cyclic voltammogram of PL6C and PL6C modified with 2% BTDA. Conditions: 50 $mV s^{-1}$, using KOH 0.1 $mol L^{-1}$ support electrolyte, pH 13, saturated with N_247
- Fig. 1.6** – Cyclic voltammogram of PL6C and PL6C modified with 2% BTDA, Conditions: 50 $mV s^{-1}$, using KOH 0.1 $mol L^{-1}$ support electrolyte, pH 13, saturated with O_2 .
.....48
- Fig. 1.7** – Linear sweep voltammogram in RRDE for PL6C and PL6C/BTDA 2%. Conditions: 50 $mV s^{-1}$, using KOH 0.1 $mol L^{-1}$ support electrolyte, pH 13, saturated with O_2 .
.....49
- Fig. 1.8** – a) Selectivity values for H_2O_2 b) Number of electrons involved in the ORR reactions for PL6C and PL6C/BTDA 2%, Conditions: 50 $mV s^{-1}$, using KOH 0.1 $mol L^{-1}$ support electrolyte, pH 13, saturated with O_251
- Fig. 1.9** – Linear sweep voltammetry in RRDE to analyze the stability of the microlayer (PL6C/BTDA 2%) Conditions: 5 $mV s^{-1}$, using KOH 0.1 $mol L^{-1}$ support electrolyte, pH 13, saturated with O_2 . Inset: Cyclic voltammogram in O_2 , KOH 0.1 $mol L^{-1}$, pH 13, potential window: 0.1 V to -0.8 V, 1000 cycles at 50 $mV s^{-1}$52

Fig. 1.10- Contact angle of the microlayers, drop volume 3uL.....	53
Fig. 1.11 – Transmission electron microscopy images of PL6C and PL6C/BTDA 2% materials at 20 and 10 nm.....	54
Fig. 1.12- Thermogravimetric analysis (TG) graphs of the materials: PL6C and PL6C/BTDA 2%.....	55

CHAPTER 2.

Fig. 1. (a) H ₂ O ₂ electrogeneration under different current densities ($j = 10, 25$ and 50 mA cm^{-2}) as a function of time using PL6C/GDE and PL6C/GDE-2%BTDA. Conditions applied – electrolyte: 0.1 mol L^{-1} of KOH at pH 13; temperature: $25 \text{ }^\circ\text{C}$ (b). Final concentrations of H ₂ O ₂ after 90 min of electrolysis for PL6C/GDE and PL6C/GDE-2%BTDA (b).....	65
--	----

Fig. 2. Apparent rate constant for H ₂ O ₂ electrogenerated ($k_{\text{H}_2\text{O}_2}$) as a function of applied current density in 20 min of electrolysis using PL6C/GDE and PL6C/GDE-2%BTDA. Conditions applied - electrolyte: 0.1 mol L^{-1} of KOH, pH 13; temperature: $25 \text{ }^\circ\text{C}$	67
---	----

Fig. 3. (a) Current efficiency (C.E.) and (b) energy consumption (E.C.) obtained from the application of PL6C/GDE and PL6C/GDE-2%BTDA as a function of applied current density. Conditions applied - electrolyte: 0.1 mol L^{-1} of KOH, pH 13; temperature: $25 \text{ }^\circ\text{C}$	68
---	----

Fig. 4. Relative percentage of CIP removed over time based on the application of different treatment processes. Conditions applied – current density: 25 mA cm^{-2} ; cathode: PL6C/GDE-2%BTDA; anode: Pt; irradiation: 9 W UVC lamp; supporting electrolyte: 0.1 mol L^{-1} of KOH at pH 13; temperature: $25 \text{ }^\circ\text{C}$	70
---	----

Scheme 1. Formation of H ₂ O ₂ in the presence of PL6C/2%BTDA under UV irradiation in alkaline solution during CIP electrolysis.....	72
---	----

Fig. 5. Electrical energy consumed in order to reduce the concentration of CIP by one order of magnitude under the application of different advanced oxidation processes. Conditions applied – current density: 25 mA cm^{-2} ; cathode: PL6C/GDE-2%BTDA; anode: titanium covered with Pt; irradiation: 9 W UVC lamp; supporting electrolyte: 0.1 mol L^{-1} of KOH at pH 13; temperature: $25 \text{ }^\circ\text{C}$	74
---	----

Fig. 6. Proposed pathway of CIP degradation based on the application of the e-H ₂ O ₂ /UVC process.....	75
--	----

Fig. 7. Evolution of short-chain carboxylic acids (a) and inorganic ions concentration (b) in 360 min treatment of CIP under the AO/e-H₂O₂/UVC process. Conditions applied – current density: 25 mA cm⁻²; cathode: PL6C/GDE-2%BTDA; anode: titanium covered with Pt; irradiation: 9 W UVC lamp; supporting electrolyte: 0.1 mol L⁻¹ of KOH at pH 13; temperature: 25 °C.....77

Fig. SM1 – LC-UV/DAD chromatogram of the degradation of CIP during different electrolysis time using the e-H₂O₂/UVC process: (a) 6, (b) 60 and (c) 360 min h. Peaks 1 to 10: degradation by-products.....86

CHAPTER 3.

Fig. 3.1 – System with discontinuous flow for electrogeneration of H₂O₂ with PEM and without PEM, and the system continuous flow in double compartment, using GDE PL6C as cathode and DSA as anode. Na₂SO₄ 0.5 mol L⁻¹, pH 2.5 adjusted with H₂SO₄, 1 L, 250 mL min⁻¹, 90 min.....95

Fig. 3.2 – Electrogeneration of H₂O₂ applying different current densities per time in a system with PEM and without PEM. **a).** Using GDE PL6C as cathode and BDD as anode. **b).** Using GDE PL6C as cathode and DSA as anode. Na₂SO₄ 0.5 mol L⁻¹, pH 2.5 adjusted with H₂SO₄, 1 L, 250 mL min⁻¹, 90 min.....98

Fig. 3.3 – **a)** Calculus of PL6C/BDD-PEM Faradaic efficiency, energy consumption and maximum of H₂O₂. **b)** - Calculus of PL6C/DSA-PEM Faradaic efficiency, energy consumption and maximum of H₂O₂.....100

Fig. 3.4 – Electrogeneration of H₂O₂ with GDE PL6C/DSA-PEM at a continuous system flow 250 mL min⁻¹ applying 150 mA cm⁻². Na₂SO₄ 0.5 mol L⁻¹, pH 2.5 adjusted with H₂SO₄.....102

Fig. 3.5 – **a)** Tangential-flow reactor 3D printed. **b)** – Flow-by reactor. Desing in the Fusion 360° Program.....103

Fig. 3.6 – Electrogeneration of H₂O₂ applying different current densities per time in tangential-flow reactor 3D printed mini and scall up reactor with PEM using a GDE PL6C as cathode and DSA as anode. Na₂SO₄ 0.5 mol L⁻¹, pH 2.5 adjusted with H₂SO₄, 250 mL min⁻¹, 90 min, with PEM.....104

Fig. 3.7 – **a)** Electrogeneration of H₂O₂ reator flow-by. **b)** – Electrogeneration of H₂O₂ tangential-flow reactor 3D printed. **c)** – Calculus of reactor flow-by Faradaic efficiency and

energy consumption. **d)** – Calculus of tangential-flow reactor 3D printed Faradaic efficiency and energy consumption. GDE PL6C and DSA, Na_2SO_4 0.5 mol L^{-1} , pH 2.5 adjusted with H_2SO_4 , 1 L, 250 mL min^{-1} , 90 min, with PEM.....105

Fig. 3.8 – **a)** RTD tangential-flow reactor 3D printed (mini). **b)** – RTD tangential-flow reactor 3D printed (scall up). **c)** – RTD reactor flow-by. Market KCl 3M, 1 mL, flow 0.250 L min^{-1} 106

Fig. 3.9 – Electrogeneration of H_2O_2 applying different current densities per time in a system with PEM. **a)** – Using GDE PL6C as cathode and DSA as anode. **b)** – Using GDE PL6C/BTDA 2% as cathode and DSA as anode. Na_2SO_4 0.5 mol L^{-1} , pH 2.5 adjusted with H_2SO_4 , 1 L, 250 mL min^{-1} , 90 min.....109

Fig. 3.10 – **a)** Comparison of maximum achieved value of H_2O_2 generation in 90 min for each electrode. **b)** – Calculus of PL6C and PL6C/BTDA 2% Faradaic efficiency, energy consumption.....110

Fig. 3.11 – Proposed of electrogeneration of H_2O_2 at the material contained BTDA.....111

CHAPTER 4.

Fig. 1. Accumulation of H_2O_2 in solution over time. Conditions: $j = 10, 25$ and 50 mA cm^{-2} , supporting electrolyte = $0.1 \text{ mol L}^{-1} \text{ K}_2\text{SO}_4$, pH ~ 7 and $T = 25 \text{ }^\circ\text{C}$. The dashed line refers to the concentration of H_2O_2 accumulated in 10 min of electrolysis.....124

Fig. 2. Current efficiency and energy consumption for 10 min of electrolysis as a function of current density. Conditions: $j = 10, 25$ and 50 mA cm^{-2} , supporting electrolyte = $0.1 \text{ mol L}^{-1} \text{ K}_2\text{SO}_4$, pH ~ 7 and $T = 25 \text{ }^\circ\text{C}$125

Fig. 3. NOR removal based on the application of the treatment processes investigated. Conditions: supporting electrolyte = $0.1 \text{ mol L}^{-1} \text{ K}_2\text{SO}_4 + 60 \text{ } \mu\text{mol L}^{-1} \text{ NOR}$, $j = 10$ and 25 mA cm^{-2} , pH ~ 7 and $T = 25 \text{ }^\circ\text{C}$. In the UVC/ ϕ - H_2O_2 processes, the electric current supply was interrupted within 10 min, and then the UVC lamp was turned on.....127

Fig. 4. TOC removal based on the application of the treatment processes investigated. Conditions: supporting electrolyte = $0.1 \text{ mol L}^{-1} \text{ K}_2\text{SO}_4 + 60 \text{ } \mu\text{mol L}^{-1} \text{ NOR}$, $j = 10$ and 25 mA cm^{-2} , pH ~ 7 and $T = 25 \text{ }^\circ\text{C}$. In the UVC/ ϕ - H_2O_2 processes, the electric current supply

was interrupted within 10 min, and then the UVC lamp was turned on for 90 min.....130

Fig. 5. H₂O₂ consumption over time using the UVC/ ϕ -H₂O₂ processes. Conditions: supporting electrolyte = 0.1 mol L⁻¹ K₂SO₄ + 60 μ mol L⁻¹ NOR, $j = 10$ and 25 mA cm⁻², pH ~7 and T = 25 °C. The dashed lines refer to the initial concentration of H₂O₂ electrogenerated after 10 min of electrolysis.....132

Fig. 6. Proposed pathway for NOR degradation based on the application of the UVC/ ϕ -H₂O₂@25 mA cm⁻² process.....135

Fig. S1 – Schematic representation of the three-electrode cell used during the electrochemical experiments for H₂O₂ accumulation at different current densities. Conditions: supporting electrolyte = 0.1 mol L⁻¹ K₂SO₄, $j = 10, 25$ and 50 mA cm⁻², electrolysis time = 60 min, pH ~7, V = 250 mL and T = 25 °C.....144

Fig. S2 – Schematic representation of the proposed UVC/ ϕ -H₂O₂ process. First step: H₂O₂ accumulation in solution by applying an electric current for only 10 min – Second step: H₂O₂ activation by UVC light and NOR degradation. Conditions: supporting electrolyte spiked with NOR = 0.1 mol L⁻¹ K₂SO₄ + 60 μ mol L⁻¹ NOR, $j = 10$ and 25 mA cm⁻², lamp power = 9 W, pH ~7, V = 250 mL and T = 25 °C. The electric current supply was interrupted within 10 min, and then the UVC lamp was turned on for 90 min.....145

Fig. S3. Zero-order kinetics fitting results for H₂O₂ accumulation at different current densities. Conditions: $j = 10, 25$ and 50 mA cm⁻², supporting electrolyte = 0.1 mol L⁻¹ K₂SO₄, pH ~7 and T = 25 °C. The dashed line refers to the concentration of H₂O₂ accumulated in 10 min of electrolysis.....146

Fig. S4 – Chromatogram of NOR-containing solutions (60 μ mol L⁻¹) after treatment using the UVC/ ϕ -H₂O₂@25mA cm⁻². The sample corresponds to the time 10 min of treatment. Peak NOR: norfloxacin; Peaks 1-14: NOR by-products.....147

LISTA DE TABELAS

INTRODUÇÃO

Tabela 1 – Sistemas homogêneos e heterogêneos usados em processos oxidativos avançados.....	29
--	----

CHAPTER 1.

Table 1.1 -Elemental Analysis CHNSO of the mass composition of the samples of carbon.....	53
--	----

CHAPTER 2.

Table 1 Pseudo-first order kinetic constant (k_{1st}) values for CIP removal.....	73
--	----

Table SM1 – LC-ESI-MS/MS analysis of CIP and main degradation by-products obtained from the application of the AO/e-H ₂ O ₂ /UVC treatment process.....	88
---	----

CHAPTER 4.

Table 1. LC-ESI-MS/MS data and the proposed chemical structure of NOR by-products detected during the treatment using UVC/ ϕ -H ₂ O ₂ @25 mA cm ⁻² process.....	137
--	-----

Table S1 – Pseudo-first order kinetic constant (k_{1st}) for NOR removal.....	146
--	-----

Table S2 – Side reactions involved in the UVC/H ₂ O ₂ processes and their kinetic constants (k).....	147
---	-----

Table S3 – Energy consumption per mass (EC _X) removed.....	147
---	-----

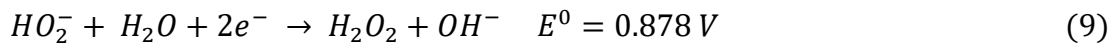
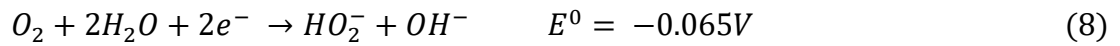
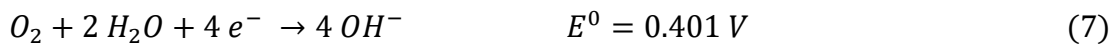
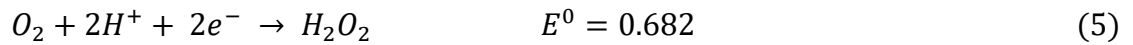
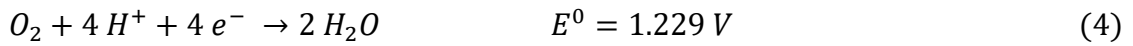
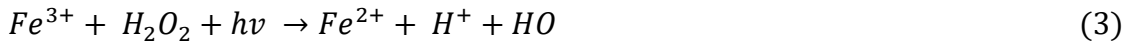
LISTA DE ABREVIACES

AOP	do ingls, <i>Advanced oxidative processes</i>
AO	do ingls, <i>Anodic <u>oxidation</u></i>
AQ	Antraquinona
BTDA	Benzofenona-3,3',4,4'-dianidrido tetracarboxlico
BDD	do ingls, <i>Boron-doped Diamond</i>
CIP	Ciprofloxacina / <i>ciprofloxacin</i>
CE	do ingls, <i>Current efficiency</i>
DE	Desreguladores endcrinos
DSA	do ingls, <i>Dimensionally stable-anode</i>
E.CNHSO	do ingls, <i>Elemental analyzer</i>
E/EO	do ingls, <i>Electrical energy per order</i>
EAOP	do ingls, <i>Electrochemical advanced oxidative processes</i>
EDG	Eletrodo de difuso gasosa
EF	Eletro-Fenton
EC	do ingls, <i>Energy consumption</i>
FE	do ingls, <i>Faradaic efficiency</i>
GDE	do ingls, <i>Gas diffusion electrode</i>
LSV	do ingls, <i>Linear sweep voltammogram</i>
IE	Interferentes endcrinos
MP	Micropoluentes
MPO	Micropoluentes orgnicos
NOR	Norfloxacina / <i>norfloxacin</i>
η_t	do ingls, <i>Number of electrons exchanged</i>
•OH	Radical hidroxila / <i>hydroxyl radical</i>
OA	Oxidao Andica
ORR	do ingls, <i>Oxygen reduction process</i>
O ₃	Oznio
H ₂ O ₂	Perxido de hidrognio/ <i>hydrogen peroxide</i>
PL6C	Printex L6 Carbono / <i>Printex L6 Carbon</i>
PEOA	Processos Eletroqumicos Oxidativos Avanados
POA	Processos oxidativos avanados

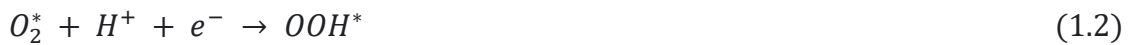
PEM	do inglês, <i>Proton exchange membrane</i>
RRO	Reação de redução de oxigênio
RTD	do inglês, <i>Residence time distribution</i>
RRDE	do inglês, <i>Rotating ring-disk electrode</i>
S% _{H2O2}	do inglês, <i>Selectivity calculations for hydrogen peroxide</i>
SHE	do inglês, <i>Standart hydrogen electrode</i>
TG	do inglês, <i>Thermogravimetric analysis</i>
TEM	do inglês, <i>Transmission Electron Microscopy</i>
TOC	do inglês, <i>Total organic carbon</i>
UV	Luz ultravioleta / <i>ultraviolet light</i>

LISTA DE EQUAÇÕES

INTRODUÇÃO



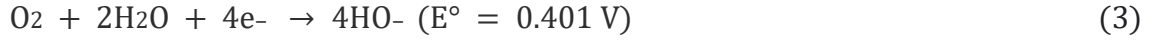
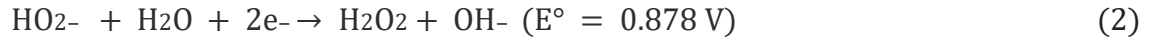
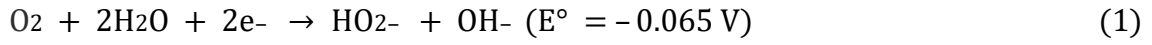
CHAPTER 1.



$$S \% H_2O_2 = \frac{(2 i_a / N)}{(i_d + i_a) / N} \times 100 \quad (1.10)$$

$$n_t = \frac{4 i_a}{(i_d + i_a) / N} \quad (1.11)$$

CHAPTER 2.



$$C_{H_2O_2}(t) = -k_{H_2O_2} t \quad (7)$$

$$\text{C. E. (\%)} = \frac{m_{H_2O_2}}{m_{H_2O_2 \text{ theoretical}}} \times 100\% = \frac{m_{H_2O_2}}{I \times t \times 34/2F} \times 100\% \quad (8)$$

$$\text{E. C. (kWh } kg^{-1}) = \frac{E_{\text{cell}} \times I \times t}{m_{H_2O_2}} \quad (9)$$

$$\text{E/EO (kWh } m^{-3} \text{ order}^{-1}) = \frac{6.39 \times 10^{-4} (E_{\text{cell}} + P_{\text{lamp}})}{V \times k_{1st}} \quad (10)$$

CHAPTER 3.



$$E(t) = \frac{C(t)}{\int_0^\infty C(t) dt} \quad (3.2)$$

$$\int_0^\infty E(t) dt = 1 \quad (3.3)$$

$$\tau = \frac{V}{v_0} \quad (3.4)$$





CHAPTER 4.

$$CE. (\%) = \frac{2 F [H_2O_2] V}{I t} \times 100\% \quad (1)$$

$$EC (kWh kg^{-1}) = \frac{1000E I t}{[H_2O_2] V} \quad (2)$$

$$EC_x (kWh g^{-1}) = \frac{E I t_1 + P t_2}{\Delta X V} \quad (3)$$



SUMÁRIO

INTRODUÇÃO	23
Processos eletroquímicos oxidativos avançado	27
Reação de Redução de Oxigênio.....	31
Eletrodo de Difusão Gasosa	32
OBJETIVOS	34
ESTRUTURA DA TESE	35
CHAPTER 1.....	37
1.1 INTRODUCTION	38
1.1.1 Organic Modifiers	42
1.2 EXPERIMENTAL PROCEDURES	44
1.2.1 Materials.....	44
1.2.2 Electrochemical Analysis	44
1.2.3 Material Characterization	45
1.3 RESULTS AND DISCUSSION.....	46
1.3.1 Cyclic voltammetry.....	46
1.3.2 ORR study using the hydrodynamic method RRDE	48
1.3.3 Physical and morphological analysis of the materials.....	52
1.4 CONCLUSION	55
CHAPTER 2.....	57
Abstract	58
Introduction	59
Experimental.....	62
Results and discussion	64
Conclusions	77
Acknowledgments.....	78

Credit authorship contribution statement	78
References.....	79
Supplementary material for:	86
CHAPTER 3.....	89
3.1 INTRODUÇÃO	90
3.1.1 New proposal of electrochemical reactor	91
3.2. MATERIAL AND METHODS	94
3.2.1 Material	94
3.2.2 Gas diffusion electrode production	94
3.2.3 Electrogeneration of H ₂ O ₂ in flow-by reactor	94
3.2.4 Electrogeneration of H ₂ O ₂ in tangential-flow reactor 3D printed	96
3.2.5 Residence time distribution analyses	96
3.3 RESULTS AND DISCUSSION.....	97
3.3.1 Optimized production of H ₂ O ₂	97
3.3.2 Electrogeneration of H ₂ O ₂ with tangential-flow reactor 3D Printed.....	102
3.4 CONCLUSÃO.....	112
CHAPTER 4.....	114
Abstract	115
Introduction	116
Materials and methods.....	118
Results and discussion	122
Conclusions	138
Acknowledgments.....	140
References.....	140
Supplementary material	144
CONCLUSÃO.....	148
REFERENCIAS BIBLIOGRAFICAS	150

INTRODUÇÃO

O peróxido de hidrogênio (H_2O_2), também conhecido como água oxigenada, é um potente agente oxidante (E° 1,77 V vs. *Standart Hidrogen Electrode* (SHE)). Por ser um produto químico versátil, é empregado em diferentes áreas e está entre os 100 principais produtos químicos produzidos e consumidos mundialmente (1). Ainda, previsões indicam o aumento da demanda por H_2O_2 , uma vez que tal oxidante encontra aplicações em diferentes áreas. Na área medicinal, o H_2O_2 é aplicado como agente desinfetante contra vírus e bactérias (2–4), como antisséptico para tratar feridas e interromper infecções e, de maneira importante, foi empregado na luta global contra a pandemia de COVID-19 sendo utilizado para desinfetar e purificar o ar (2,5). Ainda, este oxidante é aplicado em processos industriais no setor de papel e celulose assim como no setor têxtil, onde encontra aplicação como agente de branqueamento. Adicionalmente, também pode ser um componente de pasta de dente, produtos de limpeza de lentes de contato e enxaguantes bucais (6–8). Além de todas essas aplicações, há um esforço recente no emprego deste oxidante potente na remoção de contaminantes, sendo o H_2O_2 o principal reagente dos Processos oxidativos avançados (POA).

Devido às várias aplicações, industriais, comerciais e área da saúde, muitos estudos estão se concentrando na busca por novos materiais e metodologias para a produção do H_2O_2 (9,10).

Existem várias técnicas para a produção de H_2O_2 , sendo a mais utilizada comercialmente o processo de antraquinona (AQ). Esse método utiliza a reação hidrogênio-oxigênio, que é catalisada por derivados de antraquinona, a reação gera H_2O_2 concentrado, que é estabilizado e diluído com água para obter a concentração adequada. (11,12). Contudo, a síntese de H_2O_2 usando AQ apresenta algumas desvantagens relacionadas aos processos complexos e custos operativos envolvidos em sua produção. Por ser um processo complexo e de várias etapas, pode ser considerado relativamente caro e difícil de implementar, uma vez que exige ferramentas e conhecimentos específicos. Além disso, o procedimento exige o manuseio de produtos químicos perigosos, solventes orgânicos e o gerenciamento cuidadoso das condições de reação, elevando ainda mais os custos da operação (13–15).

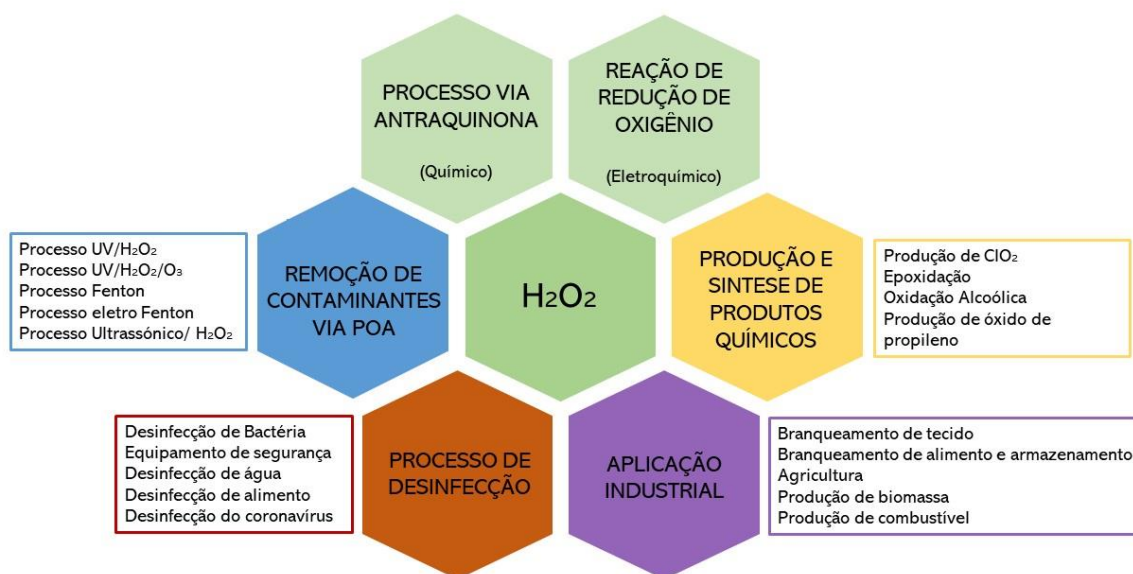
As AQ, que são utilizadas como catalisadores no procedimento, podem perder sua seletividade ao longo do tempo devido à degradação, à redução do rendimento de H_2O_2 e à necessidade de regeneração ou substituição regular do catalisador devido a essa deterioração, o que pode aumentar o custo e a complexidade do processo de fabricação. Adicionalmente, esse método tem problemas de seletividade, o que leva à criação de subprodutos indesejáveis, sendo

necessários mais estágios de purificação para produzir H_2O_2 com a pureza e a concentração desejadas. Os subprodutos gerados podem afetar a estabilidade e a qualidade do produto, exigindo processamento adicional. Outra dificuldade é aumentar a escala do método da antraquinona para a fabricação em massa que acaba sendo prejudicada pela eficácia do catalisador. O fornecimento e a acessibilidade do H_2O_2 podem ser limitados por esse problema de escala, principalmente quando há um aumento na demanda, como durante uma pandemia (13,15).

Para superar essas desvantagens, acadêmicos e pesquisadores estão procurando estratégias alternativas para a produção de H_2O_2 , o que inclui novos materiais, métodos de síntese direta, catalisadores e reatores para melhorar as condições de geração e superar as dificuldades de aumento de escala utilizando vários catalisadores e procedimentos eletrolíticos (8,16). Além de reduzir os custos, aumentar a eficiência e minimizar o efeito ambiental da geração de H_2O_2 , esses novos métodos buscam solucionar as desvantagens do processo tradicional de antraquinona. (12,15,17).

Um dos estudos atuais que pode ser destacado é o estudo da eletrogeração *in situ* desse oxidante no cátodo, por meio da reação de redução de oxigênio (RRO), uma das vantagens ambientais do uso do H_2O_2 *in situ* por processos eletroquímicos é que esse método evita a necessidade de armazenamento e transporte externos de H_2O_2 ao produzir o composto diretamente na água que está sendo tratada (18,19). Como o H_2O_2 é produzido *in situ*, ele está sempre disponível e sob controle, o que o torna extremamente eficaz e evita a necessidade de produtos químicos adicionais (20,21). Quando comparada às técnicas convencionais de síntese química, a geração eletroquímica oferece vantagens ecológicas por ser considerada uma rota verde tendo água, oxigênio e o elétrons como reagentes principais. A não necessidade de transportar e armazenar soluções de H_2O_2 (22,23), há também a redução dos riscos de acidentes nas estradas e no manuseio. Essa tecnologia por utilizar energia elétrica e leva em consideração que no Brasil a energia elétrica é proveniente majoritariamente de fontes renováveis, a eletrogeração *in situ* de H_2O_2 não colabora para a emissão de gases do efeito estufa e aquecimento global reforçando ainda mais sua sustentabilidade ambiental, (1,24–26). A Figura 1 (Fig.) resume as mais diversas aplicações nas quais o H_2O_2 pode ser empregado e seus principais meios de geração.

Fig. 1 – Principais métodos de obtenção de H₂O₂ e suas principais aplicações.



Fonte: Própria Autora.

Considerando que o H₂O₂ pode ser produzido eletroquimicamente, a concentração do mesmo pode ser modulada com o objetivo de atingir a degradação dos contaminantes e/ou desinfecção por meio da modificação dos parâmetros operacionais do sistema eletroquímico, como tempo de reação e densidade de corrente. Em particular, a aplicação do H₂O₂ como um dos principais precursores do radical hidroxila (\bullet OH) – agente altamente oxidante não seletivo capaz de degradar uma ampla variedade de compostos orgânicos em processos de tratamento de águas e efluentes - é de grande interesse e tem sido foco de intensa pesquisa (25,27,28). Principalmente, devido à contaminação da água por compostos recalcitrantes ser um dos grandes problemas enfrentados pela da sociedade atual, já que os métodos clássicos de tratamento empregados nas estações de tratamento de água e esgoto são incapazes de remover tais poluentes (29–32).

Dentre os contaminantes antropogênicos mais frequentemente detectados na água, constam os interferentes endócrinos (IE) ou também conhecidos como desreguladores endócrinos (DE) (30). Os IE podem ser definidos como substâncias químicas (naturais ou sintéticas) que podem influenciar o funcionamento de todo o sistema endócrino, até mesmo causar danos permanentes, como câncer, dificuldade na reprodução (por reduzir a quantidade de espermatozoides), atrasos de desenvolvimento neurológicos em crianças, além de lesar as

funções imunológicas (33). Ademais essas substâncias não são avaliadas apenas por seu caráter tóxico, mas também pelo mecanismo de como eles afetam os organismos, por exemplo: bloqueando os receptores celulares dos hormônios naturais, afetando a síntese, transporte, excreção desses hormônios naturais, alterando a concentração ou composição dos mesmos (30,33–37). Dentro dessa categoria, uma grande variedade de compostos químicos se inclui como IE, como pesticidas, bisfenóis, parabenos, organoclorados, ftalatos e fármacos, alguns medicamentos a longo prazo podem causar alterações irreversíveis no genoma dos microorganismos (28,38). Como exemplos desses compostos podem ser citados a ciprofloxacina (CIP) e a norfloxacina (NOR) (18,39,40). Estes fármacos são também considerados IE amplamente utilizados para o tratamento de bronquites, pneumonia, gonorreia, diarreias, febre tifoide, é um medicamento antibacteriano sintético (39,41), além disso, são medicamentos da classe dos antibiótico do grupo das fluoroquinolonas utilizados tanto na medicina humana quanto na medicina veterinária (42).

Dessa forma, o método eletroquímico é uma solução economicamente viável para o tratamento de efluentes contaminados com IE devido à sua simplicidade e capacidade de ser integrado à infraestrutura de tratamento de água existente. A aplicação de dispositivos eletroquímicos para a síntese de H_2O_2 *in situ* exige projeto, otimização e monitoramento cuidadosos. Para garantir a eletrogeração com elevados valores de eficiência de corrente, fatores como material do eletrodo, densidade de corrente e condições de reação devem ser considerados para tornar o processo ainda mais factível de ser aplicado comercialmente, isso porque consegue superar algumas limitações do processo atualmente utilizado via AQ. As vantagens do processo de eletrogeração *in situ* do H_2O_2 comparado com a geração via AQ são destacadas na Fig. 2 (43,44) .

Fig. 2 – Vantagens do processo de eletrogeração *in situ* do H_2O_2 comparado com a geração via antraquinona.



Fonte: Própria Autora.

Processos eletroquímicos oxidativos avançado

Processos Oxidativos Avançados (POA) são métodos alternativos para o tratamento de águas e efluentes que são fundamentados principalmente na geração do radical hidroxila ($\cdot OH$). Esse radical é extremamente reativo e não é seletivo, e apresenta alta capacidade oxidante devido ao seu potencial de redução (2,80 V vs SHE), sendo capaz de oxidar e degradar diversas espécies tóxicas (24,45–47). Assim, uma das principais vantagens apresentadas pelos POA é a possibilidade de conversão total dos poluentes orgânicos em espécies como dióxido de carbono, água e/ou íons inorgânicos, bem como a conversão parcial gerando espécies mais simples e/ou menos tóxicas, que possam ser biodegradadas posteriormente. Além disso, os POA são ambientalmente amigáveis, e apresentam vantagens pela possibilidade de operações em plantas de qualquer tamanho, como por exemplo: em plantas industriais onde a água é contaminada diretamente pelo resíduo industrial (48–50).

Os POAs podem ser empregados também em sistemas de purificação de água, e ainda a possibilidade de serem utilizados como um pré tratamento de água, acoplado aos processos clássicos utilizados em estações de tratamento de água (24,45–47).

O $\bullet\text{OH}$ pode ser gerado pela oxidação da água na superfície do ânodo, ou através da cisão homolítica do H_2O_2 , via processos Fenton, luz ultravioleta (UV) ou ozônio (O_3) (51–53). A obtenção de H_2O_2 através da reação de redução do oxigênio (RRO) foi reportada a primeira vez em 1930, a partir da utilização de carvão ativado como cátodo (54,55). Esta técnica foi posteriormente adaptada para produção *in situ* de peróxido de hidrogênio em meio alcalino diluído para ser comercializado para branqueamento de celulose, que foi chamado de processo Huron-Dow. Uma das variações do processo Huron-Dow, é o processo eletro-Fenton, em que o $\bullet\text{OH}$ é produzido através da mistura de H_2O_2 e do íon Fe^{2+} , o H_2O_2 é produzido eletroquimicamente *in situ*, posteriormente o $\bullet\text{OH}$ é utilizado na degradação de poluentes (9,18,56).

A obtenção do $\bullet\text{OH}$ *in situ*, pelos POA pode ser realizada utilizando um sistema homogêneo de alto poder reacional ou em sistemas heterogêneos com a utilização de materiais semicondutores catalíticos. É possível comparar brevemente os métodos de obtenção do radical, como mostra a Tabela 1, e enfatizar que o peróxido de hidrogênio aparece como principal precursor (24,57,58). Assim, os principais POA são: químicos, fotoquímicos, foto-Fenton, sonoquímicos e eletroquímicos (eletro-Fenton e fotoeletro-Fenton). Um dos pontos principais dos POA é o efeito de sinergia, como acontece no caso da degradação da Atrazina, por exemplo. Nesse caso, o melhor resultado foi alcançado quando as técnicas fotoquímicas e eletroquímica são combinadas (acontecem simultaneamente), do que quando as técnicas são simplesmente somadas (acontecem separadamente mais sequencialmente). Assim pode-se concluir que quando combina-se duas técnicas, ou mais, a eficiência é maior que elas apenas somadas ou isoladas (48,59,60).

Tabela 1 – Sistemas homogêneos e heterogêneos usados em processos oxidativos avançados.

	Fotoquímicos	Não fotoquímico
Sistemas Heterogêneos	TiO ₂ / O ₂ / UV	Eletroquímico
	TiO ₂ / H ₂ O ₂ / UV	Eletro-Fenton
	Fotoeletroquímico	
	Fotoeletro-Fenton	
Sistemas Homogêneos	O ₃ / UV	O ₃ / H ₂ O ₂
	H ₂ O ₂ / UV	O ₃ / HO ⁻
	H ₂ O ₂ / Fe ²⁺ /UV	H ₂ O ₂ / Fe ²⁺
	H ₂ O ₂ / Fe ³⁺ /UV	H ₂ O ₂ / Fe ³⁺
	UV/ Ultrassom	Ultrassom

Fonte: própria autora (46).

Dentre os principais POA químicos, o processo Fenton é o que mais se destaca, para geração do •OH. Nesse processo, o H₂O₂ é ativado na presença de íons ferro para formar •OH, e por esse radical ter alta capacidade oxidante, consegue degradar uma vasta quantidade de poluentes orgânicos. Como catalisador utiliza-se íons ferrosos (Fe²⁺) ou íons férricos (Fe³⁺), em meio ácido, como demonstra a Equação 1 (48,61).



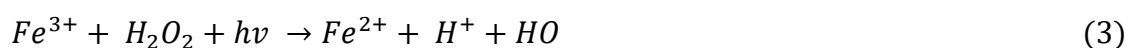
Dentre as vantagens da utilização do processo Fenton, ressaltam-se o uso de produtos químicos economicamente acessíveis, facilidade no manuseio e flexibilidade, uma vez que esta técnica pode ser acoplada a outros processos e simples. Entretanto, uma desvantagem de sua aplicação envolve a necessidade de grande quantidade de produtos químicos para que não haja variação de pH. Para o correto funcionamento do Fenton, o pH da solução deve ser mantido próximo a 3, pois em valores de pH maiores que 4 acontece a precipitação de Fe³⁺ como hidróxido de ferro e em pH com valores abaixo que 2 existe altas concentrações de H⁺ que

podem sequestrar $\bullet\text{OH}$ e, conseqüentemente, podem diminuir a velocidade de degradação do poluente (6,44,56,62).

As técnicas POA fotoquímicas se baseiam na junção da irradiação UV com agentes oxidantes fortes, como H_2O_2 , O_3 , dióxido de titânio (TiO_2) como catalizador, e incluem as técnicas H_2/UV , O_3/UV , $\text{O}_3/\text{H}_2\text{O}_2/\text{UV}$, foto-Fenton, fotocatalise heterogênea. A fotólise do H_2O_2 por irradiação UV acontece em comprimentos de onda de 200 a 300 nm (hv), que causa a quebra da ligação O-O da molécula de peróxido de hidrogênio, gerando o $\bullet\text{OH}$, como mostra a Equação 2 (44,63,64).



O processo foto-Fenton ($\text{H}_2\text{O}_2/\text{Fe}^{2+}/\text{UV}$), que consiste no processo Fenton assistido por irradiação UV, pode aumentar a produção de $\bullet\text{OH}$ devido a efeitos sinérgicos (Equação 3) (65).



Nos Processos Eletroquímicos Oxidativos Avançados (PEOA), a degradação pode ocorrer diretamente, como ocorre na Oxidação Anódica (OA) pela transferência de elétrons na superfície do eletrodo. No PEOA os radicais são formados na superfície no ânodo, de forma direta, através das moléculas de água fisio ou quimiossorvidas que são oxidadas, e/ou indiretamente como no eletro-Fenton (EF), onde agente oxidante H_2O_2 é formado na superfície do cátodo e ativado no seio da solução pela reação Fenton formando $\bullet\text{OH}$ (44,66).

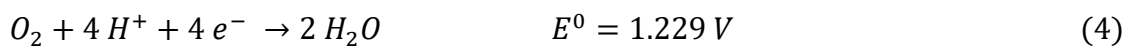
O processo combinado de H_2O_2 eletrogerado e UVC ($e\text{-H}_2\text{O}_2/\text{UVC}$) destaca-se por não depender de pH, pode ser utilizado em qualquer eluente sem a necessidade de ajustar o pH, e não há necessidade de adição de reagentes (como cloro e ferro) apresentando alta eficiência, baixo custo, facilidade no processo e a possibilidade de combinar com outros processos mais facilmente (67). Assim, os processos envolvidos nessa técnica é inicialmente a eletrossíntese de H_2O_2 e a ativação por radiação UVC.

Como já mencionado, uma das principais formas de produção de H_2O_2 é pela reação de redução de oxigênio (RRO) a qual pode acontecer em várias etapas no mecanismo reacional, por isso é uma reação eletroquímica multieletrônica, onde o O_2 pode ser convertido a H_2O ou H_2O_2 , dependendo do mecanismo. Entender como o mecanismo de reação acontece para atingir a máxima eficiência do processo de geração de H_2O_2 .

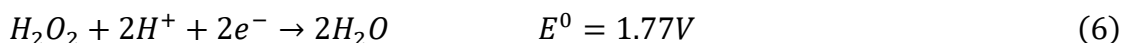
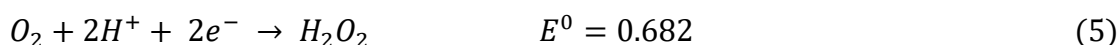
Reação de Redução de Oxigênio

Na RRO o gás O_2 que fica dissolvido na solução eletrolítica precisa ser adsorvido na superfície do eletrodo para que a reação aconteça. Como mostra as Equações 4-6, em meio ácido, quando a reação envolve 4 elétrons ($4e^-$) e 2 elétrons ($2e^-$) respectivamente, obtém-se a formação de água ou H_2O_2 . Caso o H_2O_2 reaja novamente por mais $2e^-$ o produto resultante pode ser água. No meio básico, Equação 7-9, via $4e^-$ acontece a formação de grupamentos hidroxilas e via $2e^-$ gera-se íons superóxidos. Os valores de potencial padrão de redução, são indicadas por E^0 , esses valores são referentes ao SHE (23,68,69).

Em meio ácido para 4 elétrons:



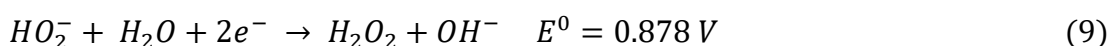
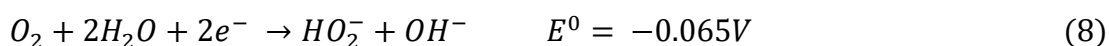
Em meio ácido para 2 elétrons:



Em meio básico para 4 elétrons ons:

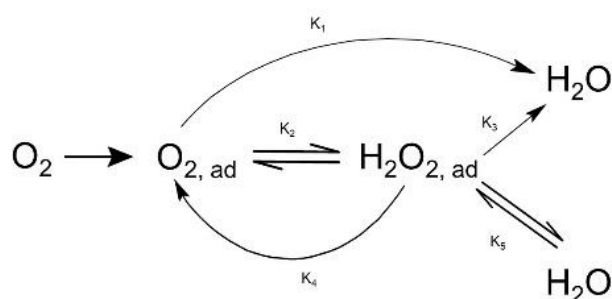


Em meio básico para 2 elétrons:



A Fig. 3 mostra o diagrama dos possíveis mecanismos da reação de redução de oxigênio.

Fig. 3 – Diagrama dos possíveis mecanismos da reação de redução do oxigênio



Fonte: Própria Autora.

A principal limitação da RRO está ligada com a necessidade de O_2 dissolvido em solução, e o posterior transporte do mesmo para a superfície do eletrodo. Isso porque a solubilidade do O_2 em temperatura ambiente é baixa, além disso a cinética da $2e^-$ RRO é lenta, por isso existe a necessidade de estudar materiais que possam ser utilizados ou combinados como catalisadores que sejam ativos para a RRO e seletivos via $2e^-$ (9,22,70).

Materiais a base carbono ou grafite podem gerar H_2O_2 , por causa dos grupos funcionais da superfície do carbono que geram sítios ativos, os quais tem uma forte interação com O_2 , além, de alguns casos onde os grupos funcionais de compostos modificadores catalíticos que podem participar das reações de RRO como: quinonas, antraquinonas, ácidos carboxílicos, são grupos encontrados em quantidades significativas na superfície do carbono (71–73).

Um dos materiais à base de carbono que têm ganhado destaque para essa aplicação por apresentar propriedades desejáveis para a RRO é o Carbono Printex L6 (PL6C). PL6C é um carbono amorfo que apresenta alta atividade catalítica devido a sua estrutura com grande quantidade de grupos funcionais em sua superfície e alta área superficial. Além disso, esse material também é vantajoso por ser abundante e, conseqüentemente, apresentar baixo custo de fabricação. Para melhorar ainda mais a eficiência da reação, materiais a base de carbono podem ser modificados com inúmeros compostos e classes de compostos (metais, óxidos metálicos, complexos, compostos orgânicos) (68,74–76).

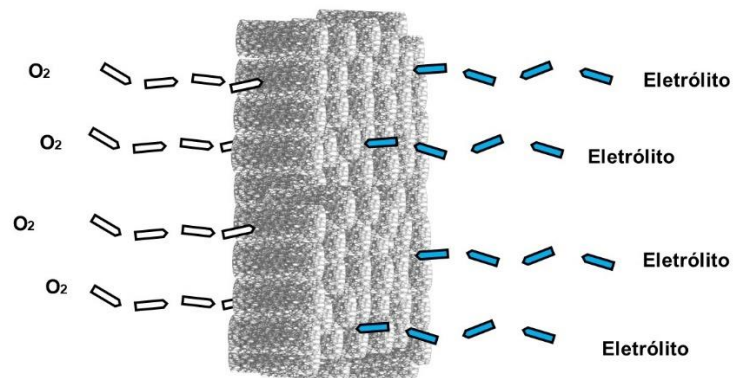
Eletrodo de Difusão Gasosa

O eletrodo de difusão gasosa (EDG) utilizado para eletrogeração de H_2O_2 é composto por uma matriz condutora, geralmente de carbono amorfo, sua principal característica é a tripla

interface gás, sólido e líquido, dessa forma o EDG permite que o gás seja suprido diretamente na superfície do eletrodo na interface sólido-líquido, por isso, a composição da matriz é importante para que essas características sejam mantidas. Essa matriz deve apresentar baixa mas presente hidrofobicidade, como objetivo evitar que o eletrodo seja permeado pela solução, e porosidade, para que a passagem do gás O_2 seja possível até os sítios ativos presentes no EDG para que a reação possa ocorrer e o H_2O_2 seja produzido (17,77). Essa propriedade (porosidade) permite a formação de uma interface tripla (gás, sólido, líquido) da superfície do eletrodo, conforme mostrado na Fig. 4, quando é permitida a interação da matriz catalítica condutora, do gás O_2 e do eletrólito. Assim, a solubilização do O_2 em solução, como no eletrodo convencional, não é mais necessária (78).

O estudo de materiais catalíticos para a RRO aplicados a sistemas escalonados é uma parte crucial para um estudo de aumento de escala do sistema. Portanto, destaca-se que, para a construção de EDG escalado, é necessária uma quantidade razoável de material catalítico (43,79), o que pode dificultar as aplicações de determinados materiais provenientes de síntese de baixo rendimento (0,1g - 1g) (77,80). Portanto, é muito importante a continuidade nos estudos de otimização de EDG para o uso de menor quantidade de material catalítico.

Fig. 4 – Representação da tripla interface do EDG.



Fonte: própria autora.

OBJETIVOS

O objetivo dessa pesquisa foi desenvolver e estudar um material carbonáceo inédito de PL6C modificado por dispersão física com 2% de Benzofenona-3,3',4,4'-dianidrido tetracarboxílico (BTDA), para ser aplicado na eletrogeração de H_2O_2 . Adicionalmente, buscou-se otimizar ao máximo os processos e as células eletroquímicas utilizadas buscando novas abordagens para evidenciar o potencial do material e aproximar de uma aplicação real para tratamento de efluentes contaminadas com interferentes endócrinos.

Assim, para atingir o objetivo geral, a pesquisa tem como objetivos específicos os seguintes tópicos:

- Estudar as propriedades morfológicas, físicas, químicas e eletroquímicas do material modificado (PL6C/BTDA 2%) para avaliar seu desempenho como catalisador para a RRO via $2e^-$.
- Produzir um EDG capaz de produzir H_2O_2 em quantidade suficiente para a degradação de molécula modelo CIP.
- Desenvolver um reator novo para eletrogeração de H_2O_2 , otimizando parâmetros operacionais para melhorar o processo
- Avaliar o desempenho do EDG (PL6C/BTDA 2%) na eletrogeração de H_2O_2 em condições otimizadas.
- Estudar proposta alternativa de abordagem para eletrogeração de H_2O_2 para degradação da molécula NOR.

ESTRUTURA DA TESE

A tese esta formatada em formato de coletânea de artigos, onde segundo regulamento pode conter capítulos independentes e ser escrito em inglês e português. Para facilitar a leitura, a tese está estruturada em uma introdução geral, seguida dos objetivos gerais da tese, em seguida são apresentados os capítulos da tese, o Capítulo 1 e Capítulo 3 são independentes por isso suas referências bibliográficas estão contidas no tópico de referências bibliográficas geral da tese ao final desse documento. Os Capítulos 2 e 4 são os artigos já publicados por isso apresentam suas referências bibliográficas dentro de seus respectivos capítulos, com suas respectivas formatações, por isso, esses capítulos não seguem a Associação Brasileira de Normas Técnicas, e sim a formatação da revista científica o qual foi publicado, assim como as disposições de tópicos e subtópicos desses capítulos.

Os capítulos giram em torno do estudo do material para aplicação em EDG e buscam aprimorar o processo e o dispositivo para que o EDG possa atuar de forma otimizada, assim explorar todo o potencial do EDG produzido com material inédito, é a principal inovação e contribuição desta pesquisa.

O processo de eletrogeração de H_2O_2 tem sido estudado para diversas finalidades, esse composto é extremamente versátil, sendo aplicado no tratamento de efluentes, os mais conhecidos Processos Oxidativos Avançados, também aplicado na indústria de branqueamento de papel, cosmética e também na desinfecção, a mais recente área de aplicação do H_2O_2 . Dentre os pontos que ainda podem ser explorados que envolvem a eletrogeração de H_2O_2 : material seletivo para RRO via $2e^-$, os parâmetros do processo, aplicação real.

Partindo do objetivo de estudar e tornar o processo o mais próximo possível de ser aplicado, essa tese vai de acordo com o projeto de doutorado direto proposto no ingresso na pós-graduação (07/2019). O projeto propunha a utilização de compostos da classe das benzofenona como modificadores catalíticos junto a matriz de carbono para produção de H_2O_2 com a finalidade de aplicação nos POA para degradação de interferentes endócrinos.

Assim, essa tese estuda e descreve a tecnologia EDG baseada em carbono para a produção de H_2O_2 . O Capítulo 1 é focado no estudo da reação RRO, como ela se processa, suas vias, o que a influência e quais produtos são formados, esta sessão da tese traz um estudo de materiais ativos para a RRO e seletivos para a via que tem o H_2O_2 como produto, a fim de entender o material e como ele influencia a reação.

Após o estudo e resultados promissores, o material foi estudado no Capítulo 2 para aplicação na tecnologia EDG e aplicado em uma célula de bancada para investigar seu

desempenho na eletrogeração, estudos de densidade de corrente, eficiência de corrente e outros parâmetros foram estudados e aplicados à degradação de uma molécula modelo. Uma vez encontrado um material que seja aplicável à tecnologia EDG e que possa ser usado para gerar H_2O_2 suficiente para ser aplicado em POA e realizar o tratamento de efluentes, o próximo passo foi estudar as formas e a otimização desse processo.

O estudo sobre o processo e as formas de otimização do EDG modificado foi discutido no Capítulo 3, com a proposta do reator que se mostra mais adequado para a aplicação de geração do oxidante de interesse, a caracterização desse reator foi feita, buscando entender como o reator proposto contribui para a melhoria da eficiência, o *layout* do sistema também foi explorado estudando reator com célula única e célula dividida, a influência do ânodo, a densidade de corrente e também a possibilidade de escalonamento, pois como o objetivo final foi viabilizar a tecnologia para aplicação real, foi necessário estudar e desenvolver reatores que sejam possíveis de escalonar. Com o estudo do processo, o EDG com material inédito e promissor foi aplicado buscando atingir a eficiência máxima.

Para explorar ainda mais as possibilidades e a versatilidade do H_2O_2 eletrogerado a partir da EDG, também foi estudada uma nova abordagem, na qual foi estudada a possibilidade de um sistema desacoplado de geração de H_2O_2 e ativação para $\bullet OH$, esse tópico é retratado no Capítulo 4. A geração *in situ* permite a possibilidade de inovar nas abordagens visando reduzir o consumo de energia sem perda da capacidade de aplicação, neste capítulo a eletrogeração de H_2O_2 acontece nos primeiros 10 min e após dentro do mesmo sistema subsequentemente é utilizada luz UVC para realizar sua ativação, essa abordagem foi aplicada para degradação de um fármaco, e analisada e monitorada para determinar o capacidade dessa nova abordagem no tratamento de efluentes.

CHAPTER 1. Study of carbonaceous material modified with organic compound benzophenone for electrosynthesis of H₂O₂ by oxygen reduction reaction

1.1 INTRODUCTION

An important point when the objective is the production of hydrogen peroxide (H_2O_2) for organic pollutants treatment is the development of novel catalytic technologies and materials capable of generating these chemical oxidants more efficiently (8,81,82). H_2O_2 is used as a hydroxyl radical ($\bullet\text{OH}$) precursor agent of advanced oxidative processes (AOP) and/or associated electrochemical EAOP, such as electro-generated/UV H_2O_2 , electro-Fenton, and photoelectro-Fenton. These wastewater treatment processes are considered green because the reaction produces innocuous products such as carbon dioxide (CO_2), H_2O , and inorganic compounds, or, in the absence of complete mineralization, oxygenated by-products whose compounds may be less toxic or have added value compared to the initial compound (6,44,62,65).

The oxygen reduction process (ORR) through 2-electron ($2e^-$) transfer has attracted a lot of interest in recent years due to its high efficiency and safe operation. The $2e^-$ process can reduce oxygen on the cathode surface to generate H_2O_2 and has the following advantages: *in situ* synthesis, eliminating the need for transportation and storage; no use of dangerous chemicals; no need for later purification procedures; and use of the green reagent, the electron (72,83,84). However, ORR is a multifaceted electrochemical reaction resulting from the fact that there is more than one step in its reaction mechanism, in instead of the production of H_2O_2 , the reaction of H_2O from 4-electron ($4e^-$) transfer is also possible, when O_2 is completely reduced to H_2O ; or H_2O_2 (formed by the $2e^-$ pathway) is reduced to H_2O by the transfer of 2 more electrons (83,85).

The major and most efficient catalysts described in the literature for the ORR via $4e^-$ are platinum-based and its metal alloys, whose materials are commonly used as cathodes in fuel cells (86,87). Carbon-based materials, on the contrary, are considered to be the most efficient catalysts for $2e^-$ ORR for their superior chemical and electrochemical properties, such as high conductivity, great stability, and particularly strong selectivity for H_2O_2 generation (26,69).

To be efficient for the synthesis of H_2O_2 from ORR via $2e^-$, a carbon-based material should have high selectivity, suppress the transfer to $4e^-$, and high catalytic activity, minimize the overpotential of ORR via $2e^-$. Carbon-based materials, according to Yeager (1986), the interaction of O_2 species with carbons proximity to functional group contained on their surface can generate H_2O_2 , the functional group contribute to the O_2 interaction by altering the electronic density (70,88).

The functional groups can change the electronic distribution of the carbons around by removing or donation electronic density, when this happen active site are form in the structure especially in the adjacent carbon of this functional group, altering the free energies of O_2 adsorption, resulting in the final product of the ORR H_2O or H_2O_2 . The interaction of O_2 with the activated sites (carbon next to the functional group) is present in the Fig. 1.1, the A is representing the functional group (23,89).

In the first stage, O_2 adsorbs on the active site, leading to the adsorbed species O_2^* (Equation 1.1). This is reduced by one electron to generate the chemical intermediate OOH^* (Equation 1.2). subsequently this, the OOH^* intermediate species combines with another H^+ to generate H_2O_2 , completing the ORR's 2-e pathway (Equation 1.3) It is important to emphasize that the sign * denotes an unoccupied active site, while the intermediate species OOH^* , OH^* , and O^* denote intermediates adsorbed on the active site (26,90,91).



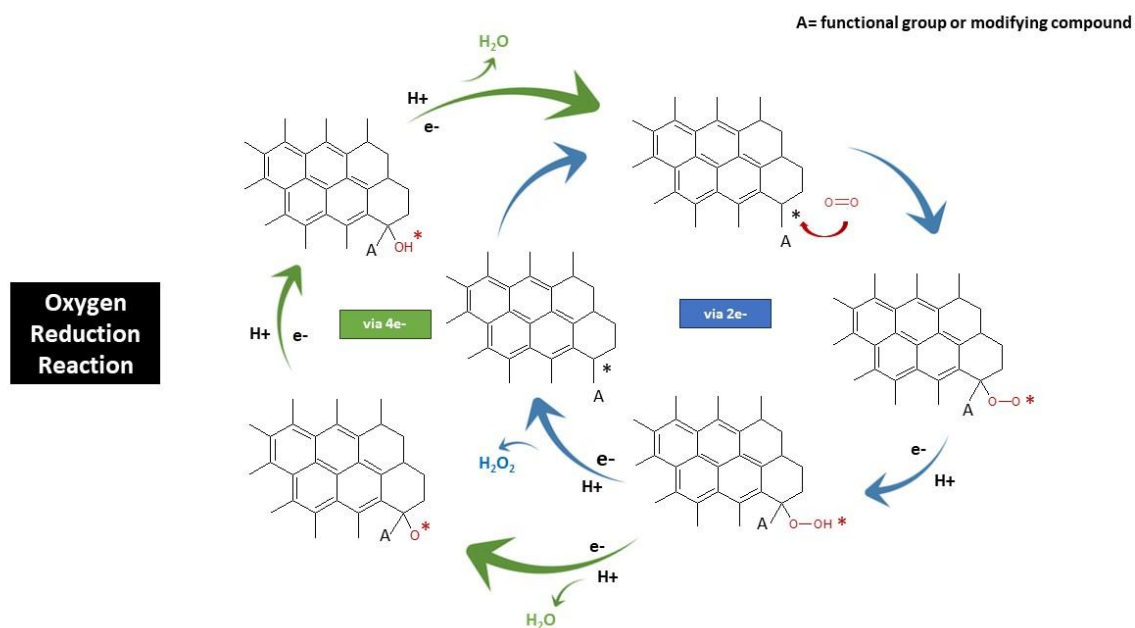
The OOH^* intermediate, on the other hand, can undergo dissociation stages to generate the other two intermediates O^* and OH^* (Equation 1.4), resulting in the creation of H_2O as the ultimate product of ORR. The $H_2O_2^*$ generated by ORR with two electrons can be reduced to H_2O , concluding the ORR mechanism with four electrons (Equation 1.4 – 1.9) (85,91).



The interaction strength of the OOH^* reaction intermediate with the active site on the surface of the carbon-based material is the essential parameter for controlling the ORR reaction path, as this is where the ORR products are produced. Thus, for a catalyst to have high activity

and selectivity for H_2O_2 generation, the O-O link of the OOH^* intermediate must be preserved, as breaking the bond will result in the development of other O^* and OH^* intermediates.

Fig. 1.1 – Depicts the mechanism involving the ORR stages on the active sites present on the surface of carbon-based materials for 4 and 2 electrons.



Source: The author herself.

As a result, an ideal carbon-based material should have a strong enough adsorption energy to preserve the O_2 molecule in the active site and induce the OOH^* intermediate formation, while the adsorption energy of this intermediate with the active site should be weak enough to induce the desorption of OOH^* and the production of H_2O_2 . If the adsorption energy between the active site and the OOH^* intermediate is high, the residence time of this intermediate will be long enough for the O-O bond to collapse and form the O^* and OH^* intermediates, and thus the ORR will tend toward the 4e- mechanism with H_2O as the final product (73,90,92).

One of the challenges for ORR via 2e- occurrence is the development of a carbon catalytic material that can make the barriers of thermodynamic and kinetic minimized for O_2 molecule adsorption and desorption, at the same time that leads to a maximization of the kinetic barriers for OOH^* dissociation to O^* and OH^* intermediates (23,83)

The advantages of employing materials based on carbon are their abundance, low cost, conductivity, and stability at acidic and basic pH, in addition to their strong selectivity for O_2

reduction via $2e^-$. The fundamental disadvantage of carbon-based materials is their poor catalytic activity, which means they have little interaction between the active site and the OOH^* intermediate. Changes in the chemical composition and surface of a carbon-based catalyst have demonstrate to be an interesting solution for overcoming this challenge. Functionalization with heteroatoms like nitrogen, oxygen, and fluorine to form functional groups near active sites, as well as the addition of defects in the surface structure of the carbon-based material, can improve the interaction with the OOH^* intermediate and favor the ORR for the production of H_2O_2 (86,89,93)

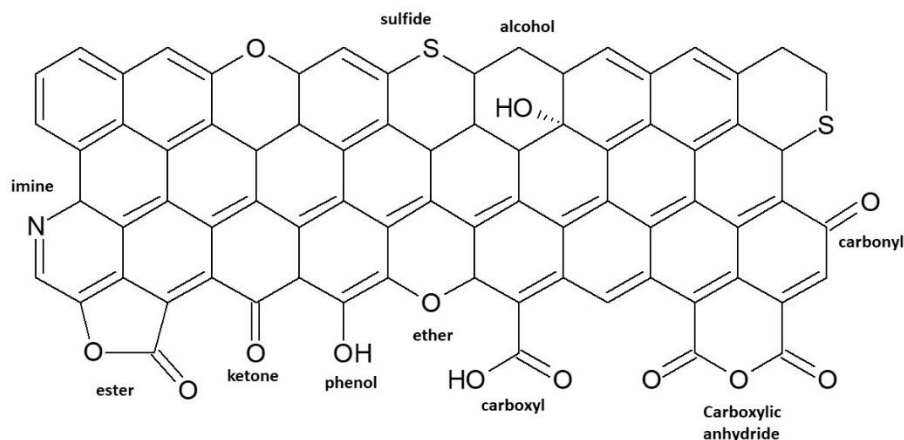
Some studies have demonstrated that the functionalization or doping of porous carbon-based materials with, fluorine, and primarily oxygen heteroatoms increase electronegativity, breaks the integrity of the conjugated system, and produces defects in the surface structure of the carbon material, and largely changes the electronic density of the active site and may favor the reduction of O_2 via $2e^-$.

Fig. 1.2 depicts several oxygenated ($-\text{COOH}$, $-\text{C}=\text{O}$, $-\text{C}-\text{O}-\text{C}$, and $-\text{COH}$) and nitrogenated (N-pyridine, N-pyrrolic, N-quaternary, and N-oxides) functional groups identified in carbon-based materials, as well as the existence of flaws or holes in the material's structural surface. Functionalization with oxygen heteroatoms at the active site has presented considerable potential to improve the selectivity and catalytic activity of ORR for $2e^-$ over nitrogenated functional groups. Oxygenated functional groups affect the surface of the carbon matrix by increasing its reactivity and wettability/hydrophobicity, allowing dissolved O_2 to be more accessible in the vicinity of the active sites. Furthermore, oxygenated functional groups found at the edges and flaws of the carbon material structure have increased ORR activity via $2e^-$ -transfer (26,83).

The presence of the oxygenated functional groups $-\text{COOH}$, $-\text{C}=\text{O}$, $-\text{CHO}$, $-\text{C}-\text{O}-\text{C}$, and $-\text{COH}$ in carbon-based materials raises ORR selectivity for H_2O_2 production, with the carboxyl ($-\text{COOH}$) and carbonyl ($-\text{C}=\text{O}$) groups bringing the highest catalytic activities for 2-electron transfer. These oxygenated functional groups, according to Kim et al (2011), can change the way of adsorption of the O_2 molecule on the active site, favoring the adsorption (70,74,94).

Commercial carbon-based materials have been used as cathode matrix for the electrochemical production of H_2O_2 , such as vitro cross-linked carbon, graphite, graphene, carbon nanotubes, and amorphous carbon. Electrical conductivity, hydrophobicity, surface area, the existence of oxygenated functional groups, and the presence of defects are all inherent properties that might have a larger or lesser interference in the selectivity and activity for H_2O_2 production (26,95).

Fig. 1.2 – Illustration of the functional groups present in carbon material surface.



Source: The author herself.

The amorphous carbon PL6C has been extensively popular among the matrices described due to its significant surface area and for present in their structure presence of oxygenated functional group, such as carboxylic acids, quinones, and anthraquinones. PL6C is an advantageous cathode material for H_2O_2 electrogeneration. The PL6C improves ORR efficiency for H_2O_2 electrogeneration when as compared to Vulcan XC-72R carbon, the difference in efficiency is attributable to the larger surface area and higher levels of oxygenated functional groups on the surface of the carbon material (95–98).

1.1.1 Organic Modifiers

The use of amorphous carbon, such as PL6C already presenting satisfactory results, but one of the advantages of using material based on carbon is the possibility of modification with catalysators to improve the catalytic activity and selectivity for ORR via $2e^-$, modifiers such as metals, metal and bimetallic oxides, organic compounds, or coordinated compounds are commonly used on amorphous carbon matrices to reduce the high overpotentials required in the process and/or increase the selectivity for H_2O_2 , resulting in a reduction in energy expenditure for H_2O_2 product (27,43,80,99–101).

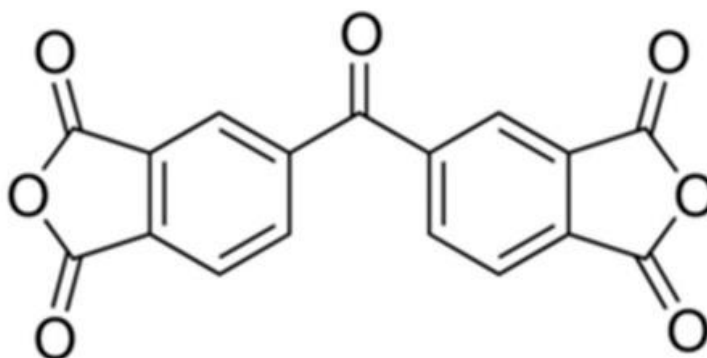
Organic compounds have been little explored and studied for H_2O_2 generation materials. Quinones, azobenzenes and phthalocyanines, have already been used to modify the carbon matrix of the gas diffusion electrode GDE, this has an effect in increasing the generation of

H_2O_2 and decrease superpowers to occur the ORR. Among the various compounds that can be used as catalytic modifiers, organic compounds are presenting satisfactory results (43,100,102).

Benzophenone is a class of organic compounds (aromatic ketones) widely used in industry, synthesis, and photochemical applications, they are water insoluble, stable and exhibit redox activity. The organic compound BTDA demonstrates promising activity and structure (Fig. 1.3) to be studied for H_2O_2 electrogeneration, because it is a ketone, it is expected to behave with a profile of quinones, since both have $C=O$ groups, and like quinones this bond contribute to an increase in H_2O_2 generation. This organic compound was explored because of the property of photogeneration of H_2O_2 , and the possibility of forming polymer and able to bond with cellulose, that possibilities the production of cellulose and functionalized cotton with H_2O_2 generation production when at the presence of a UV (103–106).

To further improve the efficiency of the oxygen reduction reaction, carbon-based materials can be modified with numerous materials ranging from metal oxides to organics. The possibility of using BTDA as a modifier to the carbon matrix to analyze the effect of benzophenones on ORR performance (H_2O_2 generation performance and on potential shift) shows promise.

Fig. 1.3 – Molecular structure of BTDA.



Source: The author herself.

The developed research consists of electrochemically evaluating the modification of PL6C carbon with the organic compound BTDA in alkaline medium.

1.2 EXPERIMENTAL PROCEDURES

This topic is divided between 2.1 Materials; 2.2 Electrochemical Analysis and 2.3 Material characterization.

1.2.1 Materials

Benzophenone-3,3',4,4'-tetracarboxylic dianhydride (BTDA; 98% from Sigma Aldrich), Printex[®] L6 carbon (PL6C; from Evonik Brazil Ltd.) and isopropyl alcohol (Sigma Aldrich) were used to prepare the material; Dimethylformamide (DMF; Sigma Aldrich) was used as the solvent for the preparation of the microlayer. Ultra-pure water from a Milipore Milli-Q system and potassium hydroxide (KOH; 90% of the solution) were used as the electrolyte.

1.2.2 Electrochemical Analysis

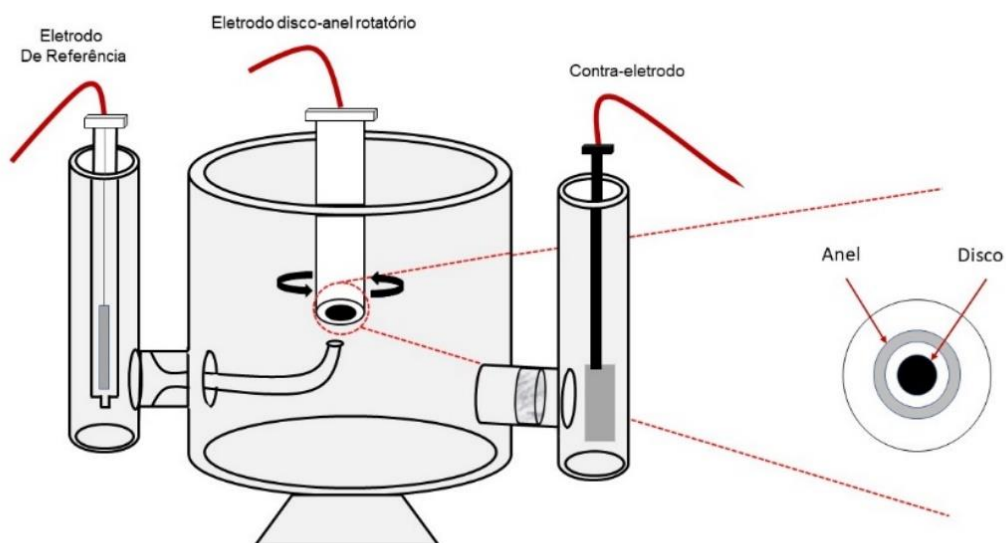
The modified material was made by physical adsorption of 2.0% BTDA in relation to the mass of PL6C to obtain 1g of modified material (PL6C/BTDA 2.0%), 20 mL of isopropyl alcohol was added and kept in magnetic stirring for 40 min, after the mass was placed in study for 3h for the material to dry, then the material was macerated with the aid of a mortar and pestle. Then a dispersion was made where the proportion was 2.5 mass to 1 solvent DMF (2.5:1) and 10 μL of this mixture was dripped onto the surface of the disk of the ring-disk electrode (Figure 1.4). where the disk is made of glassy carbon and the ring of platinum (Pt). It was then left to stand for the porous microlayer to dry.

Cyclic voltammetry analyses were performed in the potential window from 0.1 to -1.2 $\text{V}_{\text{Ag}/\text{AgCl}}$ with a scan rate of 50 mV s^{-1} . ORR was studied by linear scanning voltammetry in a potential window of 0.1 to -0.8 $\text{V}_{\text{Ag}/\text{AgCl}}$ at the scan rate of 5 mV s^{-1} under 900 rpm rotation.

The stability test was performed by applying 1000 cycles of cyclic voltammetry in the potential window 0.1 V to -0.6 V at scan rate of 500 mV s^{-1} . All electrochemical analyses were performed in a saturated medium with nitrogen (N_2) and oxygen (O_2), using 0.1 mol L^{-1} KOH electrolyte (pH 13), silver/silver chloride (Ag/AgCl 3 M) reference electrode and Platinum (Pt) counter electrode.

The equipment used was a PGSTAT 128N potentiostat from Metrohm AUTOLAB, interfaced with NOVA 2.1 software in a PINE model rotating ring-disk electrode (RRDE) rotation module, where the electrode is composed of a platinum ring (area of 0.1866 cm^2) and a glassy carbon disk (area of 0.2476 cm^2) with a collection factor of 0.37 provided by the manufacturer, in an electrochemical cell (Fig. 1.4).

Fig. 1.4 – Schematic diagram of the electrochemical cell of the RRDE.



Source: The author herself.

Selectivity calculations for H_2O_2 ($S\%_{H_2O_2}$) were performed using Equation 1.10, where i_a is the current in the ring (in A); i_d is the current in the disk (in A); and 0.37 is the collection number (N).

$$S \%_{H_2O_2} = \frac{(2 i_a/N)}{(i_d+i_a)/N} \times 100 \quad (1.10)$$

The number of electrons exchanged (n_t) for the ORR reaction to occur by Equation 1.11

$$n_t = \frac{4 i_d}{(i_d+i_a)/N} \quad (1.11)$$

1.2.3 Material Characterization

For elemental analysis assays, a Thermo Scientific FlashSmart CNHSO elemental analyzer was used under the operating conditions of 720 seconds run time and 950 °C oven temperature for CHNSO determinations.

For the thermogravimetric analysis (TG) assays, ~10 mg of PL6C/BTDA 2% sample was used at a temperature range of 30 °C to 1000 °C with a heating rate of 10 °C min⁻¹ in a synthetic air atmosphere under 50 mL min⁻¹ flow rate, the equipment used was a Mettler thermogravimetric analyzer model TGA/DSC2.

The hydrophobicity of the synthesized materials was analyzed by contact angle tests using a Tensiometer. During the analyses, a 3 μL drop of water was dropped on top of the analyzed surface, which in this case was a microlayer of the material PL6C and PL6C/BTDA 2%.

For morphological evaluation of the synthesized materials Transmission Electron Microscopy (TEM) analyses were performed. The analyses were performed using a FEI TECNAI G² F20 microscope (acceleration voltage: 200 kV), supported on copper grids covered with a carbon film (Electron Microscopy Sciences). Samples of the materials studied were drop-dried from a diluted dye of these materials. The MET analyses were done at the facilities of the Chemistry Department of the Federal University of São Carlos (UFSCar).

1.3 RESULTS AND DISCUSSION

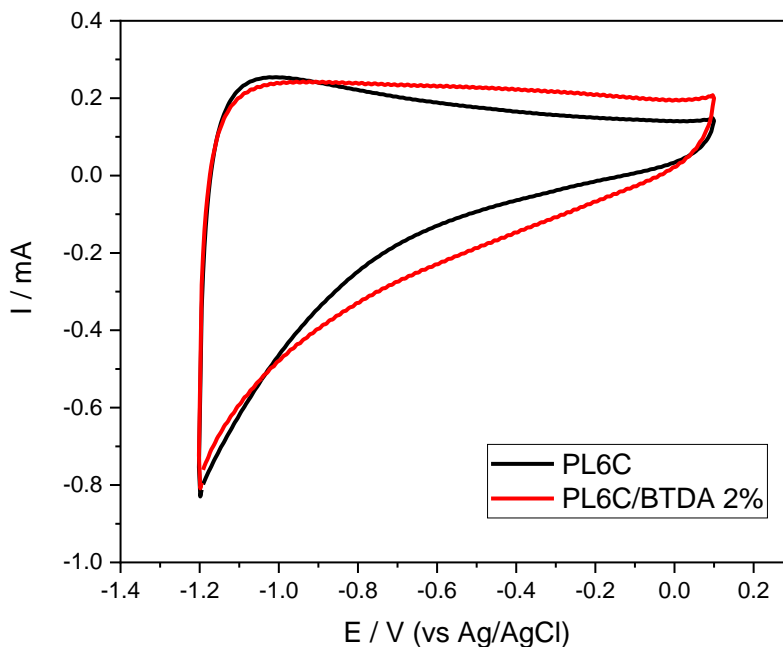
The results and discussion were divided in 3.1 Cyclic voltammetry, 3.2 ORR study using the hydrodynamic method RRDE and 3.3 Physical and morphological analysis of the materials.

1.3.1 Cyclic voltammetry

Initially, the electrochemical behavior of the catalyst materials (PL6C and PL6C/BTDA 2%) was studied by cyclic voltammeteries performed in a medium saturated with N_2 (to ensure that there is no solubilized O_2 in the reaction medium) as can be observed in Fig. 1.5. It can be noted that at potential values more negative than -1.2 V there is an increase in current due to H^+ reduction reactions generating H_2 gas, while in more positive potentials, at +0.1 V, the oxidation reaction of H_2O occurs to generate O_2 , then potential interval was based on these data, since the reaction of interest is the ORR via 2e^- to generate H_2O_2 .

It can be observed that at the potential studied no redox pairs can be attributed to BTDA in PL6C/BTDA 2%, this may occur due to the fact that possible redox pairs do not present activity in this potential range, or are being covered by the PL6 carbon, or even due to the low amount of BTDA present (2.0%) being a very low concentration, to obtain response (95,100). No peaks related to 2e^- -ORR were identified because there is no O_2 in the solution, this is important because if peaks appear in the cyclic voltametric with solution solubilized with O_2 indicates that the peaks are from ORR and not from the material.

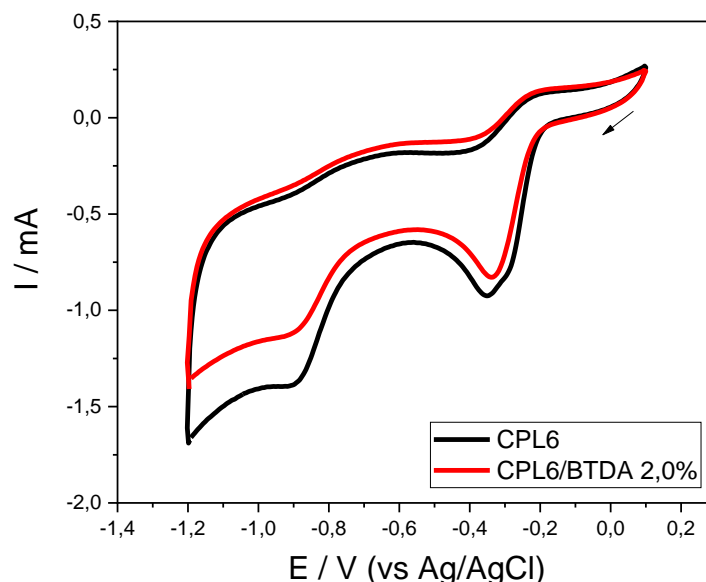
Fig. 1.5 – Cyclic voltammogram of PL6C and PL6C modified with 2% BTDA. Conditions: 50 mV s^{-1} , using KOH 0.1 mol L^{-1} as support electrolyte, pH 13, saturated with N_2 .



Source: The author herself.

In the O_2 saturated cyclic voltammetry (Fig. 1.6) it is possible to see that the cyclic voltammograms of both materials (modified and unmodified) remain with the same profile, this indicates that the modification did not change the properties of the carbon, and that despite the modification the electrochemical properties of the carbon were still mostly maintained. Two peaks can be identified when O_2 is present, one at -0.3 V and another at -0.9 V, referring to the ORR, the peaks relate to the number of electrons involved in the ORR (2e⁻ or 4e⁻) and also how O_2 is adsorbed on the active sites of the carbon (85,95).

Fig. 1.6 – Cyclic voltammogram of PL6C and PL6C modified with 2% BTDA, Conditions: 50 mV s^{-1} , using KOH 0.1 mol L^{-1} as support electrolyte, pH 13, saturated with O_2 .



Source: The author herself.

1.3.2 ORR study using the hydrodynamic method RRDE

For the electrochemical study of ORR by the linear sweep voltammetry (LSV) technique, a RRDE was used, where the disk of the electrode (glassy carbon) is the microlayer of the material studied. A constant potential of +0.45 V (vs Ag/AgCl) is applied to the ring of the RRDE, and the ring current values refer to the oxidation of H_2O_2 , which is generated in the disk. Thus, the LSV plots are divided into 2 parts: the upper part referring to the current detected in the ring, and the lower part referring to the current detected in the disk.

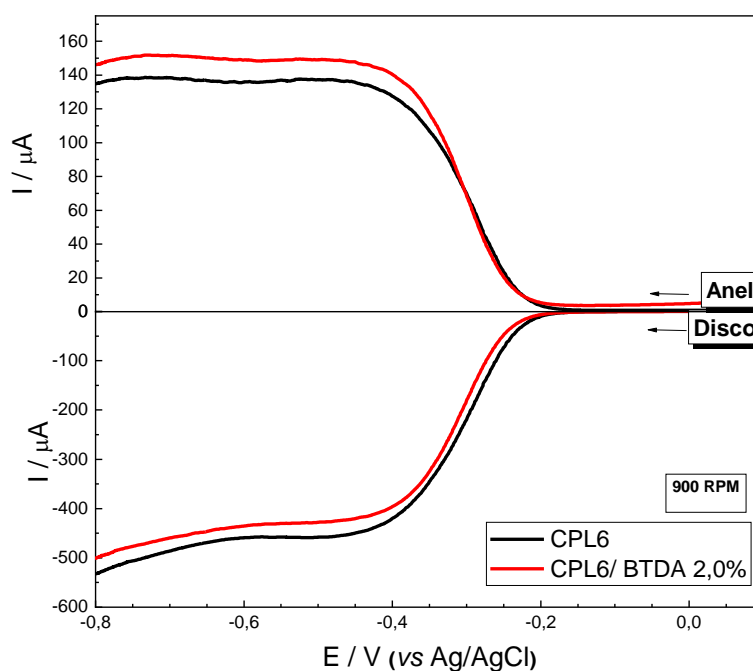
The LSV curves referring to the studied materials are in Fig. 1.7, where it is in hydrodynamic mode with rotation at 900 RPM, and the medium was saturated with O_2 to ensure the study of the ORR.

It can be seen that for PL6C and modified PL6C catalysts there are three distinct regions in the voltammogram. The first region where the potential range is +0.1 V to -0.2 V, only capacitive current is observed, so what controls the ORR is charge transfer or kinetic control. In the potential range between -0.2 V to -0.5 V, the second region, the ORR process is controlled by both charge transfer and mass transport, it is controlled by mixed regime. And in the third region, where the potential range is from -0.5 V to -0.8 V, is controlled by charge transfer, it is

possible to notice why the disk current reaches a maximum and constant value, this is because the process is limited to the amount of O_2 that reaches the surface of the disk.

The ring current values detected refer to the oxidation of the H_2O_2 generated in the disk, so it is possible to estimate and compare the materials in estimates of H_2O_2 production. Thus, the carbon without modification reached a maximum ring current of $138 \mu A$ and the carbon with organic modifier reached a maximum ring current of $151 \mu A$, thus the modification with BTDA in the proportion of 2%, improved the catalytic effect of the material, generating more H_2O_2 . There was no significant ORR shift.

Fig. 1.7 – Linear sweep voltammogram obtained used RRDE setup for PL6C and PL6C/BTDA 2%. Conditions: 50 mV s^{-1} , using $KOH 0.1 \text{ mol L}^{-1}$ as support electrolyte, pH 13, saturated with O_2 .



Source: The author herself.

Based, on the disk and ring LSV curves, the selectivity of the material was calculated. Figure 1.8a, elucidates that the modification increased the selectivity for H_2O_2 . PL6C recorded a value of $89.5 \% S_{H_2O_2}$ and PL6C/BTDA 2% recorded $97.7 \% S_{H_2O_2}$, this demonstrated that the synergism between the carbon and modifier materials were advantageous for the selectivity for

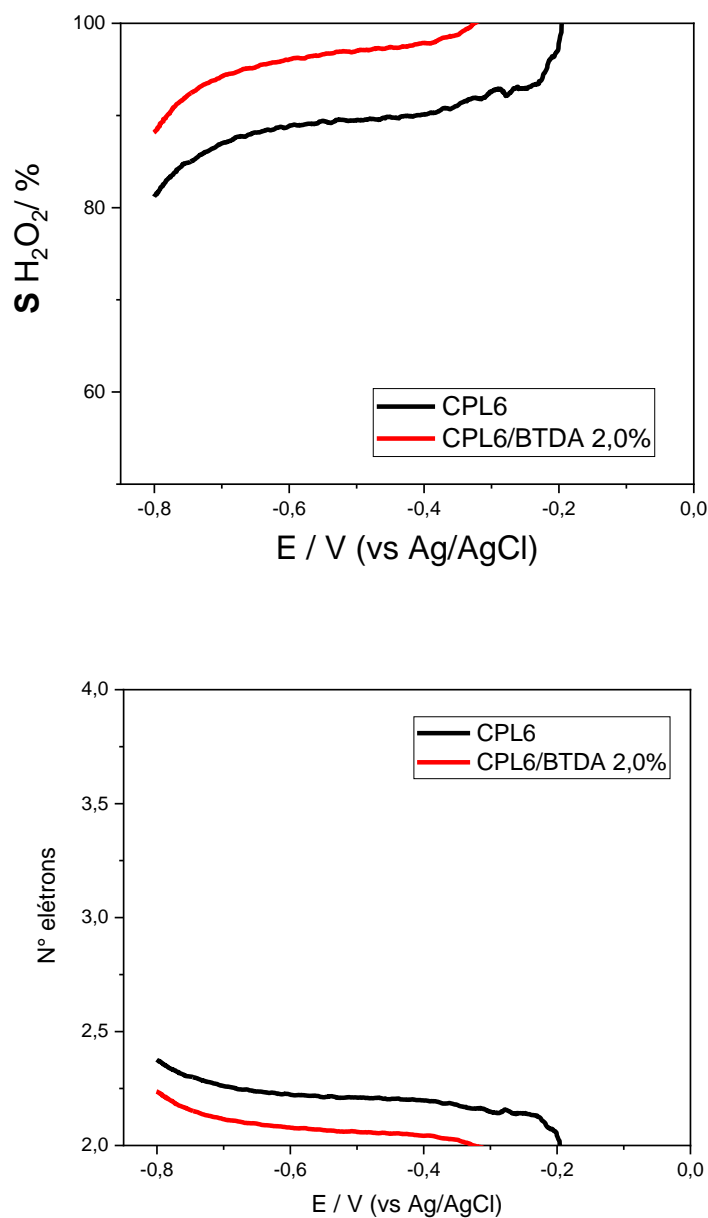
H₂O₂, the structure of benzophenone presents oxygen groups which can explain the increase in this selectivity. Moreira et al (2019), achieved a maximum selectivity of 86.2% using the same carbon matrix PL6C modified with 0.5% Sudan Red 7B, this compost has in its structure several nitrogenous groups in azo positions (-N = N-), compared to the BTDA compost, the Second is more promising because it reaches higher values of %S_{H2O2} and because oxygenated groups try to increase selectivity more than nitrogenous groups (100).

Other works in the literature such as Kronka et al (2021), presents with the PL6C material modified with 5.1% wt of ZrO₂ selectivity of 88 %S_{H2O2}, in addition to the material proposed in this research presenting higher selectivity (97.7 %S_{H2O2}), this value is reached using a lower percentage of modification (BTDA 2%). One of the works reported in the literature that reach similar selectivity values is that of Kronka et al (2023), reaching a value of 97 %S_{H2O2} with PL6C material modified with Au-ZrO₂, yet the proposed material stands out using noble metals such as Gold and for presenting a simple synthesis in a single step by physical dispersion, where the PL6C/Au-ZrO₂ material was made in two steps by hydrothermal synthesis (27,77).

Comparing with the literature it is evident that the material is extremely promising, other materials of the quinone class, which have a structure very similar to benzophenone, present better selectivity at lower concentrations such as: Carbon Black modified 1% of Alizarin (95 %S_{H2O2}) and PL6C modified 1% 1,4-naphthoquinone and PL6C modified 2% anthraquinone-2-carboxylic acid (83.8 %S_{H2O2}). This is because organic compounds at higher modification percentages tend to agglomerate, so the low amount of modification of BTDA 2% elucidates advantageous results (43,100).

The results of the selectivity for H₂O₂ is in concordance with the electron number of electrons involved in the reaction, calculated and presented in Fig. 1.8b, by the figure, is possible to note that, the modified material presented electron number values closer to 2e⁻ than the PL6C, so it is possible to understand that even though the carbon already presents high selectivity and number of electrons involved in the reaction close to 2e⁻ (reaction of interest), that is in concordance with the literature, the modification provided an even greater improvement in selectivity, a greater generation of H₂O₂ (based on the current value of the ring) and electron values closer to the reaction pathway of interest.

Figure 1.8 – a) Selectivity values for H_2O_2 b) Number of electrons involved in the ORR reactions for PL6C and PL6C/BTDA 2%, Conditions: 50 mV s^{-1} , using $\text{KOH } 0.1 \text{ mol L}^{-1}$ as support electrolyte, pH 13, saturated with O_2 .

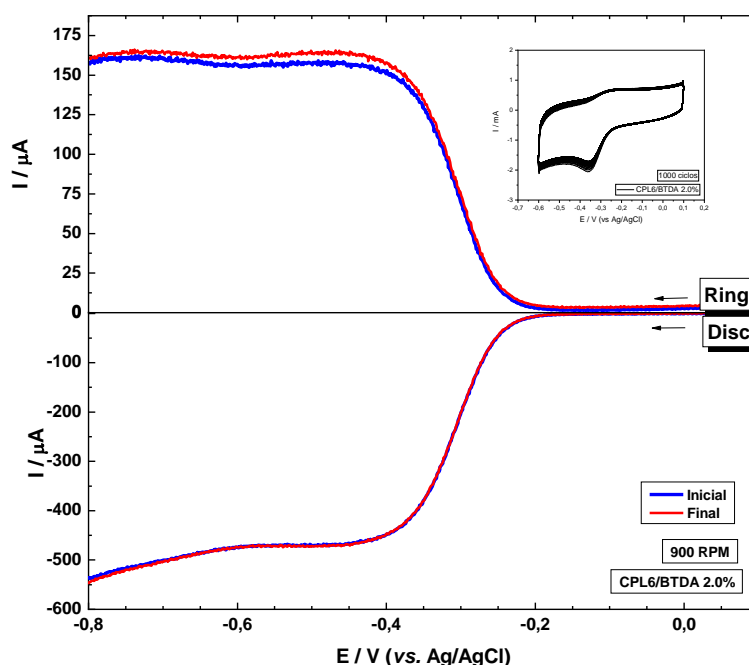


Source: The author herself.

The material electrochemical stability (microlayer) was analyzed, where the microlayer was subjected to an accelerated stress test (AST) by applying 1000 potential cycles between 0.1 to -0.6 V with a scan rate of 500 mV s^{-1} in a medium saturated with O_2 . The LSV curves obtained before and after the 1000 cyclic voltammetries are shown in Fig. 1.9.

It is possible to note that there was no loss of activity and performance of the material, elucidating the microlayer stability. This may indicate that the material was well adsorbed and the synergism between them also provides a stable material.

Fig. 1.9 – Linear sweep voltammetry to analyze the stability of the microlayer (PL6C/BTDA 2%) Conditions: 5 mV s^{-1} , using KOH 0.1 mol L^{-1} as support electrolyte, pH 13, saturated with O_2 . Inset: Cyclic voltammogram in O_2 , KOH 0.1 mol L^{-1} as support electrolyte, pH 13, potential window: 0.1 V to -0.8 V , 1000 cycles at 50 mV s^{-1} .



Source: The author herself.

1.3.3 Physical and morphological analysis of the materials.

Contact angle analyses were performed to investigate the hydrophobicity/hydrophilicity of the materials, a drop in the volume of $3 \mu\text{L}$ of ultrapure water was dripped on a microlayer of the studied materials, as shown in Fig. 1.10. It is possible to notice a change in the contact angle values for the modified material. PL6C presented contact angle 128.49° and 128.37° and PL6C/BTDA 2% 123.74° and 123.84° ; this demonstrate that both sides were quite close, and the variations can go into the error.

It is expected that the modified material has hydrophilicity like the unmodified, due to the structure of BTDA once it is contained of C=O groups, causing the material to have more polarity and thus greater interaction with water, the variation of contact angles, conversely, are low, this is also expected since the percentage of modification is only 2%. That elucidated the medicated material do not imply in properties loss of the PL6C.

Fig. 1.10 – Contact angle of the microlayers, drop volume 3 μ L.



Source: The author herself.

The results obtained from the Elemental Analysis CHNSO corroborate with the contact angle results, in Table 1.1. where is possible to analyze the mass percentage and the composition of the CHNSO elements (m/m (%)), thus, it is evident that the PL6C presents a greater amount of carbon in its composition than the PL6C/BTDA 2%, conversely, the modified material presents a greater amount of oxygen and hydrogen, this is due to the C=O and C-H groups present in the benzophenone, elucidate the modification of the material and explain the increased hydrophilicity with the increase of oxygen present in the material.

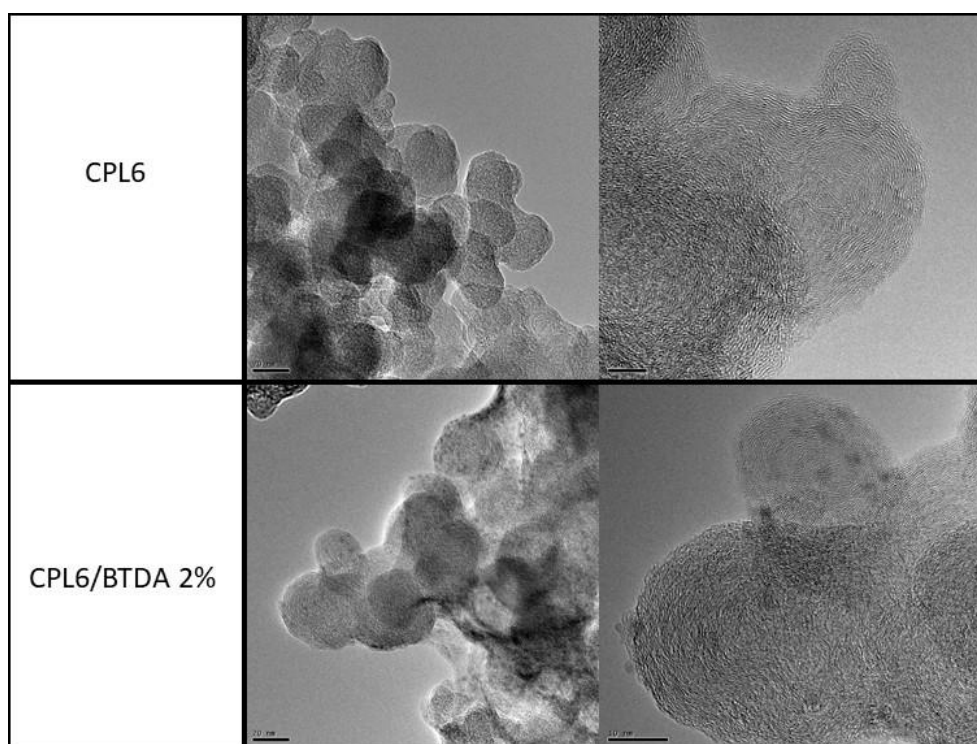
Table 1.1 – Elemental Analysis CHNSO of the mass composition of the samples of carbon.

	N	C	H	S	O*
Material	(wt. %)	(wt. %)	(wt. %)	(wt. %)	(wt. %)
PL6C	0,37	92,58	0,49	0,34	6,22
BTDA 2,0%	0,21	89,43	0,58	0,32	9,47

*Values obtained by difference. Source: The author herself.

The results obtained by TEM analysis allow to identify that the modification had no effect on the morphology of the carbon matrix (Fig. 1.11), conversely, it is possible to notice that in the modified material small dots are identified that cannot be seen in the carbon images. This could indicate that the dots the PL6C/BTDA 2% image are related to the modification with the organic compound. Just from the images it is not possible to say that it is due to modification, but there is a great indication corroborated with data obtained from CHNSO analyses.

Fig. 1.11 – TEM images obtained for PL6C and PL6C/BTDA 2% materials at 20 (second column) and 10 nm (third column).

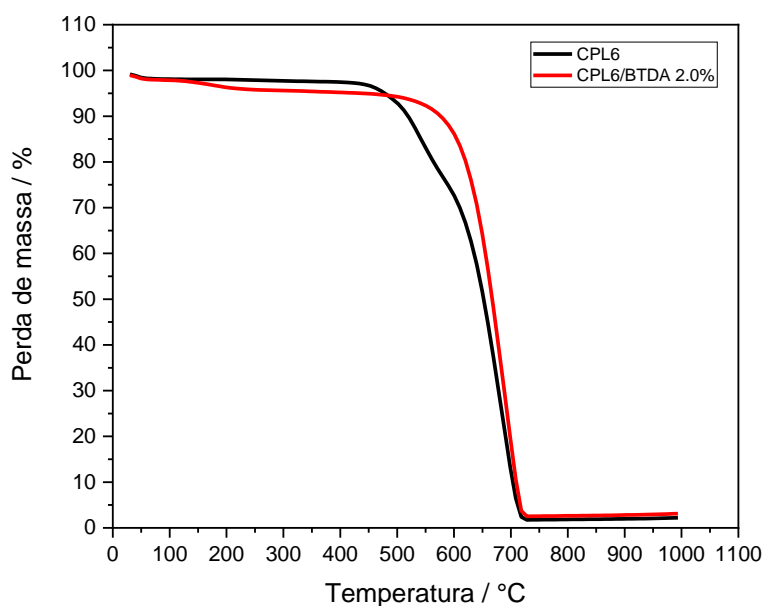


Source: The author herself.

The materials analyzed were submitted to TG, in order to observe the events of mass loss or gain of the materials (Fig. 1.12). As the temperature rises to 300°C 3% the PL6C loses 3% of its initial mass, this can be related to a possible humidity of the material, the modified material up to 300°C presents 5% of mass loss of the material, where the 2% more lost can be related to the presence of BTDA that increases the interaction of the material with water. For the next steps (application of the material in GDE) the materials will be submitted to a

temperature of 290°C, the TG analysis evidences that the materials are resistant to this temperature, and do not present significant losses that affect the performance or loss of property of these materials, and it is possible to consider this loss in the calculation of the amount of mass needed to obtain the desired amount of mass of material for application in GDE (100).

Fig. 1.12 – Thermogravimetric analysis (TG) graphs of the materials: PL6C and PL6C/BTDA 2%.



Source: The author herself.

1.4 CONCLUSION

Chapter 1 studied the effects of structural, chemical, and physicochemical properties of carbonaceous materials (unmodified and modified) for the oxygen reduction reaction to produce H_2O_2 . The results elucidate that the studied material PL6C and PL6C/BTDA 2% present themselves as favorable materials for the electrogeneration of H_2O_2 . The analyses highlight that the modification of the carbon matrix with the organic compound tends to increase the generation of H_2O_2 , the selectivity and the reactions that take place are mostly via $2e^-$ to ORR. The characterization results of the materials corroborate with the electrochemical results, the increase in hydrophobicity concur with the masses detected in the elemental analysis

and the thermogravimetric analysis, elucidating that the modified material interacts more with water, due to its molecular structure.

Thus, it is possible to conclude that the modification was successful and tends to increase the catalytic effect for H_2O_2 electrogeneration, their excellent properties such as: high electrochemical surface area, composition of oxygenated functional groups were responsible for playing a significant role in the efficiency of ORR for H_2O_2 production. The modification with BTDA contributes to the appearance of more active site, because of BTDA structure with functional groups (C-O-C and C=O). Although the carbonaceous material (PL6C) already presents high selectivity of 89.5 % $\text{S}_{\text{H}_2\text{O}_2}$, the modification made it possible to reach a selectivity value of 97,7 % $\text{S}_{\text{H}_2\text{O}_2}$, being possible to contribute beyond a contribution of the BTDA itself to electrogenerate H_2O_2 , but also contributes with its functional groups to a possible synergism with the carbon matrix.

The modification caused no loss of desirable properties of the carbon matrix and increased the thermal and electrochemical stability of the material, as presented by the TG and electrochemical stability results.

In view of the results obtained in Chapter 1, it is evident that the PL6C/BTDA 2% material is an excellent cathode material to be applied in the manufacture of gaseous diffusion electrodes for the production of H_2O_2 *in situ* and, subsequently, to be applied as cathodes in an effluent treatment system operating by means of electrochemical advanced oxidative processes, whose theme is addressed in Chapter 2.

CHAPTER 2. Using a novel gas diffusion electrode based on PL6 carbon modified with benzophenone for efficient H₂O₂ electrogeneration and degradation of ciprofloxacin

This article was published in Chemical Engineering Journal, 455, Taynara O. Silva; Lorena A. Goulart; Isaac Sánchez-Montes; Géssica O. S. Santos; Renato B. Santos; Renata Colombo; Marcos R. V. Lanza; “Using a novel gas diffusion electrode based on PL6 carbon modified with benzophenone for efficient H₂O₂ electrogeneration and degradation of ciprofloxacin”, 140697, Copyright Elsevier, 2023. DOI: <https://doi.org/10.1016/j.cej.2022.140697>.

Abstract

The present study reports the development and application of a gas diffusion electrode (GDE) based on Printex L6 carbon modified with 2.0% benzophenone-3,3',4,4'-tetracarboxylic dianhydride (PL6C/2.0-BTDA) for the efficient electrogeneration of hydrogen peroxide (H_2O_2) and degradation of ciprofloxacin (CIP) using different advanced oxidation processes (AOPs). The modified GDE was studied under different current densities and 25 mA cm^{-2} was found to be the most efficient current density, since the application of the modified GDE at this current density yielded higher amounts of H_2O_2 , greater kinetic constant and lower energy consumption compared to unmodified GDE. Based on these results, the modified GDE was used for the degradation of CIP in alkaline solutions using different AOPs, including anodic oxidation (AO), UVC photolysis, and processes based on H_2O_2 electrogeneration (AO/e- H_2O_2 /UVC and AO/e- H_2O_2). The AO/e- H_2O_2 /UVC technique was found to be the most efficient among the AOPs investigated; the application of this technique led to the complete removal of CIP ($75 \mu\text{mol L}^{-1}$) in 20 min of treatment, apart from yielding the highest kinetic constant rate and lower electrical energy per order ($2.1 \text{ kWh m}^{-3} \text{ order}^{-1}$). The oxidation by-products generated during CIP degradation via AO/e- H_2O_2 /UVC were successfully identified and a pathway for CIP degradation was proposed.

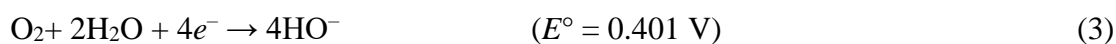
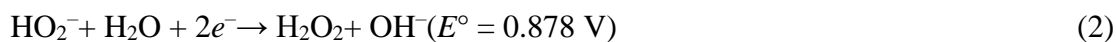
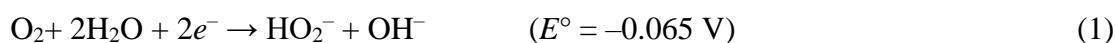
Keywords: Gas diffusion electrode; Benzophenone modifier; Hydrogen peroxide; Antibiotic degradation.

Introduction

The rampant consumption of pharmaceutical products worldwide has resulted in one of the biggest environmental challenges of our time: the significant presence of pharmaceutical contaminants in aquatic systems. The massive presence of these contaminants in water bodies can be attributed to the ineffectiveness of conventional treatment methods that are employed in water and wastewater treatment plants for the removal of these pollutants [1–3]. Even when present at low concentration levels, these pollutants have been found to pose serious risks to human and animal health [4–6]. Ciprofloxacin (CIP) is an antibiotic of the fluoroquinolone class which is widely used for the treatment of bacterial infections. CIP can cause disorders in human endocrine system and can also undermine the photosynthesis process in some plants, affecting their morphology [7,8]. Several studies reported in the literature have detected the presence of CIP at high concentrations in wastewater that has already been treated and in natural waters [9,10]. In view of that, it is essentially important to develop highly efficient technologies that are capable of removing CIP in aqueous matrices. Electrochemical advanced oxidation processes (EAOPs) are highly promising technologies which have been successfully employed for the treatment of water; the application of EAOPs has resulted in the effective removal of several classes of organic contaminants, including antibiotics, in aqueous matrices [11–15]. EAOPs are also found to be incredibly versatile once they can be employed as pre-treatment techniques prior to the application of bio-treatment processes [16,17].

The mechanism of operation of EAOPs involves the production of highly reactive and non-selective free radicals (mainly hydroxyl radicals - $\cdot\text{OH}$) which are capable of converting organic pollutants to CO_2 , H_2O and inorganic ions. $\cdot\text{OH}$ species can be produced from the activation of hydrogen peroxide (H_2O_2) which can be electrogenerated *in situ* using suitable electrode materials [11,16–20]. As reported in the literature, electrochemically-produced H_2O_2 can be activated through UVC radiation ($e\text{-H}_2\text{O}_2/\text{UVC}$), leading to the production of $\cdot\text{OH}$ species; this technique has been found to be efficient for the degradation of different classes of organic contaminants [20,21]. H_2O_2 can be generated *in situ* through oxygen reduction reaction (ORR) which occurs on the cathode surface via 2-electron ($2e^-$) pathway; the advantages of *in situ* electrogeneration of H_2O_2 are that the application of this technique helps eliminate the problems related to the storage and transport of H_2O_2 , where there can be risks of explosion at high temperatures. While it is primarily important that the ORR process follows a $2e^-$ mechanism to generate H_2O_2 as the final product of reaction, the process may occur via the $4e^-$

mechanism, which also leads to the production of H₂O [22–24]. The ORR process in basic solution under the 2e⁻ and 4e⁻ pathways is represented in Eqs. 1, 2 and 3 [25,26].



The main limitation of the ORR process lies in the low solubility of oxygen (O₂) in solution. To overcome this constraint, gas diffusion electrodes (GDE) have been successfully applied in ORR under the 2e⁻ pathway [22,24]. This strategy involves the use of the triple interface gas-solid-liquid, which facilitates the transfer of electrons and O₂ mass to the cathode surface [27–30]. GDE based on carbonaceous materials have been widely applied as cathodes for ORR due to their high electrical conductivity, large surface area, good porosity, and abundant availability [23,24,29–31]. The development of new methodologies for the preparation of GDE and the search for new materials with excellent electrochemical properties that are highly efficient for the treatment of emerging pollutants in water have become a matter of great environmental relevance [[31,32]].

Inorganic and organic modifiers have been widely employed with a view to improving the efficiency of carbon-based GDEs in H₂O₂ electrogeneration; this is mainly because these compounds can provide the device with a greater amount of oxygenated groups and redox pairs that can effectively help to enhance the selectivity and kinetics of the ORR process via the 2e⁻ mechanism. Some studies reported in the literature have successfully employed inorganic modifiers such as Nb₂O₅, RuO₂, Ta₂O₅, Fe₃O₄, ZrO₂ and V₂O₅ for the enhancement of H₂O₂ generation [33–37]. Other studies have also successfully employed organic modifiers, such as quinones and azo compounds, for the improvement of ORR thanks to the different functional groups present in the structure of these modifying agents (-OH, -C=O and -COOH) [38–40]. For illustration purposes, Moreira et al. (2019) employed quinones and azo-compounds as organic modifiers of carbon matrix for the efficient electrogeneration of H₂O₂; the authors did not, however, delve into the possible application of these materials for water and wastewater treatment, leaving that part as an object of future research. In the aforementioned study, Moreira et al. (2019) conducted their analyses using organic compounds derived from another class of organic compounds (different from Benzophenones) but did not apply their proposed technique for wastewater treatment [39]. Similarly, Rocha et al. (2020) examined the effect of different quinones where the object of their study was mainly targeted at enhancing H₂O₂ electrogeneration without effectively applying the technique toward water and wastewater

treatment [41]. Unlike the aforementioned studies, in the study reported by Kronka et al. (2020), the authors successfully demonstrated the application of quinone (4-naphthoquinone)-modified GDE for the treatment of environmental matrices [42]. Taking the above considerations into account, it is worth investigating other classes of organic modifiers which exhibit suitable electrochemical properties and their application potential when applied for the enhancement of the selectivity of carbon-based electrocatalysts toward ORR under the $2e^-$ mechanism. One of these highly promising organic modifiers are benzophenone-derivative compounds.

Benzophenone is an organic compound that contains an aromatic ketone group and which is usually used in the organic synthesis of dyes, medicines and pesticides [43][44], and as photosensitizer and photoinitiator in photochemistry [43–48]. Due to its chemical structure, the benzophenone derivative compound benzophenone-3,3', 4,4'-tetracarboxylic dianhydride (BTDA) is a highly suitable compound which can be employed as a modifier for carbonaceous materials typically used for the construction of GDEs applied for H_2O_2 electrogeneration. Among the advantages of using BTDA as an organic modifier include the following: i) ease of modifying the carbon matrix (the organic modifier is physically mixed with carbon - inorganic modifiers require the use of cumbersome preparation methods as initial preparation step), ii) different electrochemical and chemical mechanisms can be added to the process; iii) the use of the modifying agent can cause a shift in ORR potential to more negative values; and iv) an increase in current for H_2O_2 formation [39,41,42]. Among the main disadvantages of using organic modifiers include the following: i) organic modifiers are mainly associated with the possible formation of aggregates/agglomerates; and ii) difficulty encountered in the physical characterization methods that are used to confirm the modification [39]. The present study aims to develop a highly efficient GDE using Printex[®] L6 as carbon matrix modified with BTDA organic compound; due to its suitable electrochemical properties, the BTDA organic compound was used to modify the GDE-PL6C material so as to improve the efficiency of the electrocatalyst in terms of H_2O_2 generation compared to the unmodified GDE (GDE without BTDA). To the best of our knowledge, this is the first time that a benzophenone derivative has been used as an organic modifier for the study of H_2O_2 electrogeneration and contaminant degradation. The present study brings an innovative contribution to the fore and helps to widen our knowledge and understanding regarding organic modifiers, which have, in general, been little explored in the literature; essentially, the study evaluates the performance of the proposed Benzophenone-modified PL6 carbon material in terms of its application for antibiotic degradation in alkaline medium. The catalytic effects of the modified material on H_2O_2

electrogeneration and CIP degradation are also evaluated by UV-vis spectroscopy and high performance liquid chromatography (HPLC), respectively. Finally, a pathway for CIP degradation is proposed based on the data obtained from liquid chromatography - electrospray ionization - tandem mass spectrometry (LC-ESI-MS/MS) analyses.

Experimental

2.1 Chemicals

CIP ($C_{17}H_{18}FN_3O_3$; >99% - from Sigma Aldrich), potassium hydroxide (KOH; 90% - from Sigma Aldrich), potassium sulfate (K_2SO_4 ; >99% - from Neon), ammonium molybdate - $((NH_4)_6Mo_7O_{24})$ (99% - from Sigma Aldrich), sodium bicarbonate - $NaHCO_3$ (>99.7 - from Sigma Aldrich), sodium carbonate, nitric acid - HNO_3 (65% - from Synth), sulfuric acid - H_2SO_4 (98% - from Neon), acetonitrile - CH_3CN (HPLC grade - from J.T. Baker) and short-chain carboxylic acids (a.r. - from Sigma Aldrich) were used as received for the conduct of the experiments. The proposed GDE was prepared using carbon black Printex[®] L6 (PL6C - from Evonik Brazil Ltd.), benzophenone-3,3',4,4'-tetracarboxylic dianhydride (BTDA; 98% - from Sigma Aldrich) and poly(tetrafluoroethylene) (PTFE) - acquired from Sealfon. Ultrapure water, obtained from a Millipore Milli-Q system (resistivity $\geq 18.2 M\Omega cm$), was used for the preparation of all solutions.

2.2 Preparation of GDE

The catalytic mass (PL6C and PL6C/BTDA 2.0%) was prepared based on a previous technique proposed by our research group [49]. Briefly, ultrapure water was added to PL6C (or PL6C/BTDA 2%) and mixed until a homogeneous mass was obtained. After that, PTFE was added to the catalytic mass in a proportion of 20% relative to the total mass. For the preparation of the GDE, the previously prepared mass was dried at 120 °C; after that, an amount of 8 g of the mass was homogeneously dispersed in a circular-shaped metal mold (20 cm²) and subjected to a hot-pressing procedure through the application of 7.5 tons and fixed temperature of 220 °C for 2 h.

2.3 Using the modified GDE for H_2O_2 electrogeneration

To evaluate the effect of the current density (10, 25 and 50 mA cm⁻²) on H_2O_2 electrogeneration, experiments were performed in a glassy electrochemical cell equipped with Ag/AgCl ($KCl 3 mol L^{-1}$) - employed as reference electrode, a platinum-coated titanium foil (~60 cm²) - used as counter electrode, a GDE (20 cm²; placed at the bottom of the cell) - used as working electrode. For comparison purposes, control experiments were performed using

unmodified GDE/PL6C. O₂ gas was injected directly into the GDE at flow rate of 0.05 L min⁻¹ during the experiments. H₂O₂ was electrogenerated in 250 mL of KOH 0.1 mol L⁻¹ electrolyte (pH 13.0) and quantified spectrophotometrically by the molybdate method [47]. All the experiments were performed for 90 min under mechanical stirring and at constant temperature of 20 °C. A bi-potentiostat Metrohm Autolab PGSTAT-302N coupled to a high current unit of BSTR-10A was used to conduct the experiments.

2.4 Degradation experiments

Degradation assays were carried out under the same conditions applied for the H₂O₂ electrogeneration experiments; *i.e.*, using the same electrochemical cell (including the electrodes) and the same temperature and supporting electrolyte concentration. The degradation of CIP (75 μmol L⁻¹) was evaluated using the following treatment processes: anodic oxidation using GDE under N₂ flow (AO; only the electrochemical effect); anodic oxidation using GDE under O₂ flow (AO/e-H₂O₂; electrochemical and e-H₂O₂ effects); photolysis (UVC; 9 W); and e-H₂O₂ coupled with UVC (AO/e-H₂O₂/UVC). The experiments were conducted based on the application of the GDE at current density of 25 mA cm⁻²; this was the optimal current density found in the H₂O₂ electrogeneration experiments.

2.5 Analytical procedures

The evolution of CIP concentration was monitored by high-performance liquid chromatography (Shimadzu Prominence HPLC model LC-20AT) with a UV-DAD detector using Luna C18 column (Phenomenex[®]: 250 mm × 4.6 mm, 5 μm particle size) as the stationary phase and a mixture of 0.15 mmol L⁻¹ formic acid and acetonitrile (ACN - proportion 50:50) as the mobile phase, in isocratic elution mode (at 0.8 mL min⁻¹) [50]. The detection of CIP was performed at 280 nm using an injection volume of 20 μL and temperature of 40 °C. The relative percentage decay of CIP was calculated based on the following: $[CIP]/[CIP]_0 \times 100\%$, where [CIP] and [CIP]₀ are the values at a determined period of time and at the beginning of the experiment, respectively. Prior to performing the analyses, the collected samples were filtered using a 0.45 μm Chromafil[®] Xtra PET filter (Macherey-Nagel) coupled to a syringe.

Short-chain carboxylic acids and inorganic ions were identified by ion chromatography using Metrohm 850 PRO IC coupled to a 940IC Extention Module Vario, with a conductivity detector. The anions (fluorine, nitrite and nitrate) were measured using Metrosep A Supp 5 (150 mm/4.0 mm), where the eluent consisted of Na₂CO₃ (3.2 mmol L⁻¹) and NaHCO₃ (1 mmol L⁻¹) applied at a flow rate of 0.7 mL min⁻¹ with temperature of 25 °C. The ammonium cation was

identified using Metrosep C 4 (150 mm/4.0 mm), where the eluent consisted of nitric acid (1.7 mmol L⁻¹) and dipicolinic acid (0.7 mmol L⁻¹) applied at a flow rate of 0.9 mL min⁻¹ with temperature of 25 °C. Carboxylic acids (oxalic and formic acid) were measured using Metrosep A Supp 5, with H₂SO₄(0.5 mmol L⁻¹) as the eluent.

CIP degradation by-products were identified by liquid chromatography electrospray ionization-tandem mass spectrometry (LC-ESI-MS/MS); these analyses were performed using Prominence LC 20 AT modular liquid chromatograph coupled to LC/MS-8030 triple quadrupole mass spectrometer (acquired from Shimadzu, Kyoto, Japan). Separation was performed using a Shim-pack GIST C18 column (150 mm×4.6 mm, 5 μm) (from Shimadzu, Kyoto, Japan), with a mobile phase composed of water acidified with 0.1 % formic acid (solvent A) and acetonitrile (solvent B), applied at a flow rate of 0.8 mL min⁻¹. The elution mode employed was linear gradient in the following conditions: 0-5 min: 10-37%; 5-8 min: 37-100% and 8-10 min: 100-10%. The mass spectrometry screening analysis was performed using positive electrospray ionization in full scan mode in the range of m/z 50–500. The desolvation and ion source block temperatures applied were 250°C and 400°C, respectively. Nitrogen was used as a nebulizer (3 L min⁻¹) and as desolvation gas (15 L min⁻¹).

Results and discussion

4.1 H₂O₂ electrogeneration using PL6C/GDE and PL6C/GDE-2%BTDA

Experiments were conducted using the unmodified PL6C/GDE and modified PL6C/GDE-2%BTDA at current densities of 10, 25 and 50 mA cm⁻² in order to evaluate the efficiency of these electrodes in terms of H₂O₂ electrogeneration in alkaline medium. Fig. 1a shows the concentration of H₂O₂ electrogenerated based on the application of the modified and unmodified GDEs at the aforementioned current densities as a function of time. As can be observed in Fig. 1a, the PL6C/GDE electrocatalyst recorded an improvement in H₂O₂ production when the current density was increased from 10 to 25 mA cm⁻²; however, an increase in current density from 25 mA cm⁻² to 50 mA cm⁻² did not lead to a significant change in H₂O₂ concentration - the electrogenerated H₂O₂ concentration values were similar to those observed at 25 mA cm⁻² over the duration of the electrolysis (the catalyst recorded maximum H₂O₂ concentration of 155.4 mg L⁻¹). Fig. 2b shows the results obtained from the application of the PL6C/GDE-2%BTDA electrocatalyst; as can be noted, the catalyst recorded an increase in e-H₂O₂ with the increase of the current density from 10 to 25 mA cm⁻² (with 275.8 mg L⁻¹ of H₂O₂ electrogenerated); interestingly though, the application of the electrocatalyst at 50 mA cm⁻² led to a decrease in H₂O₂ electrogeneration (compared to the amount generated at 25 mA

cm^{-2}) – the electrocatalyst recorded concentration values similar to those obtained at the current density of 10 mA cm^{-2} . After 30 min of electrolysis, both the modified and unmodified GDEs saw stabilization in H_2O_2 electrogeneration at the current densities employed. This behavior can be attributed to the chemical equilibrium established between the H_2O_2 formation reactions at the cathode and the H_2O_2 degradation reactions at the anode [39].

In alkaline solutions, H_2O_2 is mainly found in the form of hydroperoxyl anion (HO_2^-) [51], and these HO_2^- species can catalyze the decomposition of H_2O_2 , especially at pH values above 9 (Eq. 4). It should be noted however that when the electrolyte is subjected to continuous stirring in a single compartment cell, two other reactions may occur simultaneously – for instance, the oxidation of H_2O_2 to O_2 at the anode (Eq. 5) and the [51] reduction of H_2O_2 to H_2O at the cathode (Eq. 6) [25].

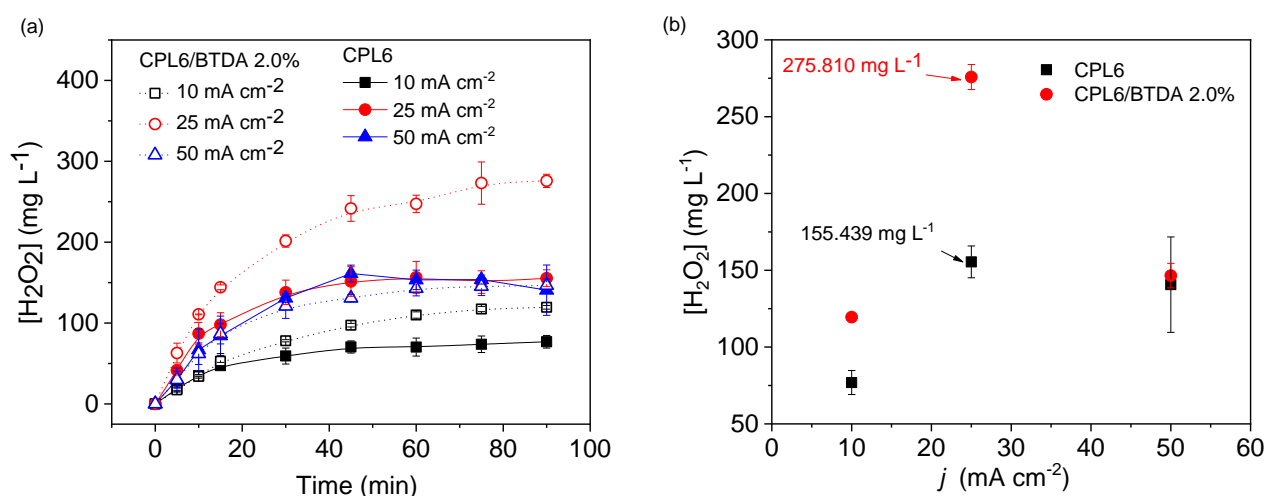


Fig. 1 – (a) H_2O_2 electrogeneration under different current densities ($j=10, 25$ and 50 mA cm^{-2}) as a function of time using PL6C/GDE and PL6C/GDE-2%BTDA. Conditions applied – electrolyte: 0.1 mol L^{-1} of KOH at pH 13; temperature: $25 \text{ }^\circ\text{C}$ (b). Final concentrations of H_2O_2 after 90 min of electrolysis for PL6C/GDE and PL6C/GDE-2%BTDA (b).

Fig. 1b shows that the highest concentration of H_2O_2 was obtained at 25 mA cm^{-2} for both electrodes at the end of each electrolysis (90 min); however, the incorporation of BTDA modifier in PL6C/GDE promoted greater selectivity of the electrocatalyst toward H_2O_2 generation reaction. Previous studies reported in the literature have already pointed out the

remarkable efficiency of organic modifiers applied in GDE in terms of catalyzing H_2O_2 generation reaction. Moreira *et al.* showed that the modification of PL6C with Sudan Red 7B organic compound can enhance H_2O_2 electrogeneration through a combination of chemical and electrochemical mechanisms [39]. According to these authors, the presence of functional groups, such as quinones, on the PL6C surface facilitates ORR reaction; in addition, the $-\text{N}=\text{N}$ groups from Sudan Red 7B can be reduced and oxidized in the presence of O_2 , leading to the generation of H_2O_2 [39]. Rocha *et al.* investigated the effects of modifying carbon-based materials with three distinct organic modifying agents containing quinone groups - Alizarin Red S, acenaphthoquinone and menadione, in terms of H_2O_2 electrogeneration [41]; in this work, the authors initially associated the ORR mechanism with the electrochemical reduction of organic compounds to hydroquinone form and their subsequent oxidation to quinone. Their findings showed that the chemical oxidation of hydroquinone by O_2 in solution led to the concomitant generation of H_2O_2 [41].

Considering the molecular structure of BTDA, with the presence of quinone groups in its composition, the process of generating H_2O_2 in the modified electrode can also occur via electrochemical and chemical mechanisms. Under this process, O_2 reduction reaction occurs on the polarized carbon surface (electrochemical mechanism) and the reduction of the BTDA molecule occurs under electrode polarization. Subsequently, the oxidation of BTDA occurs through the reduction of O_2 to H_2O_2 (chemical mechanism). Oxidation and reduction equilibrium of the modifier is then formed through the electrode polarization, catalyzing the ORR process. The commercial production of H_2O_2 occurs via a similar mechanism, with the autooxidation of anthraquinone (AQ) to alkylanthrahydroquinone (AHQ), in the presence of a catalyst (palladium) in organic medium. AHQ is then separated from the catalyst and further oxidized by O_2 (g), regenerating the initial AQ, and producing H_2O_2 [52,53]. Thus, the BTDA modifier acts like AQ, since the production of H_2O_2 occurs due to the oxidation/reduction of BTDA.

In our present study, the concentration of H_2O_2 generated in both the PL6C/GDE and PL6C/GDE-2%BTDA exhibited a linear pattern during the first 20 min of electrolysis. Thus, the kinetic rate constant in terms of H_2O_2 electrogeneration ($k_{\text{H}_2\text{O}_2}$) was calculated for the two electrodes. As the concentrations of O_2 and H_2O remain constant during the electrolysis, the process of H_2O_2 electrogeneration can be said to follow a pseudo-zero-order kinetics; here, the values of $k_{\text{H}_2\text{O}_2}$ are derived from the slope of the line, where $C_{\text{H}_2\text{O}_2(t)}$ is the concentration of H_2O_2 at time t – see Eq. 7 below [[54,55]].

$$C_{H_2O_2(t)} = -k_{H_2O_2} t \quad (7)$$

Fig. 2 shows that at current densities of 10 and 50 mA cm⁻², the kinetic constants of H₂O₂ formation are slightly higher and lower for the PL6C/GDE-2%BTDA electrode compared to the PL6C/GDE, respectively. However, at 25 mA cm⁻², the kinetic constant of PL6C/GDE-2%BTDA is 1.46-fold higher than the value obtained for PL6C/GDE; this result shows that the modifier can accelerate H₂O₂ generation.

The kinetic constant value for the modified GDE is found to be satisfactory compared to the values reported in the literature; for instance, Moreira et al. (2019) showed that the application of PL6C modified with an organic modifier (Quinones) at the current density of 25 mA cm⁻² resulted in $k_{H_2O_2}$ close to 5.0 mg L⁻¹ min⁻¹ [39]. Based on the application of 1,4-naphthoquinone-modified carbon-based GDE at current density of 25 mA cm⁻², Kronka et al. (2020) obtained $k_{H_2O_2}$ value of 1.514 mg L⁻¹ min⁻¹, which was also found to be lower than the value reported in this present work [42].

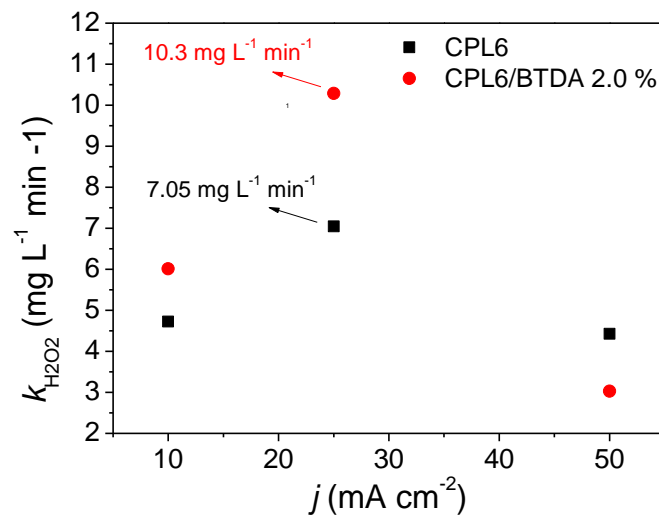


Fig. 2 – Apparent rate constant for H₂O₂ electrogenerated ($k_{H_2O_2}$) as a function of applied current density in 20 min of electrolysis using PL6C/GDE and PL6C/GDE-2%BTDA. Conditions applied - electrolyte: 0.1 mol L⁻¹ of KOH, pH 13; temperature: 25 °C.

The current efficiency (C.E.) and energy consumption (E.C.) for the electrogeneration of H₂O₂ were also calculated for both electrodes; the results obtained are shown in Fig.3. The C.E. for each electrolysis was calculated using Eq. 8 below [[39]]:

$$\text{C.E. (\%)} = \frac{m_{H_2O_2}}{m_{H_2O_2, \text{theoretical}}} \times 100\% = \frac{m_{H_2O_2}}{I \times t \times 34 / 2F} \times 100\% \quad (8)$$

where $m_{\text{H}_2\text{O}_2}$ is the mass of H_2O_2 (90 min of electrolysis) in g, I is the applied current in A, t is the electrolysis time in seconds, 2 is the stoichiometric number of electrons transferred in the process, and F is the Faraday constant (96486 C mol^{-1}).

As can be observed in Fig.3a, the current densities of 10 and 25 mA cm^{-2} recorded the highest C.E. values; overall, an increase in current density led to a decrease in C.E for both PL6C/GDE and PL6C/GDE-2%BTDA. The decrease observed in C.E. after an increase in applied current density may be related to the formation of other molecules instead of H_2O_2 (parallel reactions). The highest C.E. was obtained from the application of the GDE modified with BTDA at 25 mA cm^{-2} ; this value was found to be the optimal current density since it yielded the best result in terms of the concentration of electrogenerated H_2O_2 (275.8 mg L^{-1} of H_2O_2) and current efficiency (14.4%).

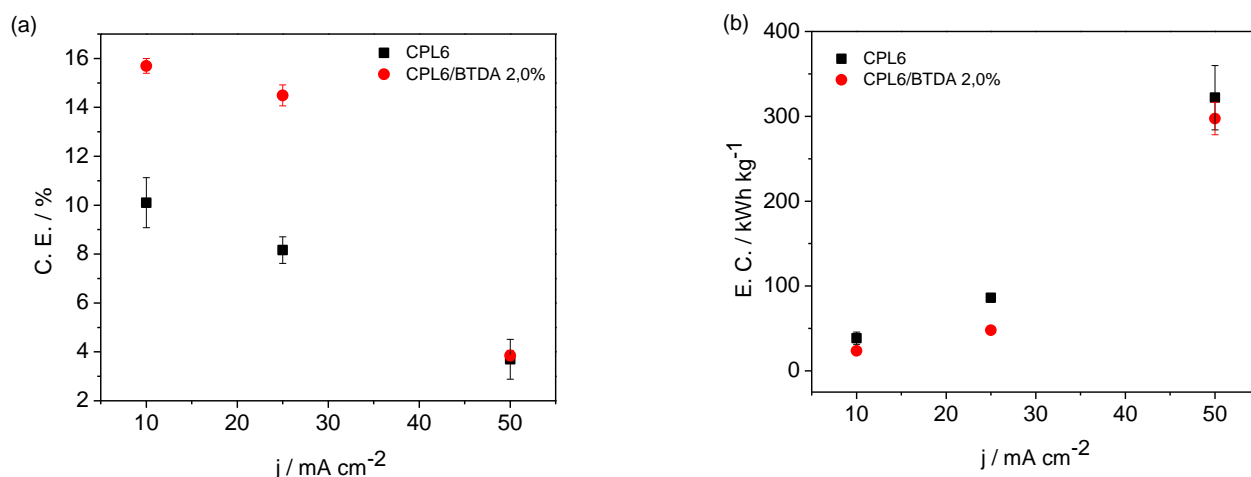


Fig. 3 – (a) Current efficiency (C.E.) and (b) energy consumption (E.C.) obtained from the application of PL6C/GDE and PL6C/GDE-2%BTDA as a function of applied current density. Conditions applied - electrolyte: 0.1 mol L^{-1} of KOH, pH 13; temperature: $25 \text{ }^\circ\text{C}$.

The energy consumption (E.C., kWh kg^{-1}) of the H_2O_2 electrogeneration process was calculated based on Eq. 9 below, where I is the current in A, E_{cell} is the electrochemical cell potential in V, t is the electrolysis time in hours, and m is the mass of H_2O_2 in kg [56].

$$\text{E.C. (kWh kg}^{-1}\text{)} = \frac{E_{\text{cell}} \times I \times t}{m_{\text{H}_2\text{O}_2}} \quad (9)$$

As can be observed in Fig. 3b, both PL6C/GDE and PL6C/GDE-2%BTDA recorded an increase in energy consumption when the applied current density was increased from 10 to 50 mA cm^{-2} . The PL6C/GDE ($321.95 \text{ kWh kg}^{-1}$) and PL6C/GDE-2%BTDA ($297.37 \text{ kWh kg}^{-1}$)

electrocatalysts recorded higher energy consumption values when applied at the current density of 50 mA cm^{-2} . At the current densities of 10 and 25 mA cm^{-2} , PL6C/GDE-2%BTDA recorded energy consumption values of 23.59 and $47.85 \text{ kWh kg}^{-1}$ respectively, while PL6C/GDE recorded energy consumption values of $38.59 \text{ kWh kg}^{-1}$ (10 mA cm^{-2}) and $86.03 \text{ kWh kg}^{-1}$ (25 mA cm^{-2}). Although the E.C. of the PL6C/GDE-2%BTDA at 25 mA cm^{-2} was twice the value obtained at 10 mA cm^{-2} , the highest concentrations of H_2O_2 (about 2.3-fold the value of H_2O_2 generated at 10 mA cm^{-2}) were obtained at the current density of 25 mA cm^{-2} (275.8 mg L^{-1}). It is also worth noting that the E.C. values obtained from the application of the PL6C/GDE-2%BTDA at different current densities were lower compared to the values obtained for the unmodified PL6C/GDE; this result points to the low energy consumption and good efficiency of the BTDA organic modifier when applied as a modifying agent in H_2O_2 generation.

Although the application of the PPL6C/GDE-2%BTDA electrocatalyst under optimal conditions in alkaline medium yielded lower H_2O_2 concentrations compared to the values reported in other works published in the literature involving the use of carbon-based GDE [33,57,58], the current density applied for H_2O_2 electrogeneration in the PPL6C/GDE-2%BTDA electrocatalyst was relatively lower (compared to the current density applied in other works), and this led to the consumption of relatively lower energy. Previous studies reported in the literature have shown that one can completely degrade organic pollutants by the application of current densities between 20 and 50 mA cm^{-2} and H_2O_2 concentrations between 100 - 500 mg L^{-1} [59–61]. An excess of H_2O_2 in solution can lead to parasitic reactions - such as the recombination of oxidant radicals formed during electrolysis, which decreases the efficiency of the process involving the electrochemical treatment of organic compounds.

The findings of our present study showed that the PL6C/GDE-2%BTDA exhibited the best results in terms of H_2O_2 electrogeneration (275.8 mg L^{-1}) when applied at the current density of 25 mA cm^{-2} ; this modified electrode (PL6C/GDE-2%BTDA) recorded kinetic constant 1.46-fold higher than the value obtained for the PL6C/GDE (unmodified electrode), current efficiency of 14.4% and energy consumption of $47.85 \text{ kWh kg}^{-1}$ - half the value obtained for the unmodified electrode.

The results obtained in this study point to the successful development and application of the PL6C/GDE-2.0% BTDA for H_2O_2 electrogeneration and ciprofloxacin degradation. BTDA has clearly proven to be a highly promising modifying agent for application in commercial scale. It is worth noting that similar studies reported in the literature (based on lab-scale reactor), including the works of Yu et al. (2014), Reis et al. (2012), and Wang et al. (2021),

were conducted using GDE with carbon base without modification. The modification of carbon-based GDE with organic BTDA can effectively lead to further improvements in the efficiency of the process, making it economically more advantageous for industrial application [22,27,62]. Considering the excellent results obtained for the PL6C/GDE-2%BTDA in terms of H_2O_2 production, this electrode was applied for the degradation of the recalcitrant organic compound CIP.

4.2 Degradation of CIP using different processes

The CIP degradation experiments were conducted using the PL6C/GDE-2%BTDA. Fig. 4 shows the relative percentage removal of CIP as a function of time under the different processes investigated.

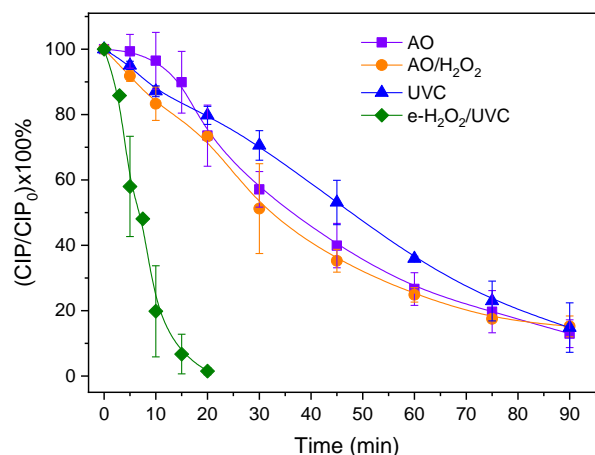


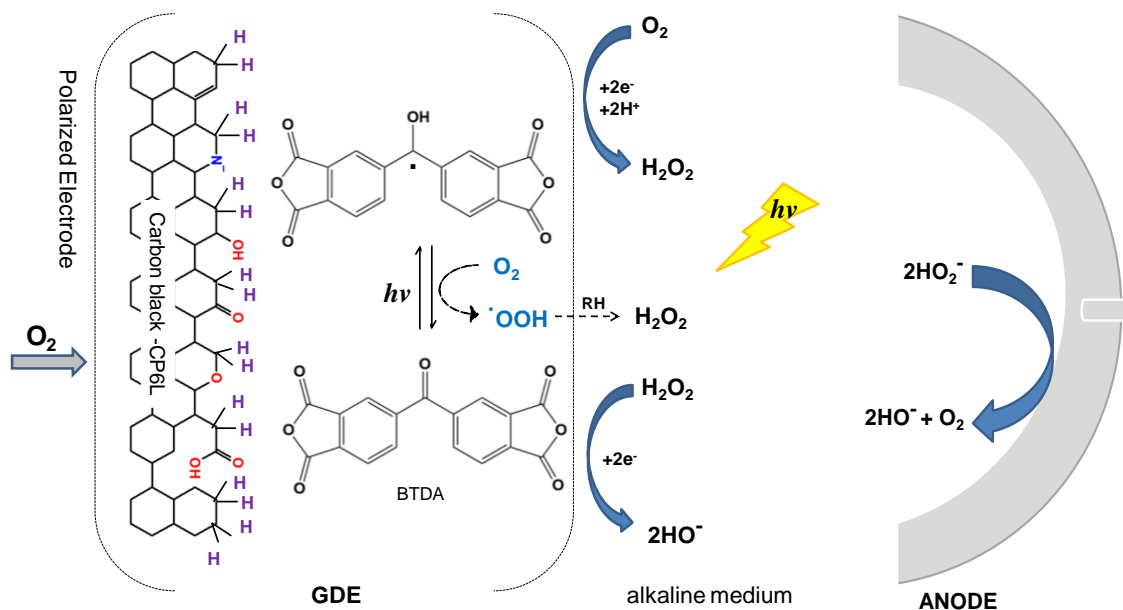
Fig. 4 – Relative percentage of CIP removed over time based on the application of different treatment processes. Conditions applied – current density: 25 mA cm^{-2} ; cathode: PL6C/GDE-2%BTDA; anode: Pt; irradiation: 9 W UVC lamp; supporting electrolyte: 0.1 mol L^{-1} of KOH at pH 13; temperature: $25 \text{ }^\circ\text{C}$.

As can be noted, a similar CIP degradation profile was observed when the following treatment processes were employed: AO, AO/ $\text{e-H}_2\text{O}_2$, and UVC processes; under these treatment processes, a significant CIP removal ($\sim 80\%$) was obtained in 90 min of treatment. With regard to the AO and AO/ $\text{e-H}_2\text{O}_2$ processes, the degradation of the CIP molecule can be attributed almost entirely to the anodic oxidation on the electrode surface; *i.e.*, the H_2O_2 electrogenerated (when O_2 flow was used) does not seem to have any positive effect on CIP degradation. This finding is in line with previous studies reported in the literature. Lima *et al.* also found no significant differences in CIP degradation profiles ($[\text{CIP}]_0 = 30 \text{ mg L}^{-1}$) when

they employed platinized titanium and GDE as anode and cathode, respectively, for CIP degradation under the AO and AO/e-H₂O₂ treatment processes [24]. With regard to the UVC process, the percentage of photodegradation obtained stems from the capacity of the CIP to absorb UV photons that are capable of inducing electronic transition states in the molecule, which eventually result in the decomposition of the excited molecules to produce mainly quinolone moieties and the deformation of the piperazine ring [63]. Although a high percentage of CIP degradation is obtained from the application of these treatment techniques, a significant amount of recalcitrant by-products can be generated during the processes and these by-products remain in solution at concentrations that pose enormous environmental risks.

As shown in Fig. 4, the combined application of e-H₂O₂ with UVC light (AO/e-H₂O₂/UVC process) led to significant improvements in the oxidation of the CIP molecule; this hybrid treatment process led to complete removal of CIP in only 20 min of treatment. The improvement observed in this hybrid treatment process is largely attributed to the action of the [•]OH species which were derived from the activation of e-H₂O₂ under UVC irradiation; these species attack the CIP molecule and its oxidation intermediates.

Studies reported in the literature show that benzophenones, such as BTDA, are classes of molecules that exhibit photosensitivity. Under UV light irradiation ($\lambda = 200\text{-}400\text{ nm}$), benzophenone can undergo transformation into an excited state, taking away a hydrogen atom from suitable donors, such as alcohol and amines – present in the carbon matrix (PL6C) in this case, and forming benzophenone ketyl radicals [46,64]. When exposed to O₂, BTDA radicals can be rapidly oxidized, forming H₂O₂, and this leads to the concomitant production of H₂O₂ [65,66]. Scheme 1 shows the mechanism involving the activation of the BTDA modifier and the generation of H₂O₂ under UV light. In addition to the electrochemical generation of H₂O₂ in the PL6/GDE-2%BTDA, the incidence of light can also contribute to the generation of H₂O₂ in solution through the photoactivation of the BTDA modifier. Thus, the combined AO/e-H₂O₂/UVC process can form more hydroxyl radicals, making the CIP antibiotic degradation process more efficient.



Scheme 1 – Formation of H₂O₂ in the presence of PL6C/2%BTDA under UV irradiation in alkaline solution during CIP electrolysis.

In *in situ* wastewater treatment, there is usually an adjustment of the pH to acid values for the application of Fenton-type processes. The simultaneous formation of H₂O₂ and OH⁻ in alkaline condition is found to affect the amount of oxidant electrogenerated compared to the isolated production of H₂O₂ in acidic condition [67]. However, the electrogeneration of H₂O₂ by GDE in alkaline solutions has the great advantage of generating the stabilizing agent *in situ* in the same reaction process. This advantage allows the application of this process for the treatment of effluents with high alkalinity; in fact, some industries, such as the textile and pulp and paper industry, produce wastewater with such alkaline characteristics, and this technology can be applied for the treatment of these industrial effluents under the proposed conditions [19,68]. The pulp and paper industry has combined H₂O₂ electrogeneration with NaOH solution for the treatment of industrial effluents produced by the industry [51,69]. The high rates of CIP degradation obtained in this work points to the great advantage of using the PL6C/GDE-2%BTDA in the electrogeneration of H₂O₂ and its highly promising application potential for the treatment of alkaline wastewater.

Table 1 presents the values of the pseudo-first-order kinetic constants (k_{1st}) calculated for the CIP degradation under the different treatment processes investigated. As expected from the degradation profiles, the AO, AO/e-H₂O₂ and UVC processes recorded similar k_{1st} values ($\sim 2 \times 10^{-2} \text{ min}^{-1}$). With regard to the AO/e-H₂O₂/UVC process, the rate constant obtained ($20.3 \pm 7.3 \times 10^{-2} \text{ min}^{-1}$) was at least 8 times higher than the values obtained under the application

of each separate process. Compared to the value obtained in our present study, Ou *et al.* obtained a relatively lower k_{1st} value ($6.7 \times 10^{-2} \text{ min}^{-1}$) corresponding to CIP ($30 \mu\text{mol L}^{-1}$) degradation based on the application of the $\text{H}_2\text{O}_2/\text{UVC}$ process (H_2O_2 was added at the beginning of the experiment) [63]. The difference observed in the k_{1st} values can be attributed to the continuous electrogeneration of H_2O_2 in the GDE, which leaves the oxidant promptly available to be activated at any time during the experiment.

Table 1 – Pseudo-first order kinetic constant (k_{1st}) values for CIP removal.

Process	$k_{1st}^*/10^{-2} \text{ min}^{-1}$	R^2
AO	2.41 ± 0.36	0.99 ± 0.001
AO/e- H_2O_2	2.21 ± 0.14	0.99 ± 0.004
UVC	2.75 ± 0.79	0.99 ± 0.008
AO/e- $\text{H}_2\text{O}_2/\text{UVC}$	20.3 ± 7.3	0.97 ± 0.070

*mean values obtained after two repetitions.

To gain a better understanding of the ability/viability of the treatment processes for CIP oxidation, a comparative analysis (of the processes) was performed in terms of electrical energy per order (E/EO) using Eq. 10 below [70]:

$$\text{E/EO (kWh m}^{-3}\text{order}^{-1}) = \frac{6.39 \times 10^{-4} (E_{\text{cell}} + P_{\text{lamp}})}{V \times k_{1st}} \quad (10)$$

where 6.39×10^{-4} is a conversion factor ($1 \text{ h}/3600 \text{ s}/0.4343$), E_{cell} is the average power of the electrochemical cell in V, P_{lamp} is the nominal power of the UVC lamp in W, k_{1st} is the pseudo-first order rate constant in s^{-1} , and V is the working volume in m^3 .

As can be observed in Fig. 5, no significant differences were observed between the AO, AO/e- H_2O_2 and UVC processes in terms of E/EO; these processes recorded electrical energy consumption higher than 15 kWh m^{-3} per order of CIP removed. Once again, the AO/e- $\text{H}_2\text{O}_2/\text{UVC}$ process exhibited the lowest E/EO value ($2.1 \text{ kW h m}^{-3} \text{ order}^{-1}$) –which was one order of magnitude lower than the E/EO values recorded by the other processes investigated in this study. Wang *et al.* obtained E/EO value of $31.6 \text{ kW h m}^{-3} \text{ order}^{-1}$ for the oxidation of CIP ($\sim 300 \mu\text{mol L}^{-1}$) based on the application of $\text{SnO}_2\text{-Sb/Ti}$ anode at 30 mA cm^{-2} [67]. Carneiro *et al.* also investigated the electrical energy consumption for the elimination of CIP ($\sim 300 \mu\text{mol L}^{-1}$) based on the application of BDD anode (10 mA cm^{-2}) and different supporting electrolytes (Na_2SO_4 , NaCl , Na_2CO_3 , among others); in all the conditions investigated, the authors reported E/EO values ranging from 0.7 to $9.5 \text{ kW h m}^{-3} \text{ order}^{-1}$ [72]. Clearly, E/EO values depend on

several variables; these variables include applied electric current density, hydrodynamic conditions, initial concentration of the contaminant, supporting electrolyte, among others.

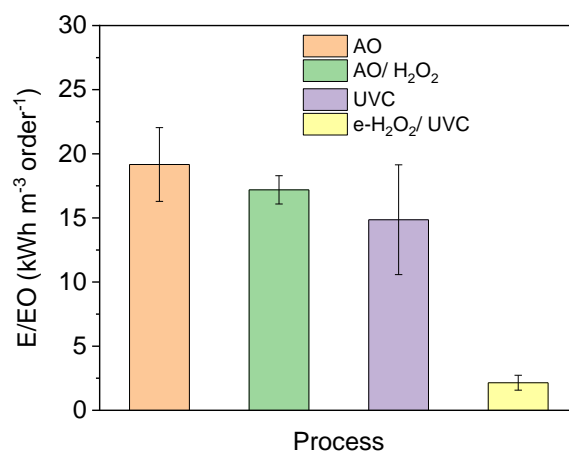


Fig. 5 – Electrical energy consumed in order to reduce the concentration of CIP by one order of magnitude under the application of different advanced oxidation processes. Conditions applied – current density: 25 mA cm⁻²; cathode: PL6C/GDE-2%BTDA; anode: titanium covered with Pt; irradiation: 9 W UVC lamp; supporting electrolyte: 0.1 mol L⁻¹ of KOH at pH 13; temperature: 25 °C.

4.3 Pathway of CIP Degradation

Prior to the application of the AO/e-H₂O₂/UVC process (*i.e.*, 0 min), the solution containing CIP was analyzed by LC-ESI-MS/MS. In this case, the antibiotic was detected in the retention time of 2.5 min where it presented molecular ion [M+H]⁺ = 332, adult ion [M+CH₃CN+H]⁺ = 373, and the following fragments (*m/z*): 140, 100, 83 and 59 Da. The adult ion ACN/proton, characteristic of this molecule, has already been reported in other studies published in the literature [73].

The results obtained from the LC-ESI-MS/MS analysis of the aliquots collected in 360 min of the AO/e-H₂O₂/UVC treatment process pointed to a progressive degradation of CIP and the formation of ten different aromatic by-products (see Fig. SM1 in the supplementary material). All the degradation products were detected within the first few minutes of treatment (Fig.SM1); this shows that CIP degradation occurs simultaneously via different routes. The polar and intermediate polarity degradation products (1-6) were completely degraded in 60 min

(Fig. SM1b), while the compounds with hydrophobic character proved to be persistent under the conditions employed and were unable to be completely degraded under the conditions employed (Fig. SM1c).

Table SM1, in the supplementary material, shows the corresponding retention times and molecular ions of the ten by-products identified. Parts of the degradation products (1, 3, 5 and 7) were identified based on the ion values characteristically obtained by LC-MS ($m/z = 306$; $m/z 263$; $m/z 320$ and $m/z 304$, respectively) and previously reported in studies involving CIP degradation via the application of other advanced oxidation processes [10,73–75]. The identification of the other seven by-products was performed based on the molecular ion and fragment values obtained from the LC-ESI-MS/MS analysis.

The structure of the by-products identified shows that the degradation process occurs mainly through the attack of $\cdot\text{OH}$ on the heterocyclic rings of the CIP molecule (Fig.6). In the case of by-products 1-6, 9 and 10, the attack occurs on the nitrogen of the piperazinyl ring, which leads to the breakage of the carbon-nitrogen bond, causing partial (1, 4-6, 9) or complete (2, 3, 10) elimination of this ring. With regard to compounds 4 and 6, the ring cleavage is followed by the addition of a hydroxyl group.

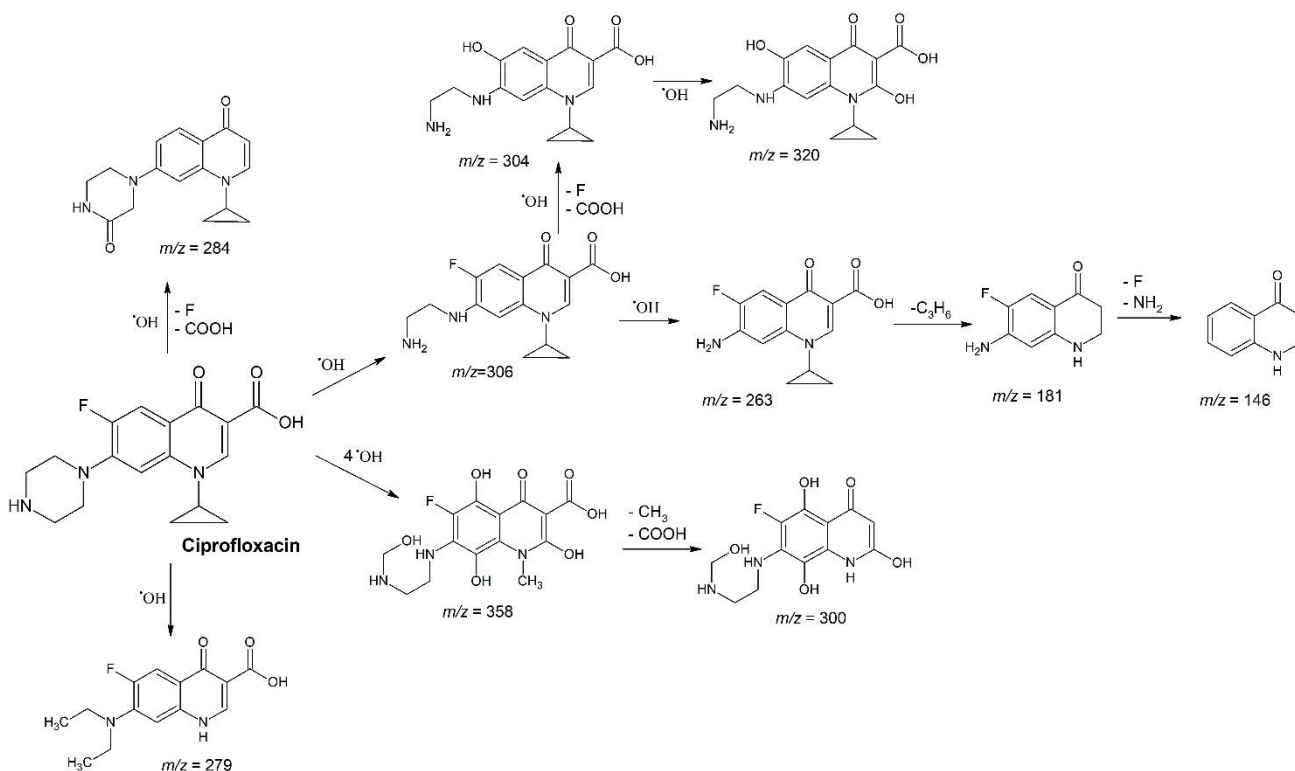


Fig. 6 – Proposed pathway of CIP degradation based on the application of the $e\text{-H}_2\text{O}_2/\text{UVC}$ process.

The $\cdot\text{OH}$ attack also occurs on the carbon of the piperazinyl ring, leading to its oxidation (by-product 8), and on the quinolone ring with the addition of hydroxyl groups (by-products 4-6). The breakage of the carbon-cyclopropyl bond is also the result of the primary attack of $\cdot\text{OH}$, as can be seen in by-products 2, 4, 6, 9 and 10.

Due to the high carbon-fluorine bond energy, the bond in the CIP molecule is difficult to break; however, the high oxidation-reduction potential of the $\cdot\text{OH}$ species ($E^\circ = 2.7 \text{ V}$) allows the species to attack and break this bond. In this study, the defluorination of the CIP molecule was observed in seven by-products (1, 3, 5, 8-10) and the carbon-fluorine bond in compound 5 was broken and substituted by hydroxyl. The by-product formation pathway also includes the loss of acid moiety from the carboxylate group of the quinolone ring (compounds 2, 6-8, 10), which leads to the generation of short chain carboxylic acids [76,77].

4.4 Short-chain carboxylic acids and inorganic ions formation

To gain a better understanding of the pathways in which CIP follows during the degradation process under the AO/e- H_2O_2 /UVC treatment process, ion chromatography was used to monitor the evolution of short-chain carboxylic acids and inorganic ions generated during the exhaustive experiment (360 min duration) (Fig. 7a). The results obtained from this analysis showed that the short-chain carboxylic acids detected during the degradation of CIP ($75 \mu\text{mol L}^{-1}$) were oxalic acid ($t_r = 18 \text{ min}$) and formic acid ($t_r = 3.6 \text{ min}$); these acids were found in quantities lower than 0.07 mg L^{-1} . As reported in previous studies, these two acids (oxalic and formic acids) are derived from the oxidative cleavage of the benzene aromatic ring of CIP [4,72,78]. Taking into account that the CIP molecule is completely removed in the first 30 min of treatment, the detection of very low amounts of oxalic and formic acids in the treatment process may be correlated to the quick destruction of the molecule by the $\cdot\text{OH}$ species. Moreover, no increase was observed in the accumulated concentration of the two acids after 60 min of treatment; the concentration of the two acids remained constant up to the end of the 360 min treatment.

With regard to inorganic ions, the main inorganic ion species formed during the mineralization of CIP were fluoride (F^-) and nitrogenous species (NO_2^- , NO_3^- , NH_4^+) (Fig.7b). F^- was detected in the early stages of degradation and its concentration remained constant until the end of the treatment process; this shows that the CIP molecule was quickly defluorinated in the AO/e- H_2O_2 /UVC process. Other studies on CIP degradation have also observed that the substitution of fluoride species by the $\cdot\text{OH}$ in the fluoroquinolones leads to the loss of fluorine [18]. While organic nitrogen was mainly converted to NH_4^+ , lower concentrations of NO_3^- and

NO_2^- were detected during CIP degradation under the AO/e- H_2O_2 /UVC treatment process [71]. The predominance of NH_4^+ over other nitrogenated species is favored by the cleavage of the C-N bond in the presence of UVC light and, subsequently, by the attack of the $\cdot\text{OH}$ species [71,79].

The results obtained from the ion chromatography analysis also showed that the NH_4^+ species exhibited maximum concentration in 60 min of treatment and a gradual decline thereafter; this shows that part of the nitrogen gas was further reduced to N_2 , NH_3 or N_2O gases [80].

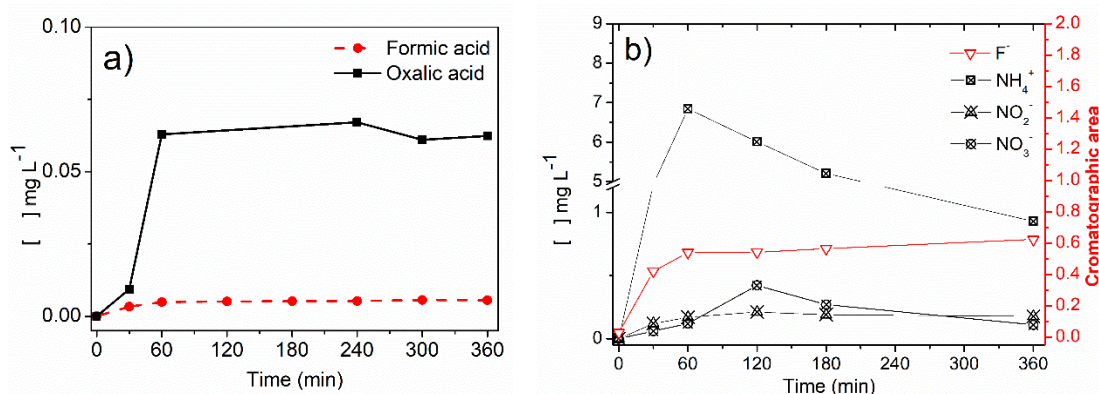


Fig. 7 – Evolution of short-chain carboxylic acids (a) and inorganic ions concentration (b) in 360 min treatment of CIP under the AO/e- H_2O_2 /UVC process. Conditions applied – current density: 25 mA cm^{-2} ; cathode: PL6C/GDE-2%BTDA; anode: titanium covered with Pt; irradiation: 9 W UVC lamp; supporting electrolyte: 0.1 mol L^{-1} of KOH at pH 13; temperature: $25 \text{ }^\circ\text{C}$.

Conclusions

The present study reported the successful development and application of PL6C/GDE modified with 2.0% BTDA for H_2O_2 electrogeneration and for the degradation of ciprofloxacin. Based on the results obtained, the following conclusions can be drawn:

- The application of the PL6C/GDE-2%BTDA at the current density of 25 mA cm^{-2} led to the production of maximum H_2O_2 concentration of $275.810 \text{ mg L}^{-1}$ in 90 min of electrolysis; this value represented an increase of 56.4% in the concentration of H_2O_2 generated compared to the value recorded for the unmodified PL6C/GDE applied under the same conditions.
- The PL6C/GDE-2%BTDA electrocatalyst recorded greater current efficiency, higher kinetic rate for H_2O_2 production, and lower energy consumption compared to the unmodified PL6C/GDE.

- Among the different EAOPs used to evaluate the efficiency of the PL6C/GDE-2%BTDA in terms of CIP degradation, the combined AO/e-H₂O₂/UVC process exhibited the best results. Under the AO/e-H₂O₂/UVC process, CIP was completely eliminated in only 20 minutes of treatment; this result may be linked to the formation of higher amounts of [•]OH species, derived from the electrochemical process, and the photo-activation of BTDA.
- Degradation by-products formed during the degradation of the CIP molecule were identified by HPLC and LC-MS/MS analyses. The detection of F⁻ ions and the formation of short-chain carboxylic acids pointed to the partial mineralization of CIP.

The results obtained in the present study point to the excellent performance of the PL6C/GDE-2.0%BTDA electrocatalyst in terms of H₂O₂ electrogeneration and its efficiency in the degradation of recalcitrant organic compounds in alkaline medium. These findings show that the proposed PL6C/GDE-2.0%BTDA electrocatalyst is a highly promising material which has great application potential for the treatment of alkaline water and wastewater.

Finally, future studies related to the practical application of organic modifier-based GDEs must focus on the following: (i) the use of flow reactors (which have not been widely explored with organic modifier-based GDEs); (ii) the application of long-term stability tests for organic modifier-based GDEs inside flow reactors; and (iii) the conduct of analysis in real samples (*e.g.*, complex aqueous matrices).

Acknowledgments

The authors gratefully acknowledge the financial support received from CNPq (grants no #465571/2014-0 and #303943/2021-1); FAPESP (grants #2014/50945-4, #2016/08760-2, #2019/08701-4, #2020/07351-7, #2020/02743-4 and #2017/10118-0) and CAPES-Finance Code 001.

Credit authorship contribution statement

Taynara O. Silva: Conceptualization, Methodology, Formal analysis, Writing - Original Draft. **Lorena A. Goulart:** Conceptualization, Methodology, Formal analysis, Writing - Original Draft. **Isaac Sánchez-Montes:** Conceptualization, Methodology, Formal analysis, Writing - Original Draft. **Géssica O. S. Santos:** Conceptualization, Methodology, Formal analysis, Writing - Original Draft. **Renato B. Santos:** Writing - Reviewing & Editing. **Renata Colombo:** Formal analysis, Writing - Review & Editing. **Marcos R. V. Lanza:** Conceptualization, Supervision, Writing - Reviewing & Editing, Funding acquisition.

References

- [1] T. Basile, A. Petrella, M. Petrella, G. Boghetich, V. Petruzzelli, S. Colasuonno, D. Petruzzelli, Review of endocrine-disrupting-compound removal technologies in water and wastewater treatment plants: An EU perspective, *Ind. Eng. Chem. Res.* 50 (2011) 8389–8401. <https://doi.org/10.1021/ie101919v>.
- [2] M.K. Kim, K.D. Zoh, Occurrence and removals of micropollutants in water environment, *Environ. Eng. Res.* 21 (2016) 319–332. <https://doi.org/10.4491/eer.2016.115>.
- [3] A. Gupta, A. Garg, Degradation of ciprofloxacin using Fenton's oxidation: Effect of operating parameters, identification of oxidized by-products and toxicity assessment, *Chemosphere.* 193 (2018) 1181–1188. <https://doi.org/10.1016/j.chemosphere.2017.11.046>.
- [4] V.S. Antonin, M.C. Santos, S. Garcia-Segura, E. Brillas, Electrochemical incineration of the antibiotic ciprofloxacin in sulfate medium and synthetic urine matrix, *Water Res.* 83 (2015) 31–41. <https://doi.org/10.1016/j.watres.2015.05.066>.
- [5] O. Golovko, A.L. Rehrl, S. Köhler, L. Ahrens, Organic micropollutants in water and sediment from Lake Mälaren, Sweden, *Chemosphere.* 258 (2020). <https://doi.org/10.1016/j.chemosphere.2020.127293>.
- [6] J. Bhagat, L. Zang, N. Nishimura, Y. Shimada, Zebrafish: An emerging model to study microplastic and nanoplastic toxicity, *Sci. Total Environ.* 728 (2020) 138707. <https://doi.org/10.1016/j.scitotenv.2020.138707>.
- [7] S. Shehu Imam, R. Adnan, N.H. Mohd Kaus, Photocatalytic degradation of ciprofloxacin in aqueous media: a short review, *Toxicol. Environ. Chem.* 100 (2018) 518–539. <https://doi.org/10.1080/02772248.2018.1545128>.
- [8] Q. Wu, Z. Li, H. Hong, R. Li, W.T. Jiang, Desorption of ciprofloxacin from clay mineral surfaces, *Water Res.* 47 (2013) 259–268. <https://doi.org/10.1016/j.watres.2012.10.010>.
- [9] D.G.J. Larsson, C. de Pedro, N. Paxeus, Effluent from drug manufactures contains extremely high levels of pharmaceuticals, *J. Hazard. Mater.* 148 (2007) 751–755. <https://doi.org/10.1016/j.jhazmat.2007.07.008>.
- [10] M.S. Yahya, N. Oturan, K. El Kacemi, M. El Karbane, C.T. Aravindakumar, M.A. Oturan, Oxidative degradation study on antimicrobial agent ciprofloxacin by electro-fenton process: Kinetics and oxidation products, *Chemosphere.* 117 (2014) 447–454. <https://doi.org/10.1016/j.chemosphere.2014.08.016>.
- [11] F.C. Moreira, R.A.R. Boaventura, E. Brillas, V.J.P. Vilar, Electrochemical advanced oxidation processes: A review on their application to synthetic and real wastewaters, *Appl. Catal. B Environ.* 202 (2017) 217–261. <https://doi.org/10.1016/j.apcatb.2016.08.037>.
- [12] S.O. Ganiyu, C.A. Martínez-Huitle, M.A. Oturan, Electrochemical advanced oxidation processes for wastewater treatment: Advances in formation and detection of reactive species and mechanisms, *Curr. Opin. Electrochem.* 27 (2021) 100678. <https://doi.org/10.1016/j.coelec.2020.100678>.
- [13] G. Boczkaj, A. Fernandes, Wastewater treatment by means of advanced oxidation processes at basic pH conditions: A review, *Chem. Eng. J.* 320 (2017) 608–633. <https://doi.org/10.1016/j.cej.2017.03.084>.

- [14] M.A. Oturan, J.J. Aaron, Advanced oxidation processes in water/wastewater treatment: Principles and applications. A review, *Crit. Rev. Environ. Sci. Technol.* 44 (2014) 2577–2641. <https://doi.org/10.1080/10643389.2013.829765>.
- [15] A. Sheikhmohammadi, E. Asgari, M. Manshouri, Enhancement the Phenylmethyl ester photo degradability in the presence of O₃ and H₂O₂, *Optik (Stuttg)*. 228 (2021) 166204. <https://doi.org/10.1016/j.ijleo.2020.166204>.
- [16] P. V. Nidheesh, M. Zhou, M.A. Oturan, An overview on the removal of synthetic dyes from water by electrochemical advanced oxidation processes, *Chemosphere*. 197 (2018) 210–227. <https://doi.org/10.1016/j.chemosphere.2017.12.195>.
- [17] J. Li, Y. Li, Z. Xiong, G. Yao, B. Lai, The electrochemical advanced oxidation processes coupling of oxidants for organic pollutants degradation: A mini-review, *Chinese Chem. Lett.* 30 (2019) 2139–2146. <https://doi.org/10.1016/j.ccllet.2019.04.057>.
- [18] M. Sayed, M. Ismail, S. Khan, S. Tabassum, H.M. Khan, Degradation of ciprofloxacin in water by advanced oxidation process: Kinetics study, influencing parameters and degradation pathways, *Environ. Technol. (United Kingdom)*. 37 (2016) 590–602. <https://doi.org/10.1080/09593330.2015.1075597>.
- [19] A. Asghar, A.A.A. Raman, W.M.A.W. Daud, Advanced oxidation processes for in-situ production of hydrogen peroxide/hydroxyl radical for textile wastewater treatment: A review, *J. Clean. Prod.* 87 (2015) 826–838. <https://doi.org/10.1016/j.jclepro.2014.09.010>.
- [20] A. Sheikhmohammadi, E. Asgari, H. Nourmoradi, M.M. Fazli, M. Yeganeh, Ultrasound-assisted decomposition of metronidazole by synthesized TiO₂/Fe₃O₄ nanocatalyst: Influencing factors and mechanisms, *J. Environ. Chem. Eng.* 9 (2021) 105844. <https://doi.org/10.1016/j.jece.2021.105844>.
- [21] L.A. Goulart, A. Moratalla, M.R.V. Lanza, C. Sáez, M.A. Rodrigo, Photoelectrocatalytic treatment of levofloxacin using Ti/MMO/ZnO electrode, *Chemosphere*. 284 (2021). <https://doi.org/10.1016/j.chemosphere.2021.131303>.
- [22] J. Wang, C. Li, M. Rauf, H. Luo, X. Sun, Y. Jiang, Gas diffusion electrodes for H₂O₂ production and their applications for electrochemical degradation of organic pollutants in water: A review, *Sci. Total Environ.* 759 (2021) 143459. <https://doi.org/10.1016/j.scitotenv.2020.143459>.
- [23] Y. Wang, R. Shi, L. Shang, L. Peng, D. Chu, Z. Han, G.I.N. Waterhouse, R. Zhang, T. Zhang, Vertical graphene array for efficient electrocatalytic reduction of oxygen to hydrogen peroxide, *Nano Energy*. 96 (2022) 107046. <https://doi.org/10.1016/j.nanoen.2022.107046>.
- [24] V.B. Lima, L.A. Goulart, R.S. Rocha, J.R. Steter, M.R.V. Lanza, Degradation of antibiotic ciprofloxacin by different AOP systems using electrochemically generated hydrogen peroxide, *Chemosphere*. 247 (2020) 125807. <https://doi.org/10.1016/j.chemosphere.2019.125807>.
- [25] X. Ge, A. Sumboja, D. Wu, T. An, B. Li, F.W.T. Goh, T.S.A. Hor, Y. Zong, Z. Liu, Oxygen Reduction in Alkaline Media: From Mechanisms to Recent Advances of Catalysts, *ACS Catal.* 5 (2015) 4643–4667. <https://doi.org/10.1021/acscatal.5b00524>.
- [26] and R.A.B. Benjamin G. Petri, 1 Richard J. Watts, 2 Amy L. Teel, 2 Scott G. Huling, 3, FUNDAMENTALS OF ISCO USING HYDROGEN PEROXIDE, 2011. https://doi.org/10.1007/978-1-4419-7826-4_5.

- [27] R.M. Reis, A.A.G.F. Beati, R.S. Rocha, M.H.M.T. Assumpção, M.C. Santos, R. Bertazzoli, M.R.V. Lanza, Use of gas diffusion electrode for the in situ generation of hydrogen peroxide in an electrochemical flow-by reactor, *Ind. Eng. Chem. Res.* 51 (2012) 649–654. <https://doi.org/10.1021/ie201317u>.
- [28] W. Zhou, X. Meng, J. Gao, A.N. Alshawabkeh, Hydrogen peroxide generation from O₂ electroreduction for environmental remediation: A state-of-the-art review, *Chemosphere*. 225 (2019) 588–607. <https://doi.org/10.1016/j.chemosphere.2019.03.042>.
- [29] W. Wang, M. He, W. Ouyang, C. Lin, X. Liu, Influence of atmospheric surface oxidation on the formation of H₂O₂ and ·OH at pyrite-water interface: Mechanism and kinetic model, *Chem. Geol.* 571 (2021) 120176. <https://doi.org/10.1016/j.chemgeo.2021.120176>.
- [30] G. Coria, T. Pérez, I. Sirés, E. Brillas, J.L. Nava, Abatement of the antibiotic levofloxacin in a solar photoelectro-Fenton flow plant: Modeling the dissolved organic carbon concentration-time relationship, *Chemosphere*. 198 (2018) 174–181. <https://doi.org/10.1016/j.chemosphere.2018.01.112>.
- [31] M.S. Kronka, P.J.M. Cordeiro-Junior, L. Mira, A.J. dos Santos, G. V. Fortunato, M.R.V. Lanza, Sustainable microwave-assisted hydrothermal synthesis of carbon-supported ZrO₂ nanoparticles for H₂O₂ electrogeneration, *Mater. Chem. Phys.* 267 (2021) 124575. <https://doi.org/10.1016/j.matchemphys.2021.124575>.
- [32] P.J.M. Cordeiro-Junior, A.S. Martins, G.B.S. Pereira, F.V. Rocha, M.A.R. Rodrigo, M.R. de V. Lanza, Bisphenol-S removal via photoelectro-fenton/H₂O₂ process using Co-porphyrin/Printex L6 gas diffusion electrode, *Sep. Purif. Technol.* 285 (2022). <https://doi.org/10.1016/j.seppur.2021.120299>.
- [33] R.B. Valim, L.C. Trevelin, D.C. Sperandio, J.F. Carneiro, M.C. Santos, L.A. Rodrigues, R.S. Rocha, M.R.V. Lanza, Using carbon black modified with Nb₂O₅ and RuO₂ for enhancing selectivity toward H₂O₂ electrogeneration, *J. Environ. Chem. Eng.* 9 (2021) 106787. <https://doi.org/10.1016/j.jece.2021.106787>.
- [34] W.R.P. Barros, Q. Wei, G. Zhang, S. Sun, M.R.V. Lanza, A.C. Tavares, Oxygen reduction to hydrogen peroxide on Fe₃O₄ nanoparticles supported on Printex carbon and Graphene, *Electrochim. Acta.* 162 (2015) 263–270. <https://doi.org/10.1016/j.electacta.2015.02.175>.
- [35] J.F. Carneiro, R.S. Rocha, P. Hammer, R. Bertazzoli, M.R.V. Lanza, Hydrogen peroxide electrogeneration in gas diffusion electrode nanostructured with Ta₂O₅, *Appl. Catal. A Gen.* 517 (2016) 161–167. <https://doi.org/10.1016/j.apcata.2016.03.013>.
- [36] J.F. Carneiro, L.C. Trevelin, A.S. Lima, G.N. Meloni, M. Bertotti, P. Hammer, R. Bertazzoli, M.R.V. Lanza, Synthesis and Characterization of ZrO₂/C as Electrocatalyst for Oxygen Reduction to H₂O₂, *Electrocatalysis*. 8 (2017) 189–195. <https://doi.org/10.1007/s12678-017-0355-0>.
- [37] A. Moraes, M.H.M.T. Assumpção, R. Papai, I. Gaubeur, R.S. Rocha, R.M. Reis, M.L. Calegari, M.R.V. Lanza, M.C. Santos, Use of a vanadium nanostructured material for hydrogen peroxide electrogeneration, *J. Electroanal. Chem.* 719 (2014) 127–132. <https://doi.org/10.1016/j.jelechem.2014.02.009>.
- [38] E. Barbosa, F. Bergamini, L.H. Marcolino-junior, A simple, fast, and cost-effective analytical method for monitoring active quinones in a H₂O₂ production process, 163

- (2021) 1–8. <https://doi.org/10.1016/j.microc.2020.105861>.
- [39] J. Moreira, V. Bocalon Lima, L. Athie Goulart, M.R.V. Lanza, Electrosynthesis of hydrogen peroxide using modified gas diffusion electrodes (MGDE) for environmental applications: Quinones and azo compounds employed as redox modifiers, *Appl. Catal. B Environ.* 248 (2019) 95–107. <https://doi.org/10.1016/j.apcatb.2019.01.071>.
- [40] Q. Chen, Development of an anthraquinone process for the production of hydrogen peroxide in a trickle bed reactor-From bench scale to industrial scale, *Chem. Eng. Process. Process Intensif.* 47 (2008) 787–792. <https://doi.org/10.1016/j.cep.2006.12.012>.
- [41] R.S. Rocha, R.B. Valim, L.C. Trevelin, J.R. Steter, J.F. Carneiro, J.C. Forti, R. Bertazzoli, M.R.V. Lanza, Electrocatalysis of Hydrogen Peroxide Generation Using Oxygen-Fed Gas Diffusion Electrodes Made of Carbon Black Modified with Quinone Compounds, *Electrocatalysis.* 11 (2020) 338–346. <https://doi.org/10.1007/s12678-020-00591-1>.
- [42] M.S. Kronka, F.L. Silva, A.S. Martins, M.O. Almeida, K.M. Honório, M.R.V. Lanza, Tailoring the ORR selectivity for H₂O₂ electrogeneration by modification of Printex L6 carbon with 1,4-naphthoquinone: A theoretical, experimental and environmental application study, *Mater. Adv.* 1 (2020) 1318–1329. <https://doi.org/10.1039/d0ma00290a>.
- [43] T.W. Schultz, J.R. Seward, G.D. Sinks, Estrogenicity of benzophenones evaluated with a recombinant yeast assay: Comparison of experimental and rules-based predicted activity, *Environ. Toxicol. Chem.* 19 (2000) 301–304. <https://doi.org/10.1002/etc.5620190208>.
- [44] H.K. Jeon, S.N. Sarma, Y.J. Kim, J.C. Ryu, Toxicokinetics and metabolisms of benzophenone-type UV filters in rats, *Toxicology.* 248 (2008) 89–95. <https://doi.org/10.1016/j.tox.2008.02.009>.
- [45] H. Yanagishita, D. Kitamoto, T. Ikegami, H. Negishi, A. Endo, K. Haraya, T. Nakane, N. Hanai, J. Arai, H. Matsuda, Y. Idemoto, N. Koura, Preparation of photo-induced graft filling polymerized membranes for pervaporation using polyimide with benzophenone structure, *J. Memb. Sci.* 203 (2002) 191–199. [https://doi.org/10.1016/S0376-7388\(02\)00006-6](https://doi.org/10.1016/S0376-7388(02)00006-6).
- [46] G.S. Kyung Hwa Hong, Benzophenone Incorporated Polyvinyl Alcohol Hydrogels as Photo-Induced Antimicrobial Materials, (2010) 1780–1787. <https://doi.org/10.1002/pen.21712>.
- [47] X.S. Chai, Q.X. Hou, Q. Luo, J.Y. Zhu, Rapid determination of hydrogen peroxide in the wood pulp bleaching streams by a dual-wavelength spectroscopic method, *Anal. Chim. Acta.* 507 (2004) 281–284. <https://doi.org/10.1016/j.aca.2003.11.036>.
- [48] G. Sun, K.H. Hong, Photo-induced antimicrobial and decontaminating agents: Recent progresses in polymer and textile applications, *Text. Res. J.* 83 (2013) 532–542. <https://doi.org/10.1177/0040517512454202>.
- [49] J.C. Forti, R.S. Rocha, M.R.V. Lanza, R. Bertazzoli, Electrochemical synthesis of hydrogen peroxide on oxygen-fed graphite/PTFE electrodes modified by 2-ethylanthraquinone, *J. Electroanal. Chem.* 601 (2007) 63–67. <https://doi.org/10.1016/j.jelechem.2006.10.023>.
- [50] A. Edson C. Paz, a, b Victor S. Pinheiro, A. Luci R. Aveiro, a Fernanda L. Souza, D. Marcos R. V. Lanzac, and M.C. Santos, Hydrogen Peroxide Electrogeneration by Gas

- Diffusion Electrode Modified With Tungsten Hydrogen Peroxide Electrogenation by Gas Diffusion Electrode Modified with Tungsten Oxide Nanoparticles for Degradation of Orange II and Sunset Yellow FCF Azo Dyes, *J. Braz. Chem. Soc.* 30 (2019) 1964–1975. <https://doi.org/10.21577/0103-5053.20190111> J.
- [51] and U.K. Thorben Muddemann, Dennis R. Haupt, Michael Sievers, Improved Operating Parameters for Hydrogen Peroxide-Generating Gas Diffusion Electrodes, (2020) 505–512. <https://doi.org/10.1002/cite.201900137>.
- [52] E. Santacesaria, M. Di Serio, A. Russo, U. Leone, R. Velotti, Kinetic and catalytic aspects in the hydrogen peroxide production via anthraquinone, *Chem. Eng. Sci.* 54 (1999) 2799–2806. [https://doi.org/10.1016/S0009-2509\(98\)00377-7](https://doi.org/10.1016/S0009-2509(98)00377-7).
- [53] T. Nishimi, T. Kamachi, K. Kato, T. Kato, K. Yoshizawa, Mechanistic study on the production of hydrogen peroxide in the anthraquinone process, *European J. Org. Chem.* (2011) 4113–4120. <https://doi.org/10.1002/ejoc.201100300>.
- [54] E. Brillas, R.M. Bastida, E. Llosa, J. Casado, Electrochemical Destruction of Aniline and 4-Chloroaniline for Wastewater Treatment Using a Carbon-PTFE O₂ - Fed Cathode, *J. Electrochem. Soc.* 142 (1995) 1733–1741. <https://doi.org/10.1149/1.2044186>.
- [55] W.R.P. Barros, R.M. Reis, R.S. Rocha, M.R.V. Lanza, Electrogenation of hydrogen peroxide in acidic medium using gas diffusion electrodes modified with cobalt (II) phthalocyanine, *Electrochim. Acta.* 104 (2013) 12–18. <https://doi.org/10.1016/j.electacta.2013.04.079>.
- [56] R.S. Rocha, A.A.G.F. Beati, J.G. Oliveira, M.R.V. Lanza, Avaliação da degradação do diclofenaco sódico utilizando H₂O₂/fenton em reator eletroquímico, *Quim. Nova.* 32 (2009) 354–358. <https://doi.org/10.1590/S0100-40422009000200016>.
- [57] W.R.P. Barros, T. Ereno, A.C. Tavares, M.R.V. Lanza, In Situ Electrochemical Generation of Hydrogen Peroxide in Alkaline Aqueous Solution by using an Unmodified Gas Diffusion Electrode, *ChemElectroChem.* 2 (2015) 714–719. <https://doi.org/10.1002/celec.201402426>.
- [58] M.H.M.T. Assumpção, A. Moraes, R.F.B. De Souza, I. Gaubeur, R.T.S. Oliveira, V.S. Antonin, G.R.P. Malpass, R.S. Rocha, M.L. Calegaro, M.R.V. Lanza, M.C. Santos, Low content cerium oxide nanoparticles on carbon for hydrogen peroxide electrosynthesis, *Appl. Catal. A Gen.* 411–412 (2012) 1–6. <https://doi.org/10.1016/j.apcata.2011.09.030>.
- [59] R.S. Rocha, R.M. Reis, A.A.G.F. Beati, M.R.V. Lanza, M.D.P.T. Sotomayor, R. Bertazzoli, Desenvolvimento e avaliação de eletrodos de difusão gasosa (EDG) para geração de H₂O₂ in situ e sua aplicação na degradação do corante reativo azul 19, *Quim. Nova.* 35 (2012) 1961–1966. <https://doi.org/10.1590/S0100-40422012001000014>.
- [60] W.R.P. Barros, S.A. Alves, P.C. Franco, J.R. Steter, R.S. Rocha, M.R. V. Lanza, Electrochemical Degradation of Tartrazine Dye in Aqueous Solution Using a Modified Gas Diffusion Electrode, *J. Electrochem. Soc.* 161 (2014) H438–H442. <https://doi.org/10.1149/2.015409jes>.
- [61] W.R.P. Barros, P.C. Franco, J.R. Steter, R.S. Rocha, M.R.V. Lanza, Electro-Fenton degradation of the food dye amaranth using a gas diffusion electrode modified with cobalt (II) phthalocyanine, *J. Electroanal. Chem.* 722–723 (2014) 46–53. <https://doi.org/10.1016/j.jelechem.2014.03.027>.
- [62] F. Yu, M. Zhou, L. Zhou, R. Peng, A Novel Electro-Fenton Process with H₂O₂ Generation in a Rotating Disk Reactor for Organic Pollutant Degradation, *Environ. Sci.*

- Technol. Lett. 1 (2014) 320–324. <https://doi.org/10.1021/ez500178p>.
- [63] H. se Ou, J. shao Ye, S. Ma, C. hai Wei, N. yun Gao, J. zhao He, Degradation of ciprofloxacin by UV and UV/H₂O₂ via multiple-wavelength ultraviolet light-emitting diodes: Effectiveness, intermediates and antibacterial activity, *Chem. Eng. J.* 289 (2016) 391–401. <https://doi.org/10.1016/j.cej.2016.01.006>.
- [64] M.H. Gutiérrez-Villarreal, J.G. Guzmán-Moreno, Surface graft polymerization of N-vinylcaprolactam onto polylactic acid film by UV irradiation, *J. Polym. Res.* 20 (2013). <https://doi.org/10.1007/s10965-013-0149-x>.
- [65] H. Gorner, Photoreduction of 9,10-Anthraquinone Derivatives: Transient Spectroscopy and Effects of Alcohols and Amines on Reactivity in Solution, (2003) 171–179.
- [66] G.S. KYUNG HWA HONG, Structures and Photoactive Properties of Poly(styrene-co-vinylbenzophenone), (2008) 2423–2430. <https://doi.org/https://doi.org/10.1002/polb.21576>.
- [67] H.U. Suess, *Pulp Bleaching Today*, (2010).
- [68] W.I. Property, I.P. Date, I.P. Number, WO 2018/048871 A1, 2019.
- [69] P.C. Foller, R.T. Bombard, Processes for the production of mixtures of caustic soda and hydrogen peroxide via the reduction of oxygen, *J. Appl. Electrochem.* 25 (1995) 613–627. <https://doi.org/10.1007/BF00241923>.
- [70] R. Montenegro-Ayo, J.C. Morales-Gomero, H. Alarcon, S. Cotillas, P. Westerhoff, S. Garcia-Segura, Scaling up photoelectrocatalytic reactors: A TiO₂ nanotube-coated disc compound reactor effectively degrades acetaminophen, *Water (Switzerland)*. 11 (2019) 1–14. <https://doi.org/10.3390/w11122522>.
- [71] Y. Wang, C. Shen, M. Zhang, B.T. Zhang, Y.G. Yu, The electrochemical degradation of ciprofloxacin using a SnO₂-Sb/Ti anode: Influencing factors, reaction pathways and energy demand, *Chem. Eng. J.* 296 (2016) 79–89. <https://doi.org/10.1016/j.cej.2016.03.093>.
- [72] J.F. Carneiro, J.M. Aquino, B.F. Silva, A.J. Silva, R.C. Rocha-Filho, Comparing the electrochemical degradation of the fluoroquinolone antibiotics norfloxacin and ciprofloxacin using distinct electrolytes and a BDD anode: evolution of main oxidation byproducts and toxicity, *J. Environ. Chem. Eng.* 8 (2020). <https://doi.org/10.1016/j.jece.2020.104433>.
- [73] I.R. Bautitz, R.F.P. Nogueira, Degradation of tetracycline by photo-Fenton process — Solar irradiation and matrix effects, 187 (2007) 33–39. <https://doi.org/10.1016/j.jphotochem.2006.09.009>.
- [74] J. Deng, G. Wu, S. Yuan, X. Zhan, W. Wang, Z.H. Hu, Ciprofloxacin degradation in UV/chlorine advanced oxidation process: Influencing factors, mechanisms and degradation pathways, *J. Photochem. Photobiol. A Chem.* 371 (2019) 151–158. <https://doi.org/10.1016/j.jphotochem.2018.10.043>.
- [75] S. Mansoori, R. Davarnejad, E.J. Ozumchelouei, A.F. Ismail, Activated biochar supported iron-copper oxide bimetallic catalyst for degradation of ciprofloxacin via photo-assisted electro-Fenton process: A mild pH condition, *J. Water Process Eng.* 39 (2021) 101888. <https://doi.org/10.1016/j.jwpe.2020.101888>.
- [76] E. Brillas, I. Sirés, M.A. Oturan, Electro-fenton process and related electrochemical technologies based on fenton's reaction chemistry, *Chem. Rev.* 109 (2009) 6570–6631.

<https://doi.org/10.1021/cr900136g>.

- [77] A. Dirany, I. Sirés, N. Oturan, M.A. Oturan, Electrochemical abatement of the antibiotic sulfamethoxazole from water, *Chemosphere*. 81 (2010) 594–602. <https://doi.org/10.1016/j.chemosphere.2010.08.032>.
- [78] M. Lanzarini-Lopes, S. Garcia-Segura, K. Hristovski, P. Westerhoff, Electrical energy per order and current efficiency for electrochemical oxidation of p-chlorobenzoic acid with boron-doped diamond anode, *Chemosphere*. 188 (2017) 304–311. <https://doi.org/10.1016/j.chemosphere.2017.08.145>.
- [79] S. Li, T. Huang, P. Du, W. Liu, J. Hu, Photocatalytic transformation fate and toxicity of ciprofloxacin related to dissociation species: Experimental and theoretical evidences, *Water Res.* 185 (2020). <https://doi.org/10.1016/j.watres.2020.116286>.
- [80] E. Guinea, J.A. Garrido, R.M. Rodríguez, P.L. Cabot, C. Arias, F. Centellas, E. Brillas, Degradation of the fluoroquinolone enrofloxacin by electrochemical advanced oxidation processes based on hydrogen peroxide electrogeneration, *Electrochim. Acta*. 55 (2010) 2101–2115. <https://doi.org/10.1016/j.electacta.2009.11.040>.

Supplementary material for:

A novel GDE based on PL6 carbon modified with benzophenone for efficient H_2O_2 electrogeneration and degradation of ciprofloxacin

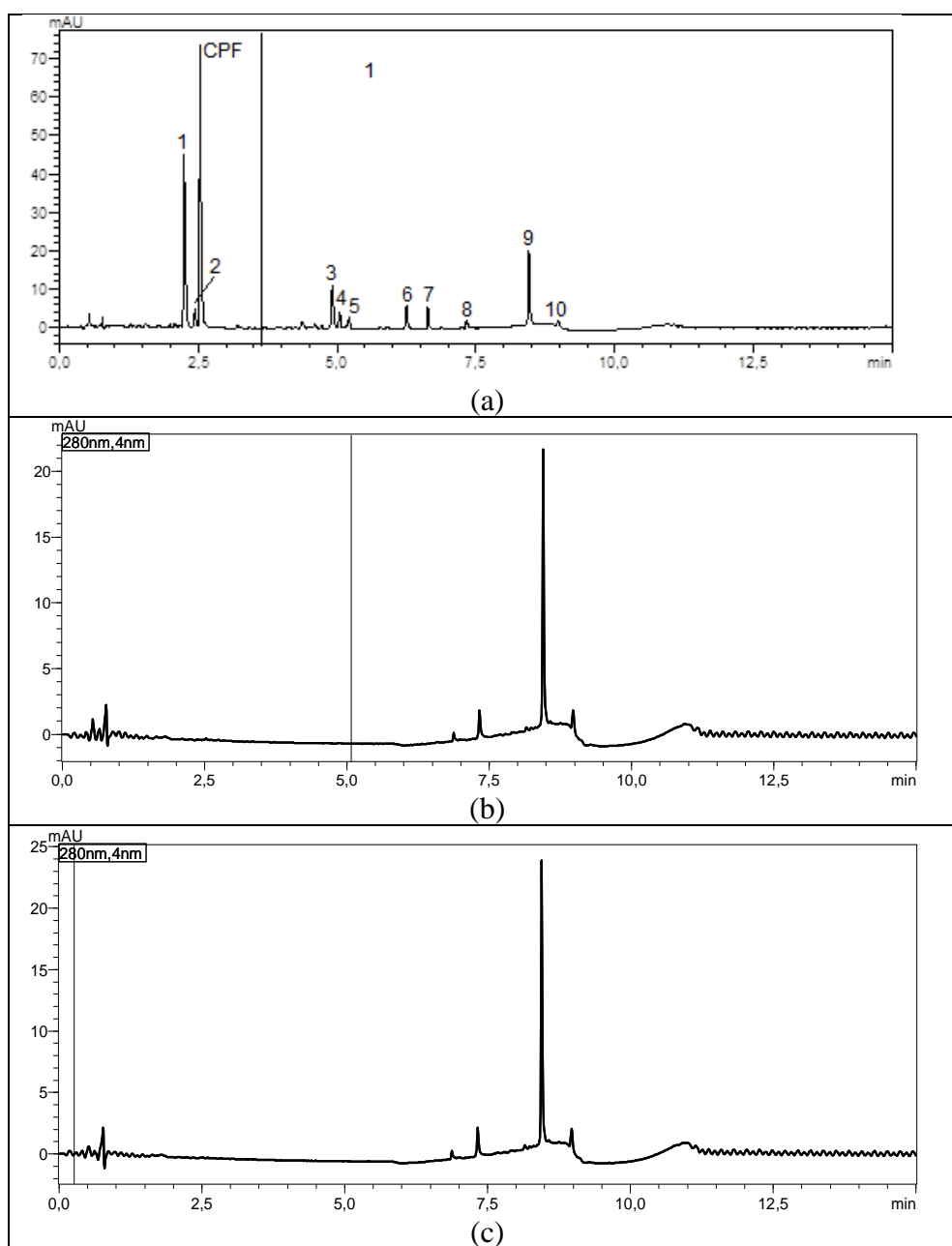


Fig. SM1 – LC-UV/DAD chromatogram of the degradation of CIP during different electrolysis time using the e- H_2O_2 /UVC process: (a) 6, (b) 60 and (c) 360 min h. Peaks 1 to 10: degradation by-products.

By-product	Retention time (min)	[M+H] ⁺ (<i>m/z</i>)	Proposed chemical structure
1	2.2	306	
2	2.4	181	
3	4.9	263	
4	5.0	358	
5	5.2	320	
6	6.2	300	
7	6.6	304	
8	7.3	284	

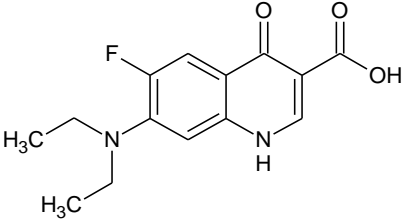
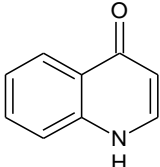
9	8.4	279	
10	8.9	146	

Table SM1 – LC-ESI-MS/MS analysis of CIP and main degradation by-products obtained from the application of the AO/e-H₂O₂/UVC treatment process.

CHAPTER 3. Study and optimization of electrochemical reactors for electrogeneration of H₂O₂ using GDE.

3.1 INTRODUÇÃO

The significance of hydrogen peroxide (H_2O_2) has been growing more and more in the recent years, not only for being a powerful oxidant in its molecular form ($E^\circ +1.77$ V vs SHE), but mainly because it can be easily activated towards powerful hydroxyl radical ($\bullet OH$) ($E^\circ +2.80$ V vs SHE), being one of the key actors in Advanced Oxidative Processes (AOPs). H_2O_2 can found a variety of applications in several fields, such as agriculture, aesthetic procedures, water and wastewater treatment, and more recently, even it was used as disinfectant against coronavirus. Its production *in situ* is a topic of a great interests, specially taking into account the high efficiencies reached compared to industrial anthraquinone process (20,83,107,108).

Thus, H_2O_2 can be electrogenerated from the oxygen reduction reaction (ORR) via $2e^-$ as presented in Equation 3.1. Carbon-based materials present high selectivity for H_2O_2 electro generation being widely applied in studies with this purpose (69,109).



Conversely, the $2e^-$ -ORR efficiency is limited by the low solubility of O_2 in water. To solve this limitation, operation at high pressures using flow-through electrodes, or even gas diffusion electrodes (GDE), are the two important approaches (43,100).

As previously commented of the approaches to overcome the limitation of O_2 solubility, the first approach is faced by raising pressure considering the almost linear increase in the solubility of oxygen with the operation pressure. In the second case, in using a GDE there is no need for O_2 solubilization, because the gas can be supplied directly and incessantly on the electrode surface not being necessary the solubilization because the formation of the H_2O_2 takes place in the triple phase boundaries of this electrode. Nevertheless, for both approaches the use of electrochemical cells with outstanding mass transport characteristics is a must in order to reach high efficiencies and currently, outstanding values have been reported in previous collaborations of our groups based on the use of specially tailored electrodes and cells (7,108,110).

Although there are numerous applications for the *in situ* production of H_2O_2 , environmental applications stand out because the transport, storage and management of the commercial product is avoided, allowing their direct application in remote sites. In this point, the electrochemical production can compete successfully with the commercial product, especially if H_2O_2 produced is able to demonstrate its effectiveness in the degradation of the

pollutant. The easiness of its activation to hydroxyl radical, by UVC light irradiation, its environmental-friendly performance (because reduction product in water) makes it more a more promising to face the removal of pollutants because not only the chemical oxidation but also the advanced oxidation processes can be developed with the same reagent (1,25).

The electrogeneration of H_2O_2 happens on the GDE cathode but other parallel reactions such as ozone (O_3), and peroxymonosulfate (SO_5^{2-}) that are considered scavengers and directly affects the efficiency of H_2O_2 generation. These species can consume H_2O_2 are call scavengers(109,111).

Looking for an approach that can overcome the generation of this predatory species, a divided cell it's one of the possibilities, that can be achieve employing a Proton exchange membrane (PEM), for example, besides the possibility to avoid the scavenger's generation and the consumption of the H_2O_2 ate the anode, possibilities to explore the anode generation of other oxidants species or anode oxidation, for example (8,112,113).

3.1.1 New proposal of electrochemical reactor

The study of the H_2O_2 electrogeneration process presents the advantage of being able to be coupled with classical water treatments. For this it is necessary that the tests and proofs of concepts carried out in the laboratory are scalable and plausible to be applied on an industrial scale and commercial application, subsequently 3 main points must be considered, the material that performs the reaction, the process that leads to the generation of the product and the electrochemical cell. Therefore, studies of different proposals of electrochemical reactors and the possibility of scaling should be analyzed and studied (9,112).

As a result, it is critical to evaluate the residence time of a fluid in the reactor. The residence time is not the same for the reactor, because this analysis depends on several parameters, liquid flow, type of fluid, temperature, the residence time distribution (RTD) determines the time in which a given fluid enters and leaves the reactor under a given condition once these conditions are changed the residence time can likewise change(114,115).

The RTD is defined as an empirical approximation that can characterize the flow in a device. One of the ideal reactor models is the plug flow which is the direct passage without distortion in flow. Real reactors do not always behave ideally and may deviate in some parameters from this ideal model, when this happens the reactor presents deviations. Reactor's designs that account for deviations from ideality, on the other hand, are more sophisticated and not yet fully developed. Deviations can be induced by channel creation, fluid recycling, the

appearance of stationary patches in the vessel, or other phenomena not considered in ideal model assumptions (115,116).

The issues of non-ideal flow are tied to scale-up, as the decision to use pilot unit is primarily determined by having control over all of the most significant factors involved in the process. In general, the amount of the flow's non-ideality is the uncontrollable component in scale-up, and this is frequently significantly different for small and big units. As a result, ignoring this element can lead to serious design flaws(117,118).

In this view, it is vital to understand what is going on inside the vessel while designing a reactor with non-ideal flow. A comprehensive velocity distribution map for the fluid, which is extremely difficult to obtain, is ideal. To address these challenges, a minimal amount of parameters must be defined in order for design to be feasible. In numerous circumstances, simply knowing how long individual molecules stay in the container, the residence time distribution of the fluid being flowed, is adequate for design(114,118).

When a fluid flows through a vessel, not all particles take the same amount of time to leave the system, and this distribution of times is measured by the tracer concentration in function of time, in a graph expressed by $E(t)$, which characterizes the distribution of the process's residence time(115,116).

Some flow phenomena in the reactor that are related to divergence from ideality may also be attributed to the following factors:

- Preferential fluid channel formation occurs when different particles flow through the pipe at different average speeds.
- Fluid recycling: occurs when sections of the fluid are recirculated to the inlet or interior of the device.
- Short-circuit: occurs when fluid particles do not travel the entire length of the vessel and escape fast.
- Dead zones or stagnation regions: form when components of the fluid become stuck in isolated regions of the equipment and do not interact with the active regions.
- Retro-mixing: occurs when sections of the fluid flow in the opposite direction as the main flow.

This deviation from ideality can be characterized through the experimental determination of the residence time distribution (RTD) of the process.

The distribution of flow times of the fluid particles leaving the system, $E(t)$ is calculated according to Equation 3.2 and has the unit of $(\text{time})^{-1}$, $C(t)$ is the output concentration of the marker at time t (114,115).

$$E(t) = \frac{C(t)}{\int_0^{\infty} C(t)dt} \quad (3.2)$$

After injection of the marker by the pulse-type technique, the curve $E(t)$ is obtained, which has the normalized form, the area under the curve is unit, according to Equation 3.3(117,118).

$$\int_0^{\infty} E(t)dt = 1 \quad (3.3)$$

The $E(t)$ curve is the distribution required to assess non-ideal flow and is greatly influenced by fluid properties such as viscosity, density, flow rate and by process conditions such as pipe diameter, length, and roughness. Another parameter that must be analyzed in an RTD analysis is the space time of a fluid, in a given system is given by the ratio between the volume of the system and the volumetric flow rate, according to Equation 3.4 (115,116).

$$\tau = \frac{V}{v_0} \quad (3.4)$$

For this condition to be valid it is necessary that the flow and the density of the fluid are constant with time, the space time is a theoretical value taking into account if the reactor was ideal (τ), θ mean residence time is the experimental value of the average time it takes for the tracer to instantly enter and exit the vessel (t_m the normalized value of $(t_m - \tau)$ where the mean residence time is subtracted from the space time, that indicates how close the reactor studied behavior is close to the ideal reactor behavior (115–117).

The magnitude of the variance σ^2 represents the square of the spread of the distribution as it passes through the vessel and is used to match the experimental curves with one of the families of theoretical curves. The larger the value of this variance, the greater the spread of the distribution. The third parameter is additionally determined around the mean and is related to the skewness of the distribution. The magnitude of this moment measures the extent of the

asymmetry (s^3) of the distribution in one direction or the other with respect to the mean (114,118).

3.2. MATERIAL AND METHODS

This topic was divided in 2.1 Materials, 2.2 Gas diffusion electrode production, 2.3 Electrogeneration of H_2O_2 in flow-by reactor, 2.3 Electrogeneration of H_2O_2 in tangential-flow reactor 3D printed and 2.4 Residence time distribution analysis.

3.2.1 Material

Sodium sulfate ($Na_2SO_4 > 99\%$ - from Merck), sulfuric acid ($H_2SO_4 > 98\%$ - from Sigma Aldrich) and Titanium (IV) oxysulfate solution ($TiOSO_4 \sim 1.9-2.1\%$ - from Sigma Aldrich) were used for characterization. Proton exchange membrane (PEM) type Cation Exchange Membrane (CMX-Neosepta- from Astom Corp.) was used to separate anodic and cathodic compartments in divided cell. The GDE was prepared using carbon black Printex® L6 (PL6C – from Evonik Brazil ltd.), poly(tetrafluoroethylene) (PTFE) – acquired from Sealfon, a carbon cloth (from Zoltek, model PX30). Ultrapure water, obtained from a Millipore Milli-Q system (resistivity $\geq 18.2 M\Omega cm$), was used for the preparation of all solutions.

3.2.2 Gas diffusion electrode production

According to the literature, the manufacture of GDE PL6C and GDE PL6C/BTDA 2% starts with the preparation of a catalytic mass, by mixing the carbon (or de PL6C/BTDA 2%) with PTFE 20% w/w in 500 mL ultrapure water (Mili-Q), under constant agitation for homogenization. After that, the catalytic mass was vacuum filtered, and 2 g of dry mass were spread on a carbon cloth ($126 cm^2$) and hot pressed for 25min at 2.5 tons at $210^\circ C$. Then, the electrode was removed from the press and cut into a circular shape of $20 cm^2$ area.

3.2.3 Electrogeneration of H_2O_2 in flow-by reactor

Discontinuous flow

The experiments of electrosynthesis of H_2O_2 in a single compartment (without membrane) were carried out using a flow-by reactor described elsewhere (109,111) connected to electric power supply (model ES030-10 (15V/10A) from Delta Elektronika) and a reservoir tank 2L capacity, coupled to a thermostatic bath (Tectron-200 27 from JP Selecta group), that kept the temperature of the system at $25^\circ C$, a peristaltic pump (Percom N-M II from JP Selecta group) with a flow rate of $250 mL min^{-1}$. In the double-compartment the reactor was equipped

with a Proton exchange membrane (PEM) type Cation Exchange Membrane (CMX-Neosepta- from Astom Corp.)

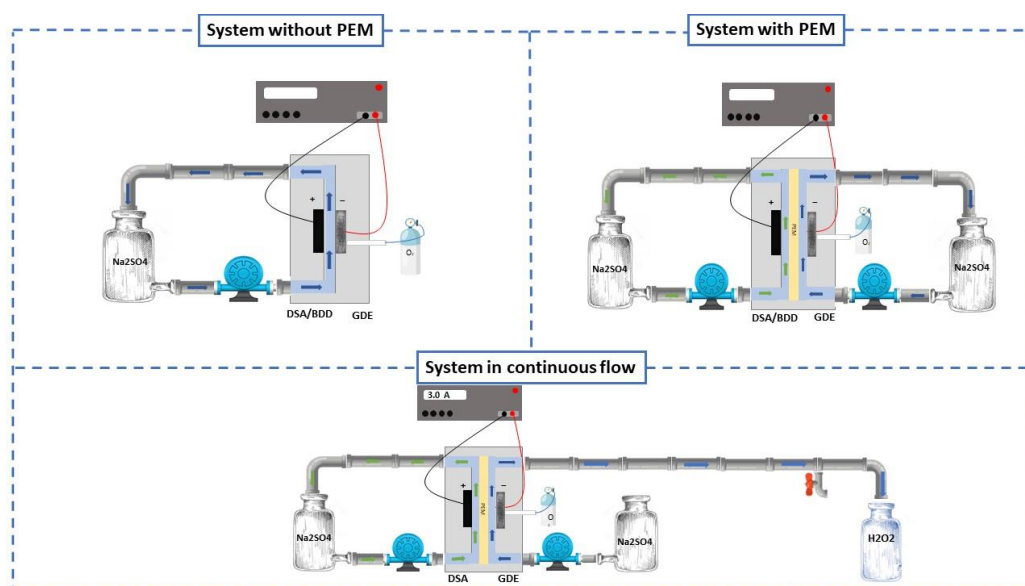
As electrolyte 1L Na_2SO_4 0.5 mol L^{-1} pH 2.5 adjusted with H_2SO_4 , a O_2 flow of 50.0 mL min^{-1} , as electrodes were employed GDE (PL6C), as an anode a dimensionally stable-anode (DSA) and a boron-doped diamond (BDD), all the electrodes have an area of 20 cm^2 . So, four system were evaluated GDE of PL6C with DSA without PEM (PL6C/DSA); GDE of PL6C with DSA with PEM (PL6C/DSA-PEM); GDE PL6C with BDD without PEM (PL6C/BDD) and GDE of PL6C with DSA with PEM (PL6C/DSA-PEM)

Continuous flow

In the system with bi-compartment (with PEM) the experimental conditions are the same both with 2 reservoir (2 L capacity). The reactor was equipped with a Proton exchange membrane (PEM) type Cation Exchange Membrane (CMX-Neosepta- from Astom Corp.) where the catholyte and the anolyte were 1L Na_2SO_4 0.5 mol L^{-1} pH 2.5 H_2SO_4 .

The effect of different current densities (50, 100, 150 and 200 mA cm^{-2} during 90 min) was evaluated. The H_2O_2 was quantified (mg L^{-1}) using titanium (IV) oxysulfate solution as an indicator reagent using UV-Vis spectroscopy (at $\lambda = 408$ nm, UV-vis 1700 Spectrophotometer from Shimadzu). Fig. 3.1 shows the schematic diagram of experiments conducted.

Fig. 3.1 – System with discontinuous flow for electrogeneration of H_2O_2 with PEM and without PEM, and the system continuous flow in double compartment, using GDE PL6C as cathode and DSA as anode. Na_2SO_4 0.5 mol L^{-1} , pH 2.5 adjusted with H_2SO_4 , 1 L, 250 mL min^{-1} , 90 min.



Source: The author herself.

3.2.4 Electrogeneration of H₂O₂ in tangential-flow reactor 3D printed

The experiments of electrosynthesis of H₂O₂ was using a tangential-flow reactor printed by a 3D printer (Form 3+ Stereolithography – from Formlabs). The electrode was connected to electric power supply (model ES030-10 (15V/10A) from Delta Elektronika), this reactor was used with a double compartment (with PEM), with reservoir tank of 2 L, that was coupled to a thermostatic bath (Tectron-200 27 from JP Selecta group) so that temperature fixed was 25 °C. The electrolyte used was 0.5 mol L⁻¹ Na₂SO₄ pH 2.5 adjusted with H₂SO₄, using a peristaltic pump (Percom N-M II from JP Selecta group) with a flow rate of 250 mL min⁻¹, and O₂ was supplied in a flow of 50.0 mL min⁻¹.

As cathode a GDE (PL6C and PL6C/BTDA 2%) was employed, as anode a dimensionally stable-anode (DSA). The first reactor was made in a small design (mini tangential-flow reactor) with dimensions of electrode area of 1.6 cm², and the volume of electrolyte of 80 mL, a scaled tangential-flow reactor was likewise 3D printed 12.5 times bigger, the tangential-flow reactor scaled (scaled) used electrodes with an area of 20 cm², and same conditions of electrolyte (concentration and flow rate) using a volume of 1 L. The H₂O₂ was quantified (mg L⁻¹) using titanium (IV) oxysulfate solution as an indicator reagent using UV-Vis spectroscopy (at $\lambda = 408$ nm, UV-vis 1700 Spectrophotometer from Shimadzu).

3.2.5 Residence time distribution analyses

The residence time distribution (RTD) analysis was done by the conductimetric technique, a compound that presents high conductivity in this technique is used as a marker, it is important that it is a non-reactive compound, that does not alter the viscosity of the liquid and that it is soluble in it (in this case, it is soluble in water), saturated potassium chloride (KCl) was used as tracer one, volume of saturated liquid with high conductivity is introduced into the system at a desired point in the process using a 5 mL syringe, causing a pulse-like disturbance by raising the electrical conductivity of the fluid. The fluid passes through the system and is detected through an online conductivity meter connected to the reactor outlet (system), recording the conductivity from the moment the marker is inserted until the moment it leaves the system completely (conductivity returns to the initial value).

The test was performed in three different reactors that were a flow-by, a tangential-flow 3D printed mini and tangential-flow 3D printed scaled). To perform the tests a 1 mL of KCl 3M was used as a marker injected in a flow of 0.250 L min⁻¹ of water, this liquid flow was the same as that used for the generation of H₂O₂ and was not changed. The passage of the fluid through the system was detected by a bench conductivity meter (EC-Meter GLP 31 from

Crison), which was directly coupled to the reactor outlet, the data acquisition frequency was 1 s from the injection of the tracer until its complete exit.

3.3 RESULTS AND DISCUSSION

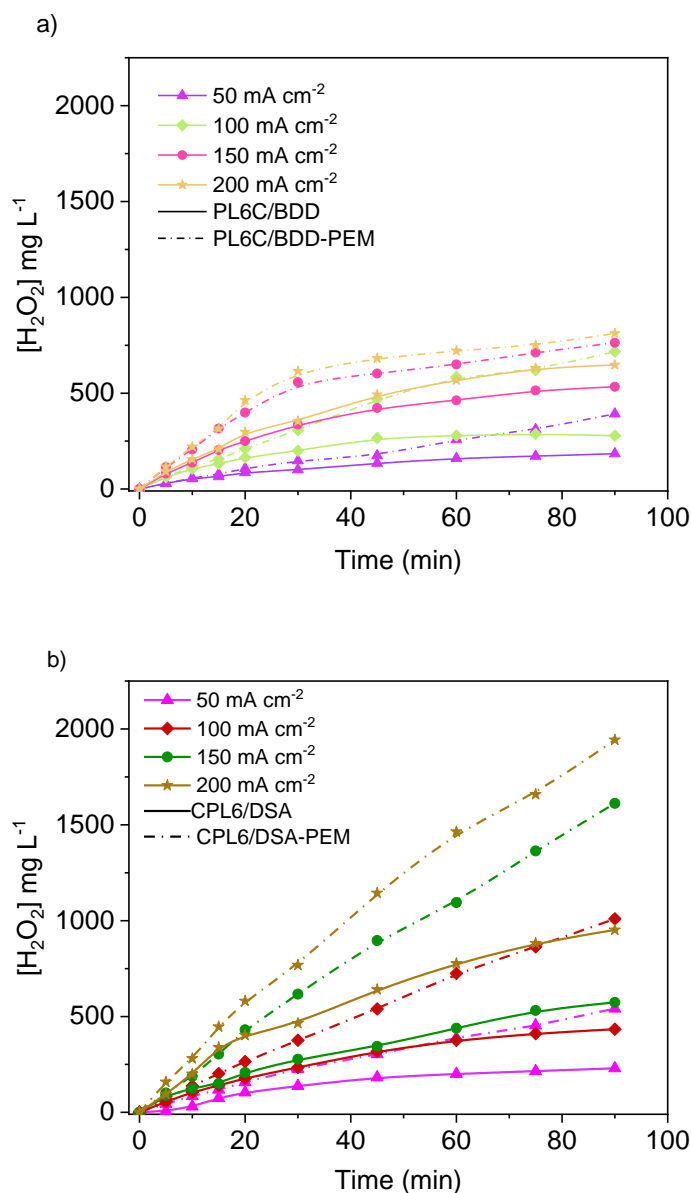
The results and discussion were divided in 3.1 Optimized production of H₂O₂, 3.2 Electrogeneration of H₂O₂ with tangential-flow reactor 3D printed and 3.3 Modification of carbon matrix.

3.3.1 Optimized production of H₂O₂

Previous work demonstrated the advantageous performance of the flow-by electrochemical reactor and GDE based on Cordeiro Junior (2022). To go further, trying to obtain a design that can be applied *in situ* for the remediation of waste in remote sites powered by solar panels, in this work we are using a cathode consisting of Printex L6 carbon (PL6C) with 20% PTFE, that is expected to improve efficiency because of the material (using less material than previously reported by Cordeiro Junior (2022)) and mainly milder manufacturing conditions, temperature of 210 °C (lower than found in the literature) and pressure of 2 tons (lower than found in the literature) (109,111) .

In addition, to prevent the effect of scavengers that are known to reduce the efficiency in the production of H₂O₂, the effect of the anode, current density, and compartmentation of the cell by using a PEM membrane are likewise evaluated. Considering that, in the Fig. 3.2a is evaluate the H₂O₂ electrogeneration using PL6C as cathode and BDD as anode at a single compartment (PL6C/BDD), and a double compartment (PL6C/BDD-PEM). Fig. 3.2b present the H₂O₂ electrogeneration with DSA as anode in a single compartment (PL6C/DSA), and a double compartment (PL6C/DSA-PEM).

Fig. 3.2 – Electrogeneration of H_2O_2 applying different current densities per time in a system with PEM and without PEM. **a)** Using GDE PL6C as cathode and BDD as anode. **b)** Using GDE PL6C as cathode and DSA as anode. Na_2SO_4 0.5 mol L^{-1} , pH 2.5 adjusted with H_2SO_4 , 1 L, 250 mL min^{-1} , 90 min.



Source: The author herself.

The application of membrane allows the separation of reactions that occurs at the anode site from the one occurring at the cathode site. The H_2O_2 electrogeneration occurs on the GDE cathode but other reactions such as ozone (O_3), and peroxymonosulfate (SO_5^{2-}) takes place on the anode site. In both system (PL6C/BDD and PL6C/DSA) the behavior of H_2O_2 generation

increase linear on the first 20 min, as a result of, a kinetic model of pseudo-zero order. After, the behavior tends to a stationary state formatting an equilibrium between the H_2O_2 electrogenerated and the consumption of the same, by scavengers, consumption at the anode surface and auto-consumption.

Ozone can be generated at the anode surface via $6e^-$ mechanism in an electrochemical process, this process is named electrochemical ozone production (EOP) as present in Equation 3.5 (63,64,111).



Since a sulfate salt was used as an electrolyte, sulfate ions are present in the medium, and peroxymonosulfate can be electrochemical generated, Equation 3.6 (119,120).



The effects that must be noted as directly interference in the decrease or stabilization of H_2O_2 generation are the scavengers (Equation 3.7 e 3.8), reaction of H_2O_2 at the anode surface (Equation 3.9) and the auto-consumption of H_2O_2 (Equation 3.10) (63,109).



This interference can be noted in both system (PL6C/BDD and PL6C/DSA), but when BDD is employed, this effect became more evidentially, on behalf of higher amounts of scavengers generated by BDD. The system with PEM avoid the scavengers species to consume H_2O_2 . Likewise, in Fig. 3.2a and 3.2b is notable that H_2O_2 electrogeneration is increase, exhibit a tendence distance from the stationary state, because the stationary state will be accomplished only when the amount of H_2O_2 were sufficiency high to dislocate the equilibrium and started to consume the H_2O_2 that will be in excess, the equation 7 will be the determinant reaction to represent that.

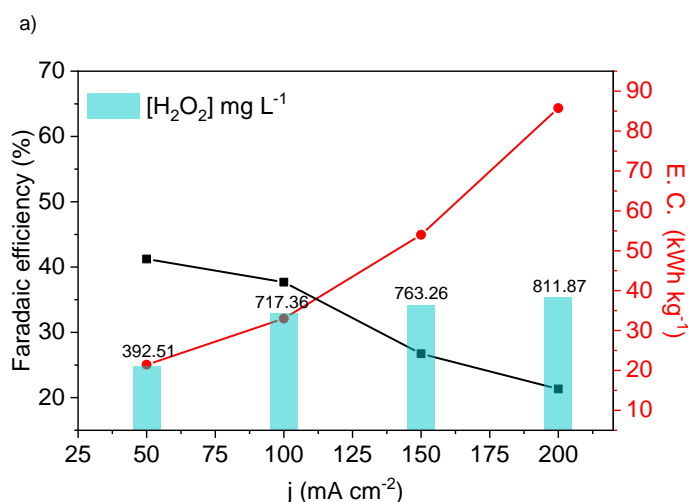
Comparing, for example, the H_2O_2 production curve of 150 mA cm^{-2} (PL6C/BDD and PL6C/BDD-PEM), in the presence of a membrane the curve steepens to continue to generate near-linear behavior, the same can be observed when DSA is used. At 60 min the system CPL6/DSA start to get a curvature to initialize the stabilization, and the system CPL6/DSA-PEM the behavior almost does not change for all the experimental time, continuous in linear production, becoming able to achieve highest values of H_2O_2 generated.

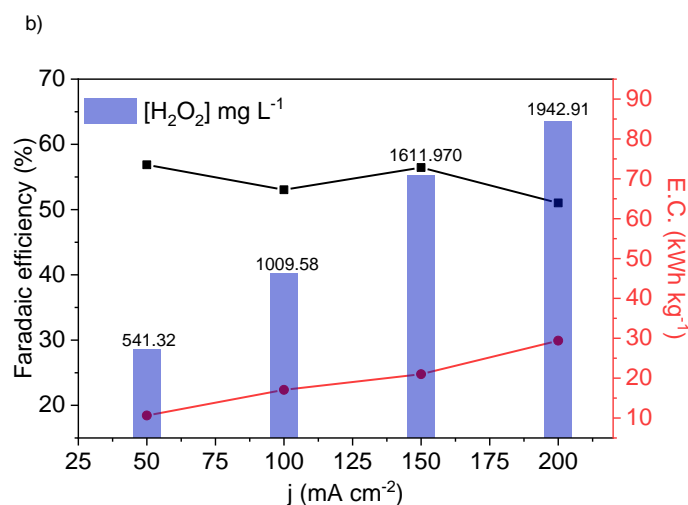
The values of maximum H_2O_2 accumulated in 90 min of electrosynthesis are higher using DSA than BDD in all four current densities applied, the maximum value achieve for each anode was 200 mA cm^{-2} , $811,87 \text{ mg L}^{-1}$ for BDD and $1942,91 \text{ mg L}^{-1}$ for DSA. With the increase of the current density the H_2O_2 values also increase.

Figure 3.3 summarizes the key performance indicators attained in the different tests made in divided cells, where the effect of the scavengers is smaller.

The energy consumption (EC) of PL6C/BDD-PEM, elucidated in Figure 3.3a, increase with the increase of density current applied, the density currents of 50, 100, 150 and 200 mA cm^{-2} obtained a value of EC of 21.44; 33.00; 54.01 and $85.73 \text{ KWh Kg}^{-1}$, respectively. The calculus of Faradaic Efficiency (FE) achieved the highest values at 50 mA cm^{-2} and sequentially 100 mA cm^{-2} , 41.24% and 37.68%, respectively, considering that these values are very similar, and the amount of H_2O_2 generated on 100 mA cm^{-2} (717.36 mg L^{-1}) was almost twice much as on 50 mA cm^{-2} (392.51 mg L^{-1}), the current density of 100 mA cm^{-2} was considered the optimal condition for BDD as anode with membrane.

Fig. 3.3 – a) Calculus of PL6C/BDD-PEM FE, EC and maximum of H_2O_2 . b) Calculus of PL6C/DSA-PEM FE, EC and maximum of H_2O_2 .





Source: The author herself.

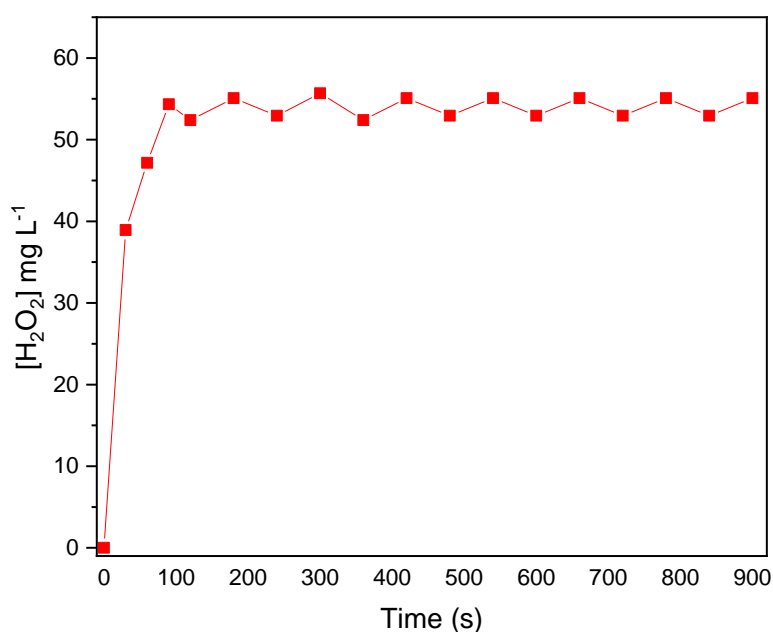
As expected, Fig. 3.3b, the PL6C/DSA-PEM system also presents its EC values increasing proportionally to the increase of current density, but with lower values than the first mentioned system, for the current densities 50, 100, 150 and 200 mA cm^{-2} , presented EC values of 10.64; 17.06; 20.99 and 29.40 kWh Kg^{-1} , respectively, the best current density in relation to the FE were 50 and 100 mA cm^{-2} , 56.87% and 56.45% respectively, in this way it is possible to consider as better current density applied 150 mA cm^{-2} taking into consideration the value of H_2O_2 generated (1611.67 mg L^{-1}) compared with 50 mA cm^{-2} that generated 3 times less. Comparing the both system is effortless notable that the use of DSA as an anode (PL6C/DSA-PEM) lead to a better FE, lower EC and higher amounts of H_2O_2 electrogenerated.

Comparing to literature, the production of H_2O_2 was very satisfaction, it was possible to achieve a value of H_2O_2 electrogenerated higher than the ones in the literature. For example, the work of Kronka et al (2023) using a GDE of PL6C applying 50 mA cm^{-2} in 120 min achieve 0.0625 $\text{mg min}^{-1} \text{cm}^{-2}$ of electrogenerated H_2O_2 ; the work of Costa et al (2021) also using a GDE of PL6C in 120 min using BDD as anode electrogenerated H_2O_2 0.100 $\text{mg min}^{-1} \text{cm}^{-2}$, and Cordeiro Junior (2022) 1.00 $\text{mg min}^{-1} \text{cm}^{-2}$, the values found in the main literature are below or close to the H_2O_2 value of this work (0.895-1.08 $\text{mg min}^{-1} \text{cm}^{-2}$), which elucidate the advantage of the system and further that even using less material, satisfactory amounts of oxidant were produced (77,111,121).

In a full scale environmental -remediation process, the operation in batch mode is not the best option, but the operation in continuous mode, which has associated the continuous

production of a stream of oxidant that can be dosed to the waste to be treated. Fig. 3.4 presents the production when the system is fed with a stream of electrolyte of 250 mL min^{-1} .

Fig. 3.4 – Electrogeneration of H_2O_2 with GDE PL6C/DSA-PEM at a continuous system flow 250 mL min^{-1} applying 150 mA cm^{-2} . Na_2SO_4 0.5 mol L^{-1} , pH 2.5 adjusted with H_2SO_4 .



Source: The author herself.

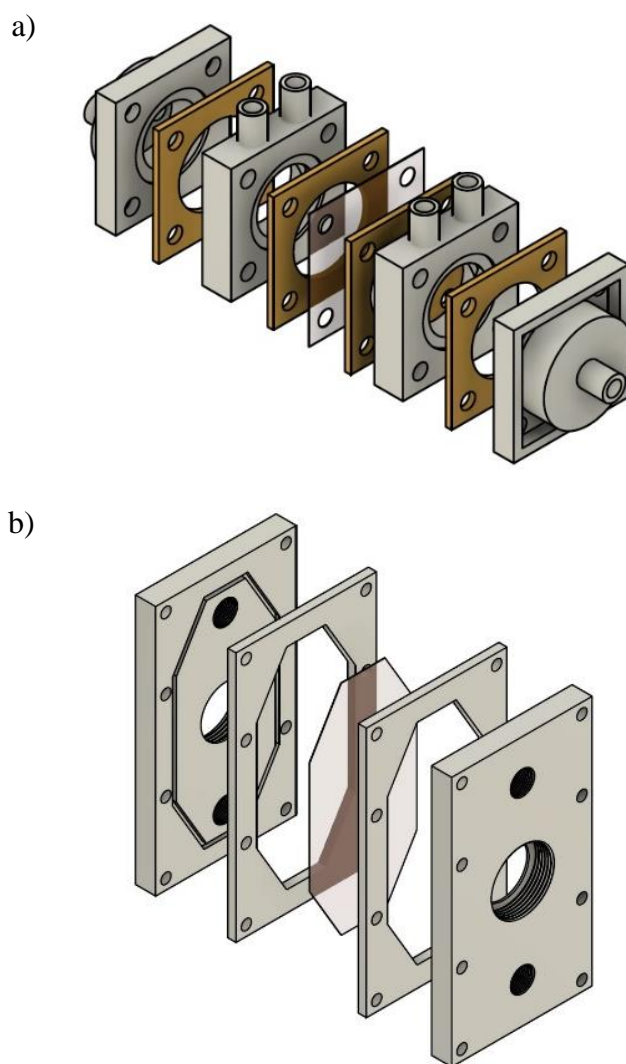
As seen, the steady state is reached in less than two minutes, from which the concentration in the outlet stream is kept in a constant value of $55.9 \text{ mg L}^{-1} \text{ s}^{-1}$, which corresponds to a production rate of $13.98 \text{ mg min}^{-1}$ (in a continuous process, the electrochemical production can be obtained as the product between the steady state concentration and the flowrate). Concentration variations after 100 s are negligible and can be explained in terms of the effects of the bubbles caused by O_2 passing through the porous GDE.

3.3.2 Electrogeneration of H_2O_2 with tangential-flow reactor 3D Printed

Another study that was carried out was a proposal of a new design reactor for H_2O_2 electrogeneration, and the study of the surface of this design, the design is in Fig. 3.5a, the proposal is a reactor 3D printed with tangential-flow creates a circular flow in the compartment and the electrolyte has more time and homogeneously in contact with the electrode surface, the

yellow part is the part made of silicone to sealing, and the PEM is represented by the grey color, Figure 3.5b illustrates a reactor already used by the group and cited in the literature, a flow-by type reactor.

Fig. 3.5 – a) Tangential-flow reactor 3D printed. b) Flow-by reactor. Desing in the Fusion 360° Program.

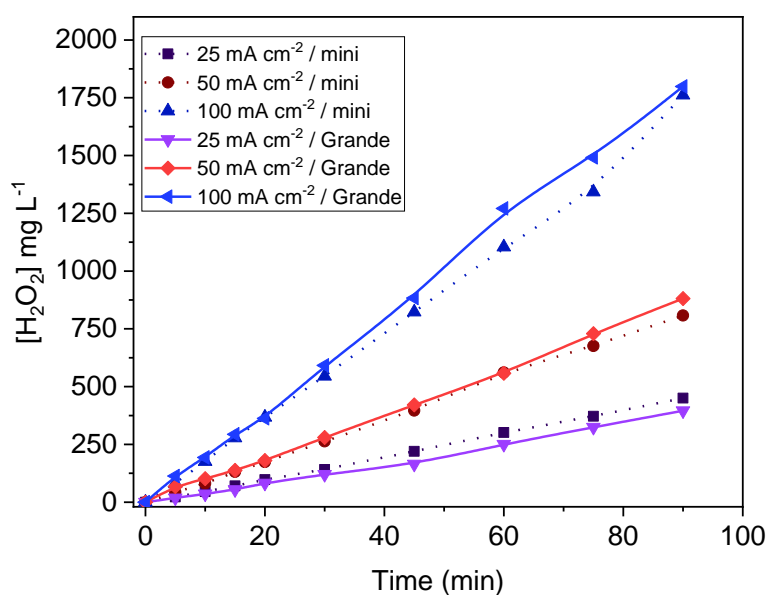


Source: The author herself.

Fig. 3.6 presents the comparison of the performance of the tangential-flow reactor 3D Printed mini reactor with its scall up version, the relation electrode area and volume of electrolyte is maintained, and the current density was calculate based on the electrode areas. The three different current densities (25, 50 and 100 mA cm⁻²) were evaluated in order to compare the performance of both reactors. As result, when compared to the same current density the performance of the two reactor is the same, considering a very little variation that

is in the error is possible to see that the reactor is scalable, which is very desirable because the technology can be applied in electrode types of industry plants and possibilities work with high volumes.

Fig. 3.6 – Electrogeneration of H_2O_2 applying different current densities per time in tangential-flow reactor 3D printed mini and scall up reactor with PEM using a GDE PL6C as cathode and DSA as anode. Na_2SO_4 0.5 mol L^{-1} , pH 2.5 adjusted with H_2SO_4 , 250 mL min^{-1} , 90 min, with PEM.



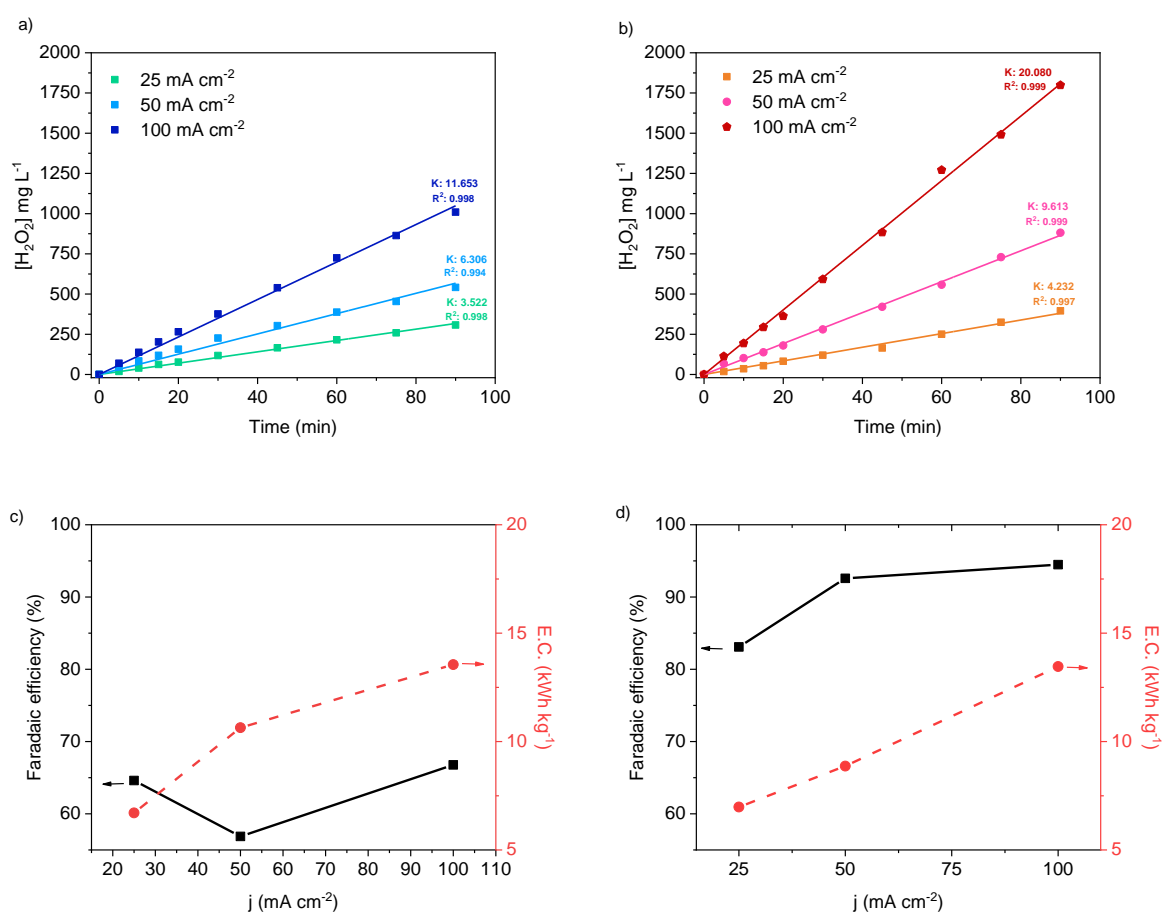
Source: The author herself.

Using the same electrode, with the same dimensions of the surface area of the electrode that is in contact with the electrolyte, the same flow rate and electrolyte, a comparison was made between the new reactor proposal and a flow-by reactor already mentioned in the literature. It is possible to see in Fig. 3.7a e 3.7b, the performance of generation and kinetics of generation in both cases, for both reactors when the current density increase the kinetic and the H_2O_2 eletrogenated additionally increase, that's because in this system the analytic and cathodic are separated with a Membrane (PEM), in the previously captured was evaluated that the use of PEM impossibility the consumption of H_2O_2 ate the surface of anode electrode.

Analyzing the Figure 3.7c e 3.7d where it expounds the EC and the FE, it is possible to notice that there is not a very big gain in relation to energy consumption, conversely, the FE is much higher, reaching very satisfactory values (above 90%) elucidating an interesting proposal in industrial applications. Among the current densities applied for the tangential-flow reactor

3D printed, the 50 mA cm^{-2} density is considered the best, because it reaches FE values practically equal to 100 mA cm^{-2} , on the other hand, it presents an EC by half, which favors the generation of H_2O_2 at this specific current density.

Fig. 3.7 – a) Electrogeneration of H_2O_2 reactor flow-by. b) Electrogeneration of H_2O_2 tangential-flow reactor 3D printed. c) Calculus of reactor flow-by FE and EC d) Calculus of tangential-flow reactor 3D printed FE and EC. GDE PL6C and DSA, Na_2SO_4 0.5 mol L^{-1} , pH 2.5 adjusted with H_2SO_4 1 L, 250 mL min^{-1} , 90 min, with PEM.



Source: The author herself.

Figure 3.8 show the RTD studies of three reactor setups, is possible to estimate the presence of non-ideal flow plug flow in the reactor that leads to a decrease in the efficiency of the reactor, comparing the, tangential-flow reactor 3D printed mini (Fig. 3.8a), scall up (Figure 3.8b) and flow-by reactor (Fig. 3.8c). The profile of the tangential-flow reactor mini is close to the plug in model reactor, it is possible to notice that the profile presented a fast inflow and outflow, a narrow peak, indicating that there is probably no dead volume in the reactor, the very

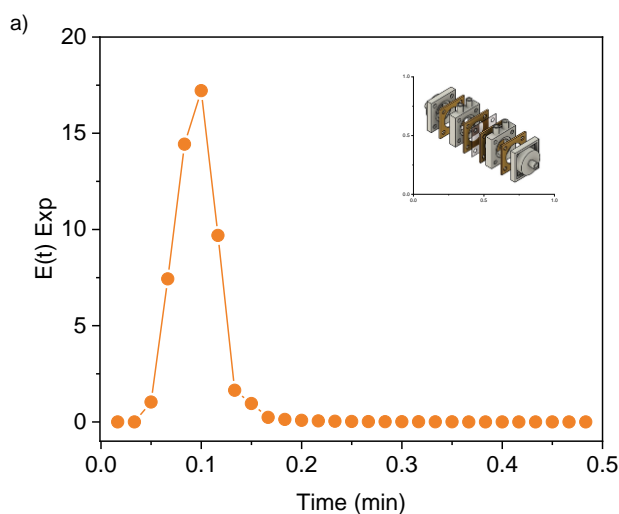
low ideality deviation, which is confirmed by the parameters, t_m 0.09 min; σ^2 0.0005; s^3 0.01; τ 0.016 min and $t_m - \tau$ 0.08 min,

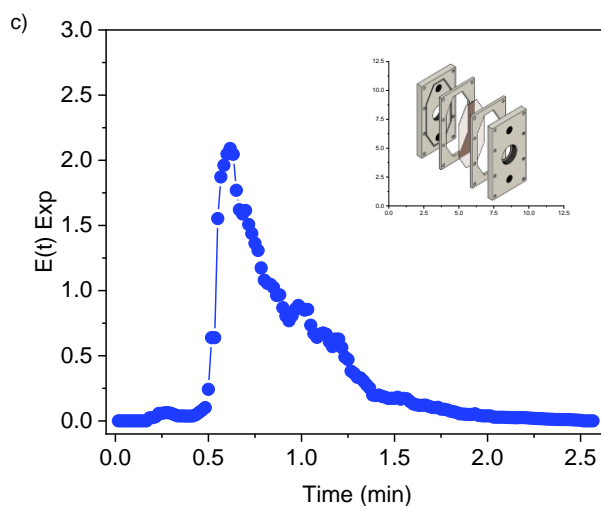
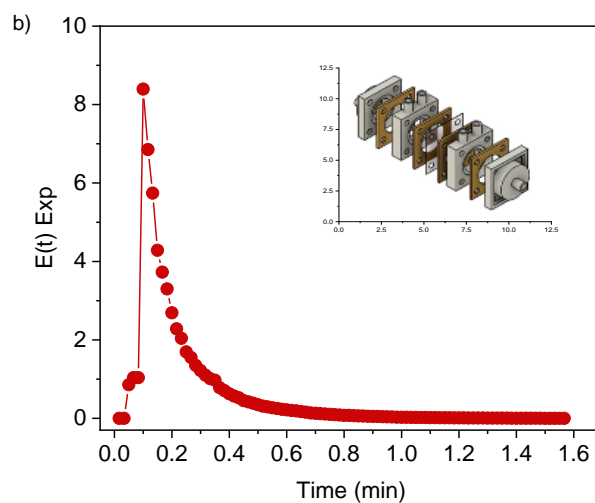
the parameters confirm that there is a low ideality deviation, low variance, and low asymmetry.

Comparing with the profile of its scall up version, the profile remains very similar, corroborating with the data of H_2O_2 electrogeneration, comparing the parameters t_m 0.22 min; σ^2 0.03; s^3 0.16; τ 0.148 min; $t_m - \tau$ 0.08 min, the scall up reactor also presents a small variance and asymmetry, indicating that the scall up reactor presents no or very little dead volume, the parameter $t_m - \tau$ of both reactors (mini and scall up) are equal, elucidating the same flow profile in the scalability of the reactor.

Conversely, the flow-by reactor presents an RTD profile and its parameters t_m 0.87 min; σ^2 0.11; s^3 0.26; τ 0.388 min; $t_m - \tau$ 0.48 min, close to reactors that contain dead volume inside, or/and the presence of preferential paths, this is characterized by the presence of a second broad peak, and also by the time of exit of the tracer being much longer than that of entry into the reactor. This possibly explains why using the same conditions and the same material in the cathode, the tangential-flow reactor electrolyzes H_2O_2 more than the flow-by one, since the flow-by reactor presents higher ideality deviation and lower process and fluid efficiencies when compared to the tangential-flow one, emphasizing that this behavior is conditioned to the flow used (0.250 L min^{-1}), once the flow is changed, the behavior can likewise change.

Fig. 3.8 – **a)** RTD tangential-flow reactor 3D printed (mini). **b)** RTD tangential-flow reactor 3D printed (scall up). **c)** RTD reactor flow-by. Market KCl 3M, 1 mL, flow 0.250 L min^{-1} .





Source: The author herself.

After studying the process and ways to improve the efficiency of the process, the study of a new reactor proposal for H_2O_2 electrogeneration presents desirable results, and exploring the material in order to increase the efficiency to the maximum is one of the objectives of this research.

3.3.3 Modification on the carbon matrix

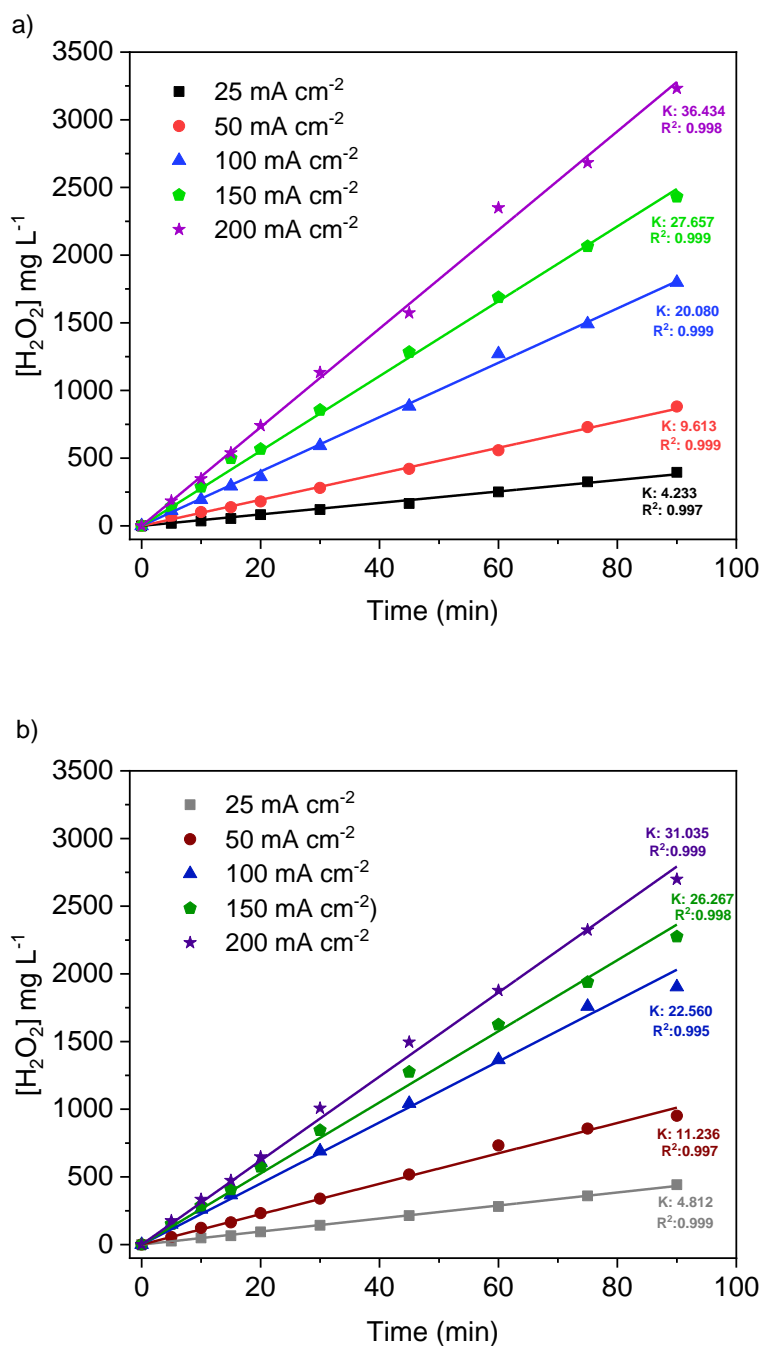
The matrix of carbon was medicated with 2% BTDA, based on previously results, the material PL6C/BTDA 2% presents high activities and selective to ORR via $2e^-$, since the study of process confirmed that the use of membrane increase the efficiency of the process and that

the tangential-flow reacted 3D printed was a new proposed with high efficiency and applicable to be utilized on industry process, the last process is to study the catalytic material in this innovative and original reactor with membrane (PEM), to investigate if the efficiency of the process, reactor and material can operate in their best.

To study the behavior of the electrodes in the electrogeneration of H_2O_2 , different current densities 25, 50, 100, 150 and 200 mA cm^{-2} were applied for the PL6C and PL6C/ BTDA 2% electrodes. Fig. 3.9 shows the electrogeneration profile of the oxidizing specie and the kinetics of generation rate for each applied current density. For both electrodes as the current density increases the generation also increases, as well as the kinetics of generation, conversely, when comparing the modified and unmodified electrodes at current densities of 25 to 100 mA cm^{-2} the material containing the organic modifier presents higher kinetics of generation rate (k : 4.812; 11.238; 22.680, respectively) than the unmodified carbon (k : 4.223; 9.818; 20.008, respectively), contrarily at currents of 150 and 200 mA cm^{-2} this profile changes, and PL6C reaches higher k values (k : 27.667; 38.434, respectively) than PL6C/BTDA 2% (k : 28.287; 31.035, respectively).

This behavior occurs because the material PL6C/BTDA 2% presents selectivity for ORR via 2 e^- at certain values of current density, once the electric current applied to the system increases, it may occur that the overpotential causes the material to lose selectivity, forcing the reaction to proceed via 4 e^- (generating H_2O), this profile has already been reported in the literature for this same material, since there is an optimal current density for the material selectivity to be maximum.

Fig. 3.9 – Electrogeneration of H_2O_2 applying different current densities per time in a system with PEM. **a)** Using GDE PL6C as cathode and DSA as anode. **b)** Using GDE PL6C/BTDA 2% as cathode and DSA as anode. Na_2SO_4 0.5 mol L^{-1} , $\text{pH } 2.5_{\text{H}_2\text{SO}_4}$, 1 L , 250 mL min^{-1} , 90 min .



Source: The author herself.

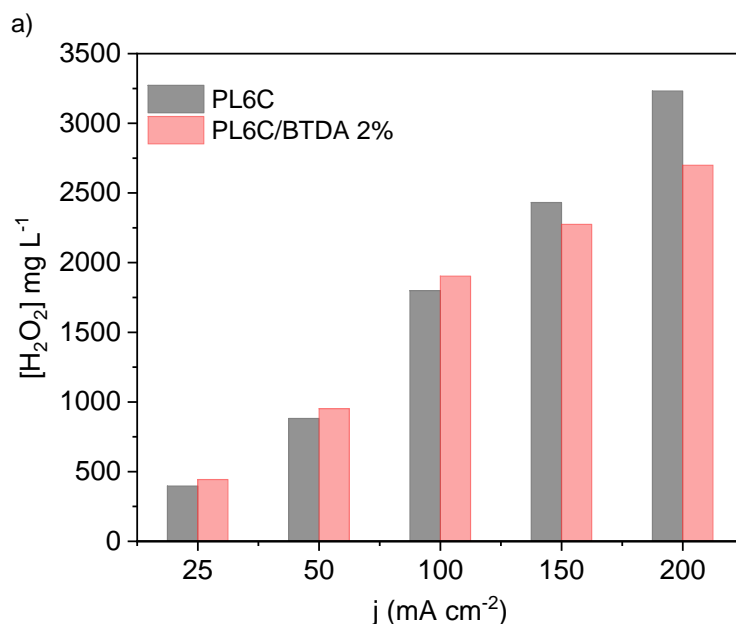
Fig. 3.10a shows the maximum values of $\text{e-H}_2\text{O}_2$ accumulated after 90 min of electrolysis, comparing the used GDE, evidencing that although with the increase of current density the values of oxidant formed continue to rise the values of the unmodified GDE reaches

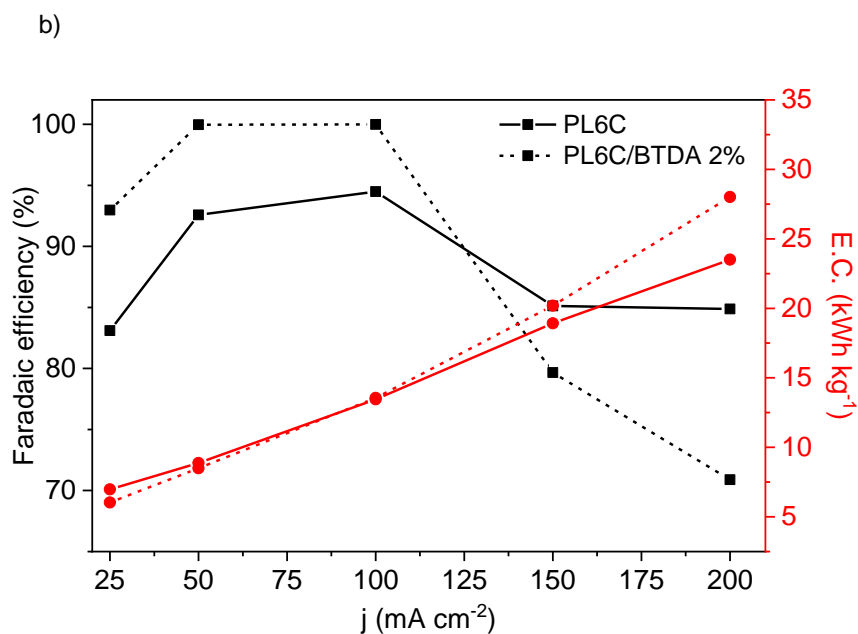
higher values in 150 and 200 mA cm⁻², this comparison is also seen in the calculations of FE EC, as shown in Fig. 3.10b.

The PL6C/BTDA 2% material, like PL6C, has an increase of FE from 25 to 50 mA cm⁻², and from 50 to 100 mA cm⁻², and both lose efficiency from 100 to 150 and 200 mA cm⁻², precisely because the increase of current density causes a loss of selectivity for e-H₂O₂. The material modified with BTDA reaches FE values of 99.97% and 99.99%, at 50 mA cm⁻² and 100 mA cm⁻², respectively, elucidate that the modification improves the performance of the GDE in electrogeneration, both current densities can be considered as FE of practically 100%, proving that the modification of the material is advantageous when compared to the PL6C GDE without modification.

The EC values at 50 and 100 mA cm⁻² are practically the same for both electrodes, demonstrate that the modification does not result in higher energy consumption, and since the F.E. values for the material with BTDA were practically the same, it is considered that the optimal condition is the PL6C/BTDA 2% material at 50 mA cm⁻², presenting an EC of 8.5 kWh kg⁻¹ compared to 13.5 kWh kg⁻¹ for 100 mA cm⁻².

Fig. 3.10 – a) Comparison of maximum achieved value of H₂O₂ generation in 90 min for each electrode. b) – Calculus of PL6C and PL6C/BTDA 2% FE, EC.

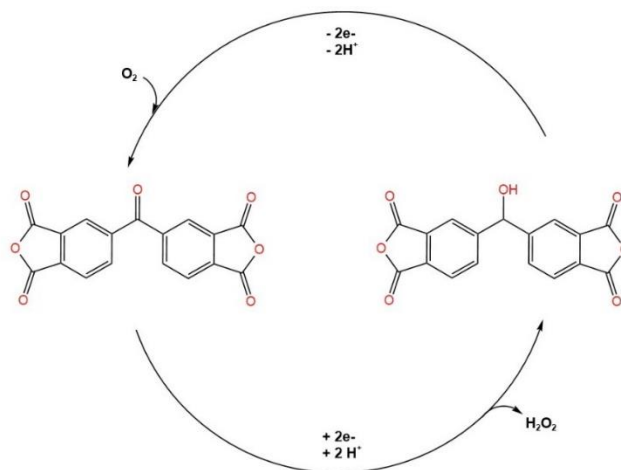




Source: The author herself.

The explanation of the high FE achieve its because of the properties of the modifier (BTDA), it's structure contained oxygens functional groups that increase the active sites in the carbon matrix, as was discussed in the Chapter 1, but there another contribution of the BTDA, as reported in the Chapter 2, presents photoactivated to produce H_2O_2 and also, present the possibility that the ketone functional group in the middle of the molecule, possibilities to the formation of H_2O_2 , the same behavior of the quinones. As demonstrate in the Fig. 3.11 the proposed mechanism for the H_2O_2 formation occurring by oxidation and reduction of the ketone group.

Fig. 3.11 – Proposed of electrogeneration of H_2O_2 at the material contained BTDA.



Source: The author herself.

The results elucidate the potential of the material, the literature confirm this potential. The modification results a more efficiency reaction without causing more energy consumption. Cordeiro Junior et al (2022), achieve a current efficiency around 85% less than this work and high consumption energy of 86.6 kWh kg^{-1} at the potential of -1.50 V , Moreira et al (2019) with the GDE of carbon modified with 0.5% Sudan Red 7B achieve only 11.1% and EC of $136.6 \text{ kWh kg}^{-1}$ applying 50 mA cm^{-2} . That's justify how promising the material and the reactor together are promising (20,100,109).

3.4 CONCLUSÃO

Analyzing all the results obtained in the different aspects of the process optimization study, it is concluded that the present research reaches optimal optimization values, confirming the importance of studying the main points to make the GDE technology industrially applicable. It is concluded that the process is directly influenced by the anode present in the reactor, in a split cell it is evident that the nodes are affected by their potential, aiming at the electrogeneration of H_2O_2 , a part of the species of interest is consumed in the BDD, because of its high potential, when compared to DSA, the latter is more conducive to the application of oxidant electrogeneration. The use of membrane prevents the appearance of scavenged species and that H_2O_2 will be consumed at the anode, thus improving the process, where the efficiency of H_2O_2 generation is increased.

After studying the parametron of single cell and split cell and concluding that split cell provides a greater generation of the species of interest. A new reactor was developed with the specific proposal of electrogeneration H_2O_2 , a cell with small dimensions was developed as a proof of concept, after proving that it is possible to generate H_2O_2 in the proposed reactor and the results are promising, it was necessary to carry out the scall up study of this reactor, in order to evaluate the scalability of the proposed design and also compare with reactors presented in the literature. From the results it is proved that the proposed reactor is scalable and further presented higher values of H_2O_2 electrogenerated and higher FE, reaching a maximum value of 94.48% at current density 100 mA cm^{-2} .

Once determined the best reactor and the best cell configuration condition, the performance of an optimal material, PL6C/BTDA 2%, is tested, seeking to achieve the highest possible efficiency, afterwards, as a final conclusion the best cell configuration was the one using PEM (divided cell), using the tangential-flow 3D printed reactor using the material of

PL6C modified with 2% with benzophenone. FE was achieved (99.99%) without causing a high energy consumption. It's possible to conclude that the study of optimization was effective.

CHAPTER 4. An innovative approach to the application of electrochemical processes based on the *in-situ* generation of H₂O₂ for water treatment

This article was published in Journal of Cleaner Production, 392, Isaac Sánchez-Montes; Géssica O. S. Santos; Taynara O. Silva; Renata Colombo; Marcos R. V. Lanza; “An innovative approach to the application of electrochemical processes based on the in-situ generation of H₂O₂ for water treatment”, 136242, Copyright Elsevier (2023). DOI: 10.1016/j.jclepro.2023.136242

Abstract

This study presents an innovative strategy for the implementation of electrochemical treatment systems based on the *in-situ* generation of H₂O₂ targeted at the removal of organic contaminants in aqueous matrices. Unlike the studies based on the continuous application of electric current, in the present work, the electric power supply was interrupted once desired concentrations of H₂O₂ were accumulated in solutions previously spiked with the contaminant. The accumulated H₂O₂ was then activated by illuminating the solution with UVC light, which gave rise to the process called UVC/ ϕ -H₂O₂. The application of current densities of 10 and 25 mA cm⁻² for only 10 min led to the efficient production of H₂O₂ in concentrations ranging from ~48-112 mg L⁻¹, which resulted in the complete degradation of the antibiotic norfloxacin (NOR; 60 μ mol L⁻¹) and high mineralization rates in the UVC/ ϕ -H₂O₂@10 mA cm⁻² and UVC/ ϕ -H₂O₂@25 mA cm⁻² processes. Moreover, no residual H₂O₂ was detected within 90 min of treatment in both conditions. Although similar results in terms of NOR degradation/mineralization were obtained from the application of the UVC/c-H₂O₂@25 mA cm⁻² process (*i.e.*, based on the continuous application of 25 mA cm⁻²), a significant residual concentration of H₂O₂ (~100 mg L⁻¹) was detected after treatment. Noticeably, the application of the UVC/ ϕ -H₂O₂@25 mA cm⁻² method led to ~26 % reduction in overall energy consumed in the mineralization process compared to the conventional system using the continuous application of electric current.

Keywords: electrochemically-driven processes; hydrogen peroxide; antibiotic degradation; residual oxidant; energy consumption.

Introduction

Over the past few decades, the use of single and hybrid electrochemically-driven processes for water remediation has gained enormous attraction among researchers worldwide (Cheng et al., 2016; Martínez-Huitle et al., 2015; Moreira et al., 2017). These electrochemical technologies have been used to eliminate organic contaminants in aqueous systems where they have been found to produce promising results in terms of degradation and mineralization efficiency (Ganiyu et al., 2018; Garcia-Segura and Brillas, 2017; Martínez-Huitle and Panizza, 2018). In particular, the use of processes based on the electrogeneration of hydrogen peroxide (H_2O_2) has become widely popular, since the *in-situ* production of this oxidant through the cathodic reduction of oxygen (O_2) helps overcome the constraints related to the storage, transportation and management of the reagent (Zhou et al., 2019).

Due to the low solubility of O_2 in aqueous solutions, gas diffusion electrodes (GDE) have been found to be suitable for application as electrode material in the cathodic generation of H_2O_2 with moderate efficiency (Wang, J. et al., 2021). The formation of a triple interface (gas-solid-liquid) in the GDEs contributes significantly toward circumventing the problems related to O_2 solubility and improving H_2O_2 generation compared to the used of planar electrodes (Cordeiro Junior et al., 2022a; Moreira et al., 2019). GDEs have also been applied for water treatment, since H_2O_2 can be activated in solution (*e.g.*, by UVC light) to produce hydroxyl radicals (HO^\bullet), leading to high rates of organic contaminants removal (Dong et al., 2020; Frangos et al., 2016; Khorsandi et al., 2019).

Although the combination of UVC light and electrogenerated H_2O_2 has been extensively studied, especially using the continuous application of electric current (which is referred to as the UVC/*c*- H_2O_2 process in the present work), most of these works have solely been confined to the analysis of the degradation efficiency with no concern for residual H_2O_2 in solution after treatment (Dong et al., 2020; Geraldino et al., 2020; Ye et al., 2019). The continuous application

of current at the cathode and the low quantum efficiency of the photolysis of H_2O_2 at 254 nm ($\Phi_{254\text{nm}} = 0.5 \text{ mol Es}^{-1}$) (Li et al., 2017) can lead to the accumulation of high concentrations of H_2O_2 which remain in solution without activation. As H_2O_2 is a mild oxidizing agent, the discharge of treated water containing high residual levels of H_2O_2 into the environment could be potentially dangerous for phytoplankton, directly impacting aquatic life (Sánchez-Quiles and Tovar-Sánchez, 2014).

Several studies based on the activation of H_2O_2 (not electrogenerated) by UVC light have reported that concentrations of H_2O_2 between 50 and 200 mg L^{-1} are enough for the efficient degradation of different classes of organic pollutants (Cuerda-Correa et al., 2019; Cunha and Teixeira, 2021; Michael et al., 2020); in this sense, the *in-situ* production of H_2O_2 concentrations above this range not only leads to the accumulation of the oxidant at the end of the treatment but also increases the overall energy consumption of the UVC/*c*- H_2O_2 process.

Taking this into account, it is worth to devise strategies in the application of systems based on H_2O_2 electrogeneration that simultaneously helps minimize energy consumption and avoid the accumulation of high residual concentrations of the oxidant after treatment. In this frame, the present study proposes the production of H_2O_2 *in-situ*, electrogenerated for a period of time (*i.e.*, not continuous, namely here as ϕ - H_2O_2), with subsequent activation using UVC light to generate HO^\bullet species capable of oxidizing NOR and its by-products. It is important to emphasize that this processes in different from other studies reported to date where H_2O_2 is added to the reaction medium (*ex-situ* process) (Jung et al., 2012; Lekkerkerker-Teunissen et al., 2012; Wang et al., 2022) or continuously generated and activated (conventional *in-situ* process) (Cordeiro Junior et al., 2022b; Da Costa et al., 2021; Kronka et al., 2023).

The implementation of the UVC/ ϕ - H_2O_2 process was applied to the removal of norfloxacin (NOR) – one of the most widely consumed antibiotics in the world and which is commonly detected in urban wastewater and natural water (Hernandez et al., 2019; Ma et al., 2015;

Tamtam et al., 2008; Zhou et al., 2013). High-performance liquid chromatography (HPLC) and total organic carbon (TOC) analyses were conducted to evaluate the efficiency of the proposed two-step approach in the degradation and mineralization of NOR. Moreover, energetic parameters and residual concentrations of H_2O_2 were also evaluated. Finally, liquid chromatography coupled with mass spectrometry (LC-ESI-MS/MS) was used to detect the main oxidation by-products of the UVC/ ϕ - H_2O_2 process and a suitable NOR degradation pathway was proposed.

Materials and methods

The material and methods section encompasses six main blocks: chemicals, preparation of gas diffusion electrode (GDE), effect of the current density on the accumulation of H_2O_2 , activation of ϕ - H_2O_2 and degradation experiments in the system: UVC/ ϕ - H_2O_2 process, analytical procedures and energetic parameters.

2.1 Chemicals

The following chemicals were used for the conduct of the experiments without any further purification: NOR ($\text{C}_{16}\text{H}_{18}\text{FN}_3\text{O}_3$; >98 % Sigma Aldrich), potassium sulfate (K_2SO_4 ; >99 % Neon), ammonium molybdate ($(\text{NH}_4)_2\text{MoO}_4$; 99 % Sigma Aldrich), hydrochloric acid (HCl ; 37 % Panreac), formic acid (CH_2O_2 ; 85 % Sigma Aldrich) and acetonitrile (CH_3CN ; HPLC grade J.T. Baker). Carbon black (Printex[®] L6; Evonik Ltd.) and poly(tetrafluoroethylene) (PTFE hydrophobic binder; Sealfon) were used for the preparation of the catalytic mass. Commercial carbon cloth was obtained from Zoltek. Ultrapure water (Millipore Milli-Q system, $\rho \geq 18.2$ M Ω cm) was used for the preparation of all solutions.

2.2 Preparation of gas diffusion electrode (GDE)

Commercial carbon cloth modified with a catalytic mass prepared by mixing Printex[®] L6 carbon (*w/w* 80 %) and PTFE (*w/w* 20 %) was used to fabricate the GDE; this was done based on the procedure described in a previous study conducted by the research group to which the

authors belong (Cordeiro Junior et al., 2022a). Briefly, 10 g of the wet catalytic mass was homogeneously dispersed on rectangular carbon cloth (geometric area: 120.2 cm²) and heated at 120 °C for 15 min. Then, the electrode was subjected to hot pressing with the application of 5 tons (in weight) and a fixed temperature of 290 °C for 2 h. Finally, three circular-format GDEs were obtained with a geometric area of 20 cm² each. For further experimental details and morphological and electrochemical characterizations of the electrode, see (Cordeiro Junior et al., 2022a).

2.3 Effect of the current density on the accumulation of H₂O₂

The influence of different current densities ($j = 10, 25$ and 50 mA cm^{-2}) on the accumulation of H₂O₂ in solution was evaluated. All electrolyses were conducted for 60 min using 250 mL of 0.1 mol L⁻¹ K₂SO₄ solution as supporting electrolyte (pH ~7) and temperature of 25 °C. Experiments were performed using a three-electrode cell equipped with an Ag/AgCl (3 mol L⁻¹ KCl) reference electrode, a Pt-coated Ti foil as a counter electrode and a GDE as working electrode. O₂ was injected directly into the GDE (placed at the bottom of the cell) at 0.05 L min⁻¹ and maintained throughout the experiment. A PGSTAT 302N Autolab bipotentiostat controlled by the Nova software was used as a power supply. A schematic representation of the experimental setup can be found in Fig. S1 in the Supplementary Material.

The H₂O₂ accumulated was analyzed spectrophotometrically at 350 nm (Shimadzu UV-1900) following the addition of 0.5 mL of the sample to 4.0 mL of 2.4 mmol L⁻¹ (NH₄)₂MoO₄ solution (Cordeiro Junior et al., 2022b). Based on the H₂O₂ accumulated in solution, current densities of 10 and 25 mA cm⁻² applied for 10 min were selected to be employed for NOR degradation/mineralization under the proposed two-step treatment approach (see next section). At these conditions (10 and 25 mA cm⁻²; 10 min), concentrations of H₂O₂ close to the levels generally employed in the UVC/H₂O₂ (not electrogenerated) process were obtained (Cuerda-Correa et al., 2019; Cunha and Teixeira, 2021; Michael et al., 2020; Rizzo et al., 2018).

2.4 Activation of ϕ -H₂O₂ and degradation experiments in the system: UVC/ ϕ -H₂O₂ process

The rampant disposal of antibiotics into the environment has become a major environmental concern since their presence in aquatic ecosystems has been found to lead to the occurrence of bacterial resistance which poses potential risks to human health (Ben et al., 2019; Polianciuc et al., 2020). Therefore, in the present work, the antibiotic NOR was selected to be studied as a model contaminant.

In the system, H₂O₂ was accumulated in 250 mL of the supporting electrolyte previously spiked with NOR (0.1 mol L⁻¹ K₂SO₄ + 60 μ mol L⁻¹ NOR) by applying 10 and 25 mA cm⁻² to the GDE for 10 min, at which time the electric current was interrupted. Since the application of electric current is interrupted, the process is referred as UVC/ ϕ -H₂O₂, to distinguish it from the conventional approach involving the continuous application of electric current (UVC/*c*-H₂O₂). After that, samples were collected to verify the effect of the anodic oxidation on NOR concentration. The H₂O₂ concentrations obtained in the first 10 min were activated under UVC irradiation for 90 min in order to eliminate NOR and its oxidation by-products from the solution. For the conduct of these experiments, a 9 W UVC lamp (Philips: emission at 254 nm) covered with a quartz tube was introduced into the system. A schematic representation of the experimental setup of the UVC/ ϕ -H₂O₂ process is shown in Fig. S2. To compare the efficiency of the proposed two-step method, experiments were conducted using the UVC/*c*-H₂O₂ system (continuous application of electric current). A control experiment was also carried out using UVC radiation only.

2.5 Analytical procedures

Prior to performing the analyses, the collected samples were filtered using a 0.45 μ m Chromafil[®] Xtra PET filter (Macherey-Nagel) attached to a syringe. The evolution of NOR concentration was monitored by HPLC-UV/DAD (Shimadzu Prominence model LC-20AT) using a Luna C18 column (Phenomenex[®]: 250 mm \times 4.6 mm, 5 μ m particle size) as the

stationary phase and a mixture of 0.15 mmol L⁻¹ formic acid and ACN as the mobile phase. NOR was detected at 275 nm using a gradient elution mode varying the proportion of ACN as follows: from 10 % to 60 % in 6 min, then from 60 % to 100 % in 3 min, and maintained at 100 % for another 3 min. The flow rate was 1 mL min⁻¹, injection volume was 25 µL and temperature of the column was 40 °C. NOR removal was expressed as $(\text{NOR}_t/\text{NOR}_0) \times 100 \%$, where NOR_t and NOR_0 are the values at time t and prior to the experiment.

The mineralization rate (*i.e.*, conversion to CO₂, H₂O and inorganic ions) was monitored by total organic carbon concentration ([TOC]) analysis (Shimadzu model TOC-VCPN) and calculated as $(\text{TOC}_t/\text{TOC}_0) \times 100 \%$, with TOC_t and TOC_0 representing the values at time t and before the experiment.

The oxidation by-products were identified by liquid chromatography coupled to mass spectrometry (LC-ESI-MS/MS); a modular LC system (Shimadzu Prominence LC-20AT) coupled with a triple quadrupole mass spectrometer (Shimadzu LC/MS-8030) was used to conduct these analyses. Separation was carried out using a Shim-pack XR-ODS II column (Shimadzu: 100 mm × 3.0 mm, 2.2 µm particle size) as the stationary phase and a mixture of 0.15 mmol L⁻¹ formic acid and ACN as the mobile phase, at flow rate of 0.8 mL min⁻¹. The gradient elution mode was applied by varying the proportion of ACN according to the following protocol: from 10 % to 37 % in 5 min, then from 37 % to 100 % in 3 min, and finally back to 10 % in 2 min. The mass spectrometer was operated in full scan mode (m/z 50–500) using positive electrospray ionization. The temperatures applied for the desolvation block was 250 °C and to the ion source was 400 °C. Nitrogen was used as a nebulizer (3 L min⁻¹) and desolvation gas (15 L min⁻¹).

2.6 Energetic parameters

The current efficiency (CE) and electrical energy consumption (EC) of the H₂O₂ electrogeneration process were calculated based on eqs. 1 and 2 (Barros et al., 2015; Fortunato et al., 2020):

$$CE (\%) = \frac{2 F [H_2O_2] V}{I t} \times 100\% \quad (1)$$

$$EC (\text{kWh kg}^{-1}) = \frac{1000 E I t}{[H_2O_2] V} \quad (2)$$

where 2 is the number of electrons exchanged for the reduction of O₂ to H₂O₂, F is the Faraday constant (96485 C mol⁻¹), [H₂O₂] is the H₂O₂ concentration (mol L⁻¹ (eq.1) and mg L⁻¹ (eq. 2)), V is the working volume (L), I is the applied electric current (A), E is the cell potential (V) and t is the electrolysis time (s (eq.1) and h (eq. 2)).

To evaluate the electrical energy consumption of the UVC/ ϕ -H₂O₂ and UVC/ c -H₂O₂ processes for NOR and TOC removal, the energy consumption per unit mass (EC_x) was evaluated based on the following equation:

$$EC_x (\text{kWh g}^{-1}) = \frac{E I t_1 + P t_2}{\Delta X V} \quad (3)$$

where E is the cell potential (V), I is the applied electric current (A), P is the nominal power of the UVC lamp (W), ΔX is the concentration variation of NOR or TOC (mg L⁻¹), V is the working volume (L), and t_1 and t_2 are the periods of time (h) associated with the use of electric current and UVC radiation.

Results and discussion

UV-Vis was used to investigate the H₂O₂ accumulated during the experiments, while HPLC, TOC and LC-ESI-MS/MS were the main techniques used to follow NOR degradation and detect the main oxidation by-products.

3.1 Influence of applied electric current density on H₂O₂ accumulation

Since the concentration of H₂O₂ derived from the reduction of O₂ on carbon-based cathodes is the backbone of many electrochemically-driven processes (anodic oxidation, UVC/c-H₂O₂, electro-Fenton, photoelectro-Fenton, among others), analyzing the effects of the applied experimental parameters on the *in-situ* electrogeneration of H₂O₂ is found to be crucially important. Bearing that in mind, an analysis was carried out to evaluate the effect of different current densities (ranging from 10 to 50 mA cm⁻²) on the generation and accumulation of H₂O₂ in 60 min of electrolysis.

It can be observed in Fig. 1 that there is a linear increase in H₂O₂ concentration in the first 20 min of electrolysis (please see Fig. S3 and Table S1 for pseudo-order-zero kinetics constants), where H₂O₂ is produced via the reduction of O₂ through the widely accepted two-electron (2e⁻) transfer mechanism (Barros et al., 2015; Pan et al., 2018). However, after 30 min of electrolysis, the concentration of H₂O₂ reaches or is near to reach a steady-state; this phenomenon can be attributed to the side/parallel reactions that promote the decomposition of H₂O₂ via different pathways, including self-decomposition (eqs. 4-6), cathodic reduction to H₂O₂ (eq. 7) and O₂ formation via anodic oxidation (eq. 8) (Barros et al., 2015; Pan et al., 2018; Rosales et al., 2012).



The huge amount of H₂O₂ produced at the end of the experiments (*e.g.*, >500 mg L⁻¹ based on the application of 50 mA cm⁻² in 60 min) is found to be higher than the quantity typically employed/required for the degradation of pollutants in advanced oxidation processes (AOPs).

However, suitable amounts of H_2O_2 (ranging from 48 to 200 mg L^{-1}) were accumulated in the system in only 10 min of electrolysis after the application of 10, 25 and 50 mA cm^{-2} (see dashed line in Fig. 1). As mentioned above, concentrations in this range have been efficiently applied for the degradation of organic pollutants after the activation of the H_2O_2 under UVC light. So, 10 min was selected as the suitable electrolysis time for application in the first step of the UVC/ ϕ - H_2O_2 treatment system proposed in this study.

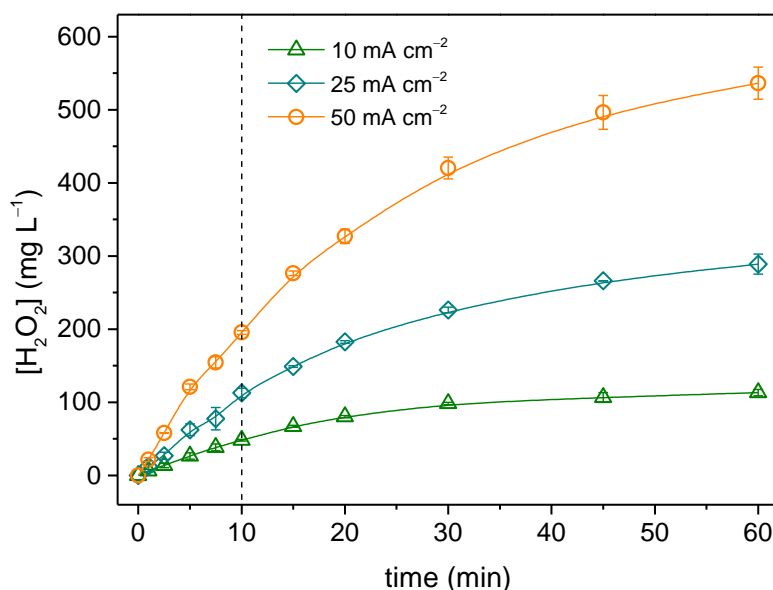


Fig. 1. Accumulation of H_2O_2 in solution over time. Conditions: $j = 10, 25$ and 50 mA cm^{-2} , supporting electrolyte = $0.1 \text{ mol L}^{-1} \text{ K}_2\text{SO}_4$, $\text{pH} \sim 7$ and $T = 25 \text{ }^\circ\text{C}$. The dashed line refers to the concentration of H_2O_2 accumulated in 10 min of electrolysis.

Considering that current efficiency (CE) and energy consumption (EC) are among the key parameters for determining the economic viability of an electrochemical system applied toward H_2O_2 production, these parameters were calculated based on eqs. 1 and 2, for 10 min of electrolysis. As seen in Fig. 2, although the application of current densities of 10 ($56.5 \pm 1.4 \%$) and 25 mA cm^{-2} ($53.1 \pm 2.3 \%$) yielded similar CE values, there was an increase in EC from 8.6 ± 0.2 to $15.1 \pm 0.9 \text{ kWh kg}^{-1}$, respectively. A further increase in current density to 50 mA cm^{-2} also led to an increase in EC ($24.3 \pm 0.3 \text{ kWh kg}^{-1}$); however, the CE percentage was found to be lower than 50 % probably due to increased side reactions caused by the rise in current

density. Although the application of current density of 25 mA cm^{-2} resulted in a 1.75-fold increase in EC compared to the value obtained at 10 mA cm^{-2} , the amount of H_2O_2 produced at 25 mA cm^{-2} in 10 min was 2.34-fold higher than the amount produced at 10 mA cm^{-2} . Based on these observations, 10 and 25 mA cm^{-2} were selected as current densities for the conduct of subsequent experiments involving NOR degradation and mineralization.

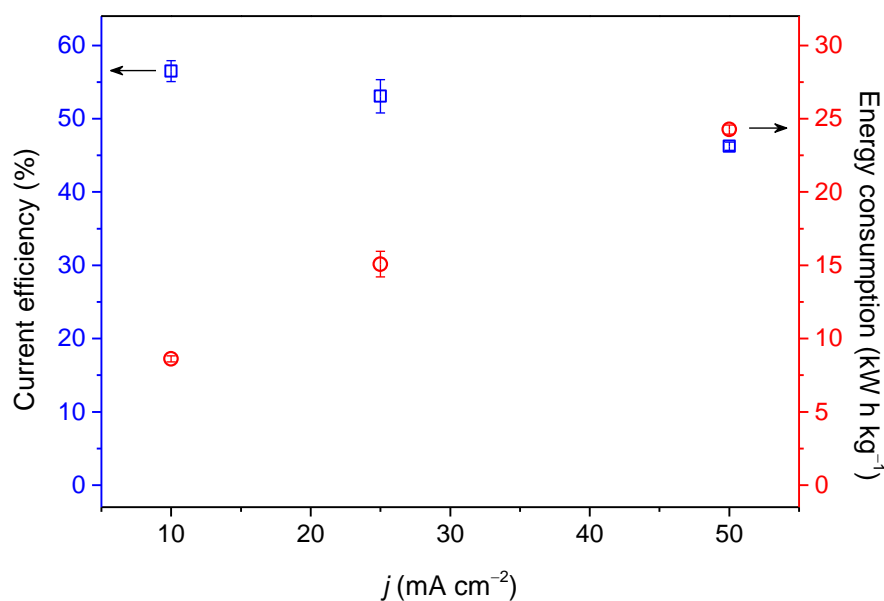


Fig. 2. Current efficiency and energy consumption for 10 min of electrolysis as a function of current density. Conditions: $j = 10, 25$ and 50 mA cm^{-2} , supporting electrolyte = $0.1 \text{ mol L}^{-1} \text{ K}_2\text{SO}_4$, pH ~ 7 and $T = 25 \text{ }^\circ\text{C}$.

3.2 Application of the UVC/ ϕ - H_2O_2 process on NOR oxidation

Fig. 3 shows the percentage of NOR degradation over time based on the application of different treatment processes. First, a control experiment was carried out in order to evaluate the extent of NOR photodegradation ($60 \text{ } \mu\text{mol L}^{-1}$) in aqueous solution using only UVC radiation (*i.e.*, without H_2O_2 electrogeneration). As can be noted, a significant amount of NOR was removed (45 %) in 12.5 min of irradiation under UVC light. Several fluoroquinolone antibiotics, including NOR, have been reported to undergo oxidation reactions by UVC radiation even under a short period of exposure (Snowberger et al., 2016). The main reactions involved in the phototransformation of NOR are the cleavage of the quinolone and piperazine rings (Babić et

al., 2013). However, it should be noted that although a high percentage of degradation was achieved in the present study, a high number of recalcitrant by-products may remain in solution at relevant environmental concentrations.

The degradation of NOR was also evaluated through the application of the UVC/*c*-H₂O₂ and UVC/*ϕ*-H₂O₂ systems. In the UVC/*c*-H₂O₂ process, current density (only for 25 mA cm⁻²) and UVC irradiation were applied simultaneously and continuously throughout the treatment, whereas in the UVC/*ϕ*-H₂O₂ process, the concentrations of H₂O₂ were accumulated in only 10 min of electrolysis by applying current densities of 10 (~48 mg L⁻¹) and 25 mA cm⁻² (~112 mg L⁻¹) and subsequently irradiating the system with UVC light to initiate the experiment. For the UVC/*ϕ*-H₂O₂ experiments, nearly 20 % of NOR degradation was observed after application of 10 and 25 mA cm⁻² for 10 min in dark conditions, *i.e.*, before turning on the UVC lamp. Due to this, the degradation percentage was normalized as a function of the NOR₀ concentration in the UVC/*ϕ*-H₂O₂ processes, as can be seen in Fig. 3.

As can be seen, the application of the UVC/*c*-H₂O₂@25 mA cm⁻² system and both UVC/*ϕ*-H₂O₂ (@10 and 25 mA cm⁻²) processes led to the complete removal of NOR within 12.5 min of treatment. The effect of H₂O₂ electrogenerated continuously (namely *c*-H₂O₂@25 mA cm⁻²) was also evaluated. As expected, the effect of H₂O₂ alone towards NOR degradation was low (62.8 % NOR removal in 20 min with no TOC removal) as previously reported in literature for other antibiotics of fluoroquinolone class (Lima et al., 2020; Silva et al., 2022). The significant improvement in NOR degradation can mostly be attributed to the activation of H₂O₂ by UVC radiation according to eq. 9 (Oh et al., 2016; Zhang et al., 2019) to produce mainly HO[•] species, which in turn react with NOR and its degradation by-products via hydroxylation reactions (section 3.4).



Interestingly, although in the UVC/ ϕ -H₂O₂ processes the power supply was interrupted in 10 min, no significant differences in NOR degradation were observed between these processes and the UVC/*c*-H₂O₂ system where electric current was applied continuously.

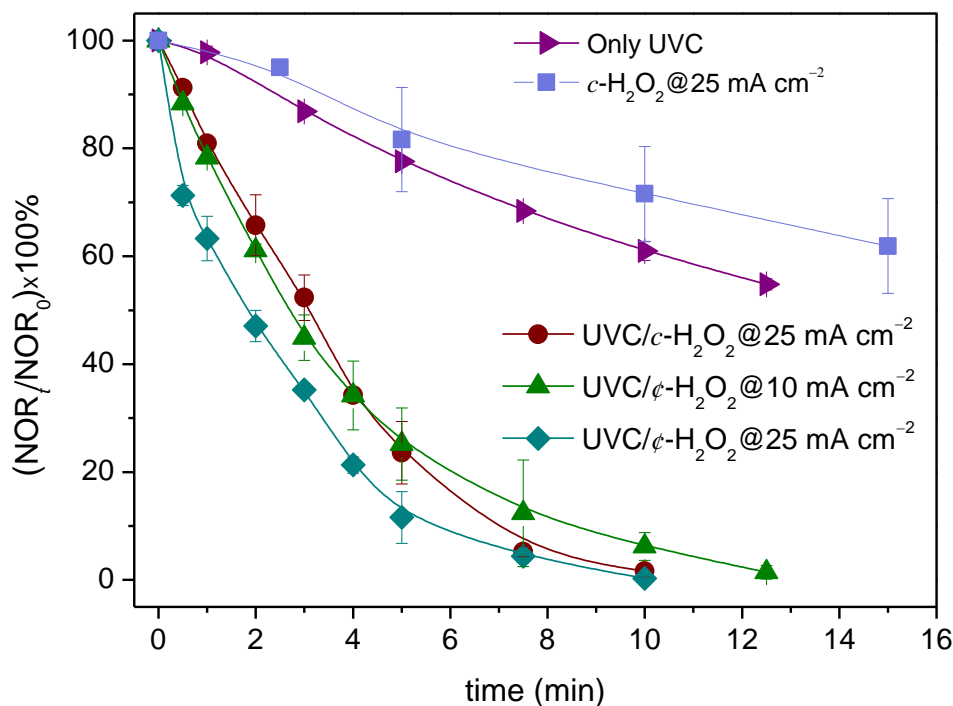


Fig. 3. NOR removal based on the application of the treatment processes investigated. Conditions: supporting electrolyte = 0.1 mol L⁻¹ K₂SO₄ + 60 μmol L⁻¹ NOR, $j = 10$ and 25 mA cm⁻², pH ~7 and T = 25 °C. In the UVC/ ϕ -H₂O₂ processes, the electric current supply was interrupted within 10 min, and then the UVC lamp was turned on.

The pseudo-first order kinetic constant (k_{1st}) values obtained relative to NOR degradation is presented in Table S2. As expected, the photochemical process recorded a lower degradation rate ($0.5 \pm 0.04 \times 10^{-1} \text{ min}^{-1}$; $R^2 = 0.99 \pm 0.0$) compared to the other treatment processes. The k_{1st} obtained for the coupled processes exhibited the following order: UVC/ ϕ -H₂O₂@25 mA cm⁻² > UVC/*c*-H₂O₂@25 mA cm⁻² > UVC/ ϕ -H₂O₂@10 mA cm⁻², with values of $5.4 \pm 0.5 \times 10^{-1}$ ($R^2 = 0.94 \pm 0.01$), $4.4 \pm 0.8 \times 10^{-1}$ ($R^2 = 0.96 \pm 0.03$) and $3.4 \pm 0.2 \times 10^{-1}$ ($R^2 = 0.94 \pm 0.06$) min⁻¹, respectively. For the UVC/ ϕ -H₂O₂ processes, the rate constant obtained from the application of the current density of 25 mA cm⁻² was found to be slightly higher (1.6 times) than that obtained

at 10 mA cm^{-2} ; this is probably due to the higher amount of HO^\bullet produced at 25 mA cm^{-2} , since there was a greater amount of H_2O_2 available to be activated.

On the other hand, as it has been well established in the literature, when the system contains a high initial concentration of H_2O_2 (over 100 mg L^{-1}), secondary/parallel reactions (radical recombination, self-scavenging reactions, etc.) that occur alongside the main reaction tend to have a negative effect on the efficiency of the AOPs in the removal of organic contaminants (Table S2: secondary reactions of the UVC/ H_2O_2 process). Santos *et al.* investigated the application of the UVC/ H_2O_2 (oxidant was added at the beginning of the experiment) process for NOR degradation at neutral pH using different concentrations of H_2O_2 ; based on their findings, the use of H_2O_2 concentrations higher than $\sim 120 \text{ mg L}^{-1}$ did not have any positive effect on the contaminant degradation kinetics (de Souza Santos *et al.*, 2015). The authors also observed that complete removal of NOR ($45 \text{ } \mu\text{mol L}^{-1}$) was only achieved after 100 min of treatment.

Shankaraiah *et al.* (2016) also investigated NOR ($\sim 470 \text{ } \mu\text{mol L}^{-1}$) degradation by the application of the UVC/ H_2O_2 process at neutral pH where the authors observed that increasing H_2O_2 concentration enhances oxidation to a certain level, since H_2O_2 acts as a free-radical scavenger itself; the authors also showed that an increase in the concentration of H_2O_2 from 100 to 200 mg L^{-1} only resulted in 10 % improvement in the percentage of NOR degradation (from 60 to 70 %), which decreased to 65 % when the concentration of the oxidant was increased to 250 mg L^{-1} (Shankaraiah *et al.*, 2016). Taking these observations into account, it is clear that the strategy involving the electrogenerating H_2O_2 in concentrations higher than 100 mg L^{-1} is not the most suitable for the degradation of contaminants, since increases the energy consumption of the process and high concentrations of the oxidant may affect the kinetics and removal efficiency of the system. In the present work it was observed that that continuous electrogeneration of H_2O_2 (which also led to higher H_2O_2 concentrations - up to about 287 mg

L^{-1}) does not lead to an improvement in degradation compared to the proposed approach (UVC/ ϕ -H₂O₂@25 mA cm⁻²). This is probable evidence that excessive H₂O₂ concentrations may not be beneficial for the degradation processes.

At this point, it is important to consider the TOC removal data to obtain information about the mineralization extent at the end of the different treatments employed, which were photochemical only, UVC/*c*-H₂O₂ and UVC/ ϕ -H₂O₂ processes (see Fig. 4). As expected, NOR photodegradation did not lead to a high mineralization rate (*i.e.*, less than 15 % of TOC removal), showing that although the NOR molecule is photosensitive, the by-products formed are recalcitrant toward oxidation by UVC light. Furthermore, the mineralization percentage after electrolysis in dark conditions at 10 and 25 mA cm⁻² in 10 min was negligible.

In contrast, high percentages of TOC removal could be attained with the combination of H₂O₂ electrogenerated and UVC light. As can be observed in Fig. 4 the UVC/ ϕ -H₂O₂@25 mA cm⁻² process was slightly more efficient than the UVC/*c*-H₂O₂@25 mA cm⁻² in terms of TOC removal attaining 80.3±3.6 % mineralization. Although the difference in mineralization between the UVC/ ϕ -H₂O₂@25 mA cm⁻² and UVC/*c*-H₂O₂@25 mA cm⁻² (76.8±5.0 %) processes is not quite obvious, the continuous application of electric current in the latter process has a significant impact on the overall energy consumption of the process (see discussion in section 3.3). Finally, the lowest TOC removal was observed for the UVC/ ϕ -H₂O₂@10 mA cm⁻² (64.5±7.8 %) system, which can be explained by the lower amount of H₂O₂ accumulated, which in turn led to less oxidant activation (less amount of HO[•] species).

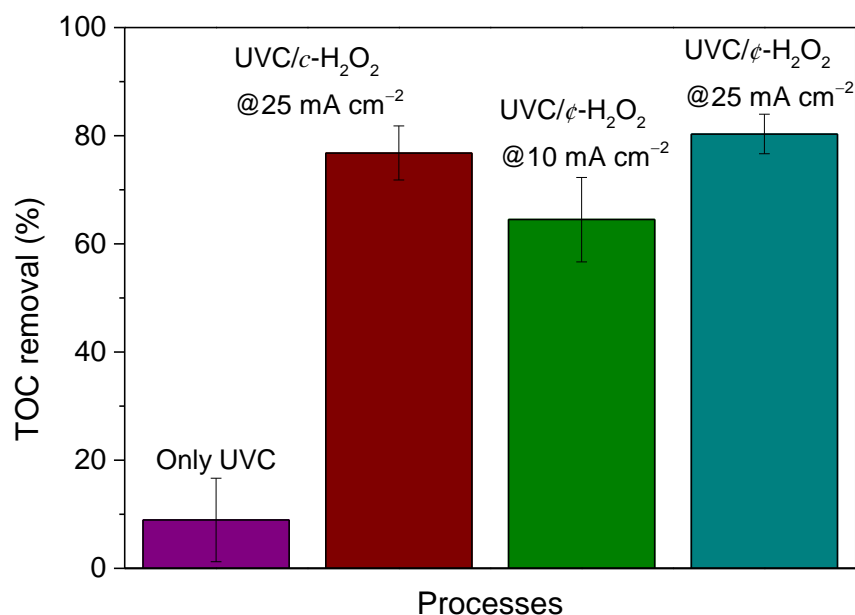


Fig. 4. TOC removal based on the application of the treatment processes investigated. Conditions: supporting electrolyte = 0.1 mol L⁻¹ K₂SO₄ + 60 μmol L⁻¹ NOR, $j = 10$ and 25 mA cm⁻², pH ~7 and T = 25 °C. In the UVC/*φ*-H₂O₂ processes, the electric current supply was interrupted within 10 min, and then the UVC lamp was turned on for 90 min.

For purposes of comparison, Santos *et al* (2015). reported to have obtained only 32 % of TOC removal after 60 min of treatment under the UVC/H₂O₂ process (de Souza Santos et al., 2015). Sánchez-Montes *et al.* (2018) obtained ~70 % of TOC removal after 720 min of electrolysis which was conducted using an electrochemical system with Ti/β-PbO₂-PTFE anode (Sánchez-Montes et al., 2018). Özcan *et al.* (2016) also reported to have obtained a high rate of NOR mineralization (~98 %) in 300 min of electrolysis based on the application of the electro-Fenton process using boron-doped diamond (as the anode) and carbon felt (as the cathode) in the presence of 0.1 mmol L⁻¹ Fe³⁺ ion (Özcan et al., 2016).

A matter scarcely addressed in processes involving continuous and *in-situ* H₂O₂ electrogeneration is the monitoring of the residual oxidant concentration. Most studies in the literature have been confined solely to the analysis in terms of contaminants removal without concern for the residual H₂O₂ which remains in the bulk solution after electrolysis. GDE mainly

based on carbonaceous materials have been widely applied for H₂O₂ production and electrochemical degradation of organic pollutants in aqueous media. Typically, the H₂O₂ concentrations accumulated in these GDE carbon-based systems range between 50 and 700 mg L⁻¹ or even higher depending on the carbon matrix used, the current density applied, the electrolysis time and other variables (Fortunato et al., 2020; Wang, J. et al., 2021; Zhang et al., 2022). In this regard, monitoring H₂O₂ concentration during and after treatment in these systems is an important issue that needs be addressed.

Fig. 5 shows the results obtained from the analysis of H₂O₂ consumption over time using the UVC/ ϕ -H₂O₂ processes. The dashed lines in the figure refer to the average initial H₂O₂ concentration accumulated after 10 min of electrolysis. Here, it is worth noting that the percentage of H₂O₂ consumption was almost 100 % in both conditions (UVC/ ϕ -H₂O₂@10 mA cm⁻² and UVC/ ϕ -H₂O₂@25 mA cm⁻²); in other words, there was no significant concentration of H₂O₂ in the solution after treatment. Interestingly, the residual concentration of H₂O₂ in the treated solution by using the UVC/ c -H₂O₂@25 mA cm⁻² process was ~100 mg L⁻¹ after 90 min of treatment (data not shown). These results show that the methodology proposed in this study is highly efficient for obtaining high rates of degradation and mineralization without generating residual H₂O₂ concentration observed under the conventional approach which involves the continuous application of electric current in the treatment process.

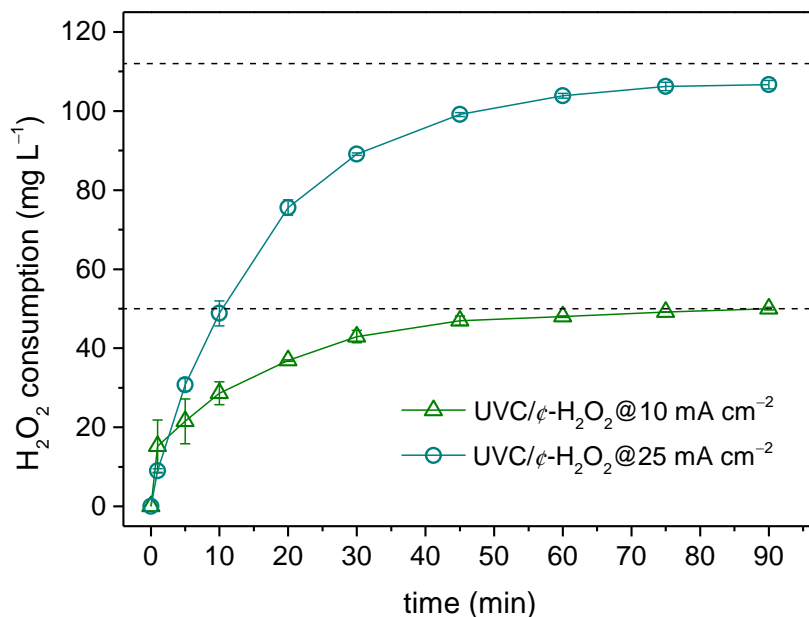


Fig. 5. H₂O₂ consumption over time using the UVC/ ϕ -H₂O₂ processes. Conditions: supporting electrolyte = 0.1 mol L⁻¹ K₂SO₄ + 60 μ mol L⁻¹ NOR, j = 10 and 25 mA cm⁻², pH \sim 7 and T = 25 °C. The dashed lines refer to the initial concentration of H₂O₂ electrogenerated after 10 min of electrolysis.

On the other hand, the consumption rates of H₂O₂ in 90 min under the application of the UVC/ ϕ -H₂O₂@10 mA cm⁻² and UVC/ ϕ -H₂O₂@25 mA cm⁻² processes were 0.55 ($R^2 = 0.81$) and 1.2 mg L⁻¹ ($R^2 = 0.86$) H₂O₂ min⁻¹, respectively. Although these values point to a linear relationship with the initial accumulated H₂O₂ concentration, as discussed above, the efficiency of the process and the initial concentration of H₂O₂ are correlated up to a certain level. It should be pointed out however that the main limitations H₂O₂-based process lie in its intrinsic properties – one such property is the low quantum yield (0.5 mol Es⁻¹ at 254 nm) (Li et al., 2017) measured for H₂O₂ photolysis, which is a major constraint specially in systems based on the continuous electrogeneration of H₂O₂ – such as UVC/ c -H₂O₂.

3.3 Analysis of energetic parameters

An analysis was carried out in order to evaluate the energy consumption per mass (EC_X) of NOR and TOC removed based on the application of the UVC/ c -H₂O₂@25 mA cm⁻² and

UVC/ ϕ -H₂O₂ processes (see Table S3). Although the pseudo-first order kinetic constant for NOR removal was higher for the UVC/ ϕ -H₂O₂@25 mA cm⁻² system compared to the UVC/*c*-H₂O₂@25 mA cm⁻² and UVC/ ϕ -H₂O₂@10 mA cm⁻², no significant differences were observed in terms of kWh g⁻¹ NOR removed when these processes were applied (EC_{NOR} values were ~0.4 kWh g⁻¹ NOR). Nevertheless, from an environmental viewpoint, TOC removal is a more suitable parameter to evaluate the efficiency of a treatment technology, since not only the removal of the target molecule is considered but also that of its oxidation by-products. In this study, EC_{TOC} values were found to be significantly higher than those obtained for NOR removal (at least 14 times higher), this is essentially because the mineralization of an organic molecule is a much more difficult process to achieve.

According to current density applied in the UVC/ ϕ -H₂O₂ processes different amount of H₂O₂ is generated initially. As previously commented the lower amount of H₂O₂ accumulated is correlated with less oxidant activation by UVC light. As expected, a positive effect on the EC_{TOC} values by using ~112 mg L⁻¹ at current density of 25 mA cm⁻² (5.7±0.22 kWh g⁻¹ TOC) can be observed, while in the same period the application of an initial H₂O₂ concentration of ~48 mg L⁻¹ at current density of 10 mA cm⁻² yielded a value of 6.9±0.35 kWh g⁻¹ TOC. Most importantly, the EC_{TOC} value obtained for the UVC/ ϕ -H₂O₂@25 mA cm⁻² process was found to be lower than the obtained for the UVC/*c*-H₂O₂@25 mA cm⁻² system. The amount of energy consumed under the UVC/ ϕ -H₂O₂@25 mA cm⁻² process was found to be approximately 26 % lower compared to the conventional process which involves the continuous supply of electric current. Clearly, the new treatment approach proposed in this study has proven to be highly more efficient and represents a significant energy-saving mechanism for the treatment of pollutants in water matrices.

3.4 Identification of by-products and NOR degradation pathway

To verify whether the main oxidation mechanism of the UVC/ ϕ -H₂O₂@25 mA cm⁻² process occurs through the attack of HO[•] species produced by the activation of accumulated H₂O₂, the by-products generated during the degradation of NOR were identified by LC-ESI-MS/MS analysis. Based on the values of molecular ions and fragments obtained and a comparative analysis conducted using previous studies, it is possible to identify the chemical structures of the main by-products detected (see Table 3). Throughout the degradation process, fourteen by-products were identified (Fig. S4 shows the chromatographic peaks of NOR and its oxidation by-products relative to retention time).

As can be noted in Fig. 6, it was confirmed that the degradation of NOR occurred mainly through the attack of HO[•] on the rings (piperazine and quinolone) of the target molecule or on the organic substituents (fluorine and acid moieties) present on these rings. The formation of the fourteen by-products followed the next three pathways: I) defluorination, II) dehydroxylation and III) simultaneous or successive transformations of the piperazine ring. The occurrence of these different pathways is mainly due to the different attack positions of HO[•] on the target molecule; however, it can be noted the existence of a dominant route related to the radical attack on the NOR molecule in the piperazine ring (pathway III).

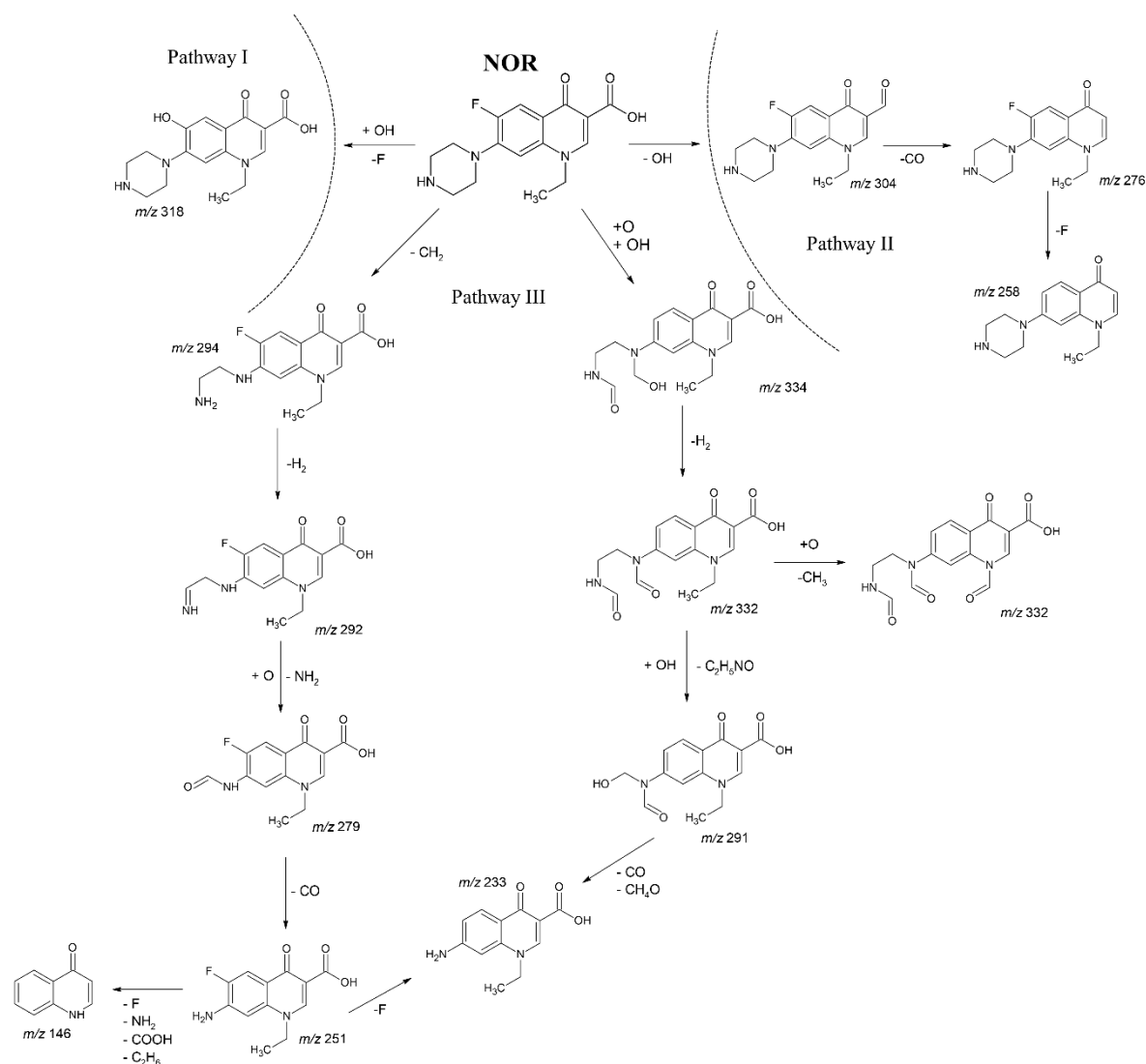


Fig. 6 – Proposed pathway for NOR degradation based on the application of the UVC/ ϕ - H_2O_2 @25 mA cm^{-2} process.

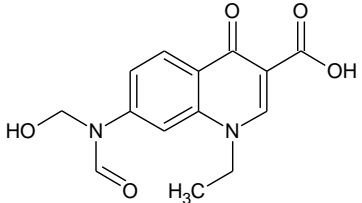
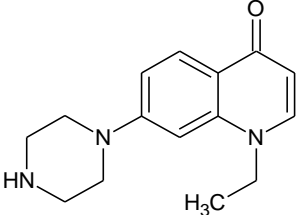
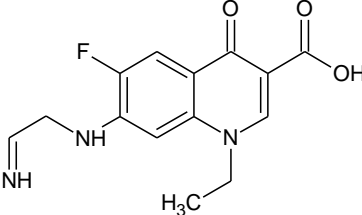
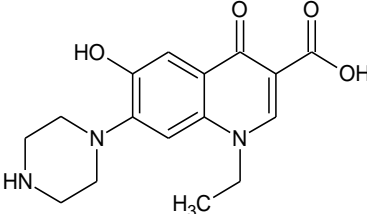
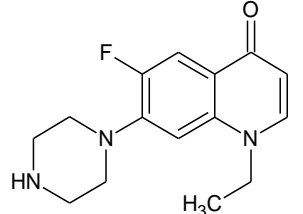
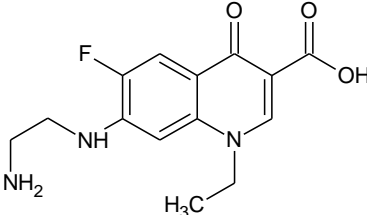
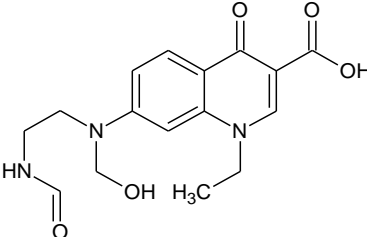
Under the degradation pathway I, defluorination occurred initially and this was followed by hydroxylation, giving the formation of the by-product **4** (m/z 318). Under pathway II, dehydroxylation occurred in NOR, and this yielded by-products **2** (m/z 258), **5** (m/z 276) and **11** (m/z 304). The structure of by-product **11** was characterized by the loss of the hydroxyl group (17 Da) from the acid moiety and this was confirmed by the characteristic fragments of this compound which have already been reported in previous studies involving NOR degradation (Guo et al., 2016). Compound **5** was identified by the loss of a unit of the carbonyl group (28 Da) from the by-product **11**. The decarboxylation reaction of NOR has also been

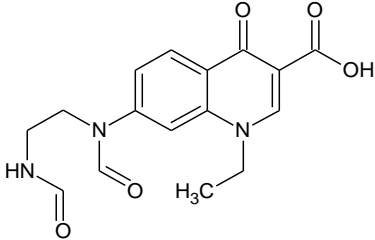
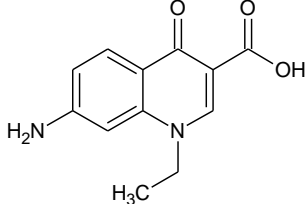
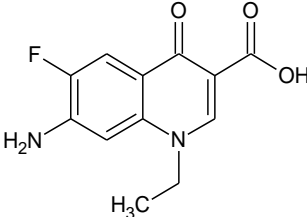
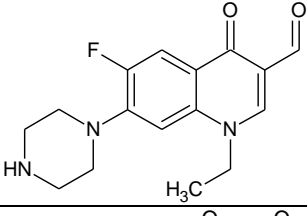
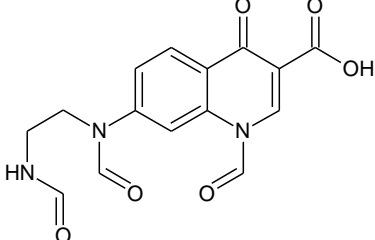
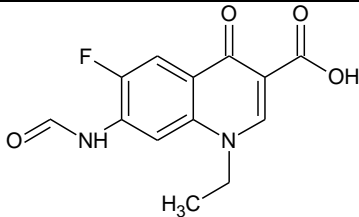
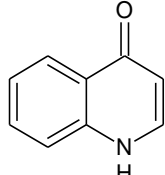
previously reported in previous studies (Wang, C. et al., 2021; Zhang et al., 2021). By-product **2** was formed after compound **5** via the cleavage of the C-F bond on the quinolone ring and the consequent loss of fluorine.

The following ten by-products were identified under pathway III: **1** (m/z 291), **3** (m/z 292), **6** (m/z 294), **7** (m/z 334), **8** (m/z 332), **9** (m/z 233), **10** (m/z 251), **12** (m/z 332), **13** (m/z 279) and **14** (m/z 146). These by-products were generated through the attack of $\cdot\text{OH}$ radical on the nitrogen of the piperazine ring, leading to its cleavage; this phenomenon was either accompanied or not by the loss of fluorine in the NOR structure. Compounds **1**, **7**, **8**, **12** and **13** were derived from the simultaneous or successive oxidation that occurred in the piperazine ring. With the exception of by-product **13**, the oxidation was accompanied by the defluorination of NOR. The complete cleavage of the piperazine ring led to the formation of by-products **9** and **10**. In the case of by-product **10**, the cleavage of the piperazine ring was accompanied by defluorination. Compounds **3** and **6** were derived from the partial elimination of the piperazine ring and, in the case of compound **3**, by the formation of the imine group (Babić et al., 2013; Ding et al., 2017; Zhang et al., 2021). Finally, by-product **14** was probably derived from compound **10** through the loss of $-\text{NH}_2$ (18 Da) and $-\text{C}_2\text{H}_6$ (30Da) and the occurrence of defluorination and decarboxylation of the piperazine ring.

In essence, although these pathways have been previously reported in studies involving NOR degradation based on the application of a wide range of AOPs (photocatalysis, ozonation, thermal activation of persulfate, among others (Jin et al., 2019; Wang, C. et al., 2021; Zhang et al., 2021), to the best of our knowledge, this is the first study that has been able to identify the formation of by-products **1**, **2**, **3**, **13** and **14**.

Table 3 – LC-ESI-MS/MS data and the proposed chemical structure of NOR by-products detected during the treatment using UVC/ ϕ -H₂O₂@25 mA cm⁻² process.

By-product	Retention time (min)	[M+H] ⁺ (<i>m/z</i>)	Proposed chemical structure
1	0.52	291	
2	0.78	258	
3	1.08	292	
4	1.59	318	
5	1.78	276	
6	2.12	294	
7	2.22	334	

8	3.42	332	
9	3.77	233	
10	4.61	251	
11	6.89	304	
12	7.33	332	
13	8.46	279	
14	9.01	146	

Conclusions

An alternative approach to the continuous application of electric current in systems based on the *in-situ* generation of H₂O₂ was successfully applied in the present study, where the H₂O₂ is

still produced *in-situ* (for a period of time of 10 min) but not continuously in a process named as UVC/ ϕ -H₂O₂. From this study the main conclusions can be drawn:

- The application of a current density of 25 mA cm⁻² for only 10 min were effective to generate concentrations of H₂O₂ ~112 mg L⁻¹. Under these conditions, the UVC/ ϕ -H₂O₂@25 mA cm⁻² process was found to be equally efficient as the UVC/*c*-H₂O₂@25 mA cm⁻² system (continuous application of electric current) when it comes to the complete degradation of NOR in short periods of treatment.
- Although similar results were obtained for TOC removal in 90 min of treatment using the two experimental approaches investigated. Compared to the residual H₂O₂ concentration of ~100 mg L⁻¹ detected in the UVC/*c*-H₂O₂ system, the UVC/ ϕ -H₂O₂ process exhibited no significant residual oxidant concentration after treatment. Evidently, from an environmental viewpoint, the conventional approach which involves the continuous application of electric current is less suitable because the treated solution requires an additional treatment prior to its “safe” disposal into the environment.
- The energy consumptions for NOR and TOC removal were found to be lower in the UVC/ ϕ -H₂O₂@25 mA cm⁻² process compared to the other treatment processes. Notably, EC_{TOC} value in the UVC/ ϕ -H₂O₂@25 mA cm⁻² process was ~26 % lower compared to the UVC/*c*-H₂O₂ system.
- LC-EIS-MS/MS analysis led to the detection of several hydroxylated by-products, confirming that degradation of NOR occurs through the attack of the HO[•] species generated during the UVC/ ϕ -H₂O₂@25 mA cm⁻² treatment.

Therefore, the approach proposed in the present study is a suitable way to apply electrochemical systems based on the *in-situ* generation of H₂O₂, apart from leading to high rates of organic

compounds oxidation, helps prevent the accumulation of residual concentrations of H₂O₂ in the treated solution and reduces the overall energy consumption of the process.

Finally, future scope for this application includes involves upscale studies in large scale flow reactors using real water matrices, since the present study was conducted at a laboratory scale using a model antibiotic contaminant. This approach can be also applied for the generation of other oxidants of interest and would be valuable to elucidate mechanisms by means of scavenger experiments at batch and flow conditions in future studies.

Acknowledgments

The authors are grateful to the following Brazilian research funding agencies for the financial assistance provided in support of this research: São Paulo Research Foundation (FAPESP grants: #2014/50945-4, #2017/10118-0, #2020/07351-7, #2020/02743-4 and #2019/08701-4), National Council for Scientific and Technological Development (CNPq grants: #303759/2014-3 and #303943/2021-1) and the Coordination for the Improvement of Higher Education Personnel (CAPES: Finance Code 001).

References

- Babić, S., Periša, M., Škorić, I., 2013. Photolytic degradation of norfloxacin, enrofloxacin and ciprofloxacin in various aqueous media. *Chemosphere* 91(11), 1635-1642.
- Barros, W.R., Ereno, T., Tavares, A.C., Lanza, M.R., 2015. In situ electrochemical generation of hydrogen peroxide in alkaline aqueous solution by using an unmodified gas diffusion electrode. *ChemElectroChem* 2(5), 714-719.
- Ben, Y., Fu, C., Hu, M., Liu, L., Wong, M.H., Zheng, C., 2019. Human health risk assessment of antibiotic resistance associated with antibiotic residues in the environment: A review. *Environ. res.* 169, 483-493.
- Cheng, M., Zeng, G., Huang, D., Lai, C., Xu, P., Zhang, C., Liu, Y., 2016. Hydroxyl radicals based advanced oxidation processes (AOPs) for remediation of soils contaminated with organic compounds: a review. *Chem. Eng. J.* 284, 582-598.
- Cordeiro-Junior, P.J.M., Jiménez, C.S., de Vasconcelos Lanza, M.R., Rodrigo, M.A.R., 2022a. Electrochemical production of extremely high concentrations of hydrogen peroxide in discontinuous processes. *Sep. Purif. Technol.* 300, 121847.
- Cordeiro-Junior, P.J.M., Martins, A.S., Pereira, G.B.S., Rocha, F.V., Rodrigo, M.A.R., de Vasconcelos Lanza, M.R., 2022b. Bisphenol-S removal via photoelectro-fenton/H₂O₂ process using Co-porphyrin/Printex L6 gas diffusion electrode. *Sep. Purif. Technol.* 285, 120299.

- Cuerda-Correa, E.M., Alexandre-Franco, M.F., Fernández-González, C., 2019. Advanced oxidation processes for the removal of antibiotics from water. An overview. *Water* 12(1), 102.
- Cunha, I.L.C., Teixeira, A.C.S.C., 2021. Degradation of pesticides present in tomato rinse water by direct photolysis and UVC/H₂O₂: optimization of process conditions through sequential Doehlert design. *Environ. Sci. Pollut. Res.* 28(19), 24191-24205.
- Da Costa, A.J., Kronka, M.S., Cordeiro-Junior, P.J., Fortunato, G.V., dos Santos, A.J., Lanza, M.R., 2021. Treatment of Tebuthiuron in synthetic and real wastewater using electrochemical flow-by reactor. *J. Electroanal. Chem.* 882, 114978.
- de Souza Santos, L.V., Meireles, A.M., Lange, L.C., 2015. Degradation of antibiotics norfloxacin by Fenton, UV and UV/H₂O₂. *J. Environ. Manage.* 154, 8-12.
- Ding, D., Liu, C., Ji, Y., Yang, Q., Chen, L., Jiang, C., Cai, T., 2017. Mechanism insight of degradation of norfloxacin by magnetite nanoparticles activated persulfate: identification of radicals and degradation pathway. *Chem. Eng. J.* 308, 330-339.
- Dong, H., Dong, B., Sun, L., Chi, Z., Wang, M., Yu, H., 2020. Electro-UV/H₂O₂ system with RGO-modified air diffusion cathode for simulative antibiotic-manufacture effluent treatment. *Chem. Eng. J.* 390, 124650.
- Fortunato, G.V., Kronka, M.S., dos Santos, A.J., Ledendecker, M., Lanza, M.R., 2020. Low Pd loadings onto Printex L6: synthesis, characterization and performance towards H₂O₂ generation for electrochemical water treatment technologies. *Chemosphere* 259, 127523.
- Frangos, P., Shen, W., Wang, H., Li, X., Yu, G., Deng, S., Huang, J., Wang, B., Wang, Y., 2016. Improvement of the degradation of pesticide deethylatrazine by combining UV photolysis with electrochemical generation of hydrogen peroxide. *Chem. Eng. J.* 291, 215-224.
- Ganiyu, S., Zhou, M., Martínez-Huitle, C., 2018. Heterogeneous EF and photoEF processes: a critical review of fundamental principles and application for water/wastewater treatment. *Appl Catal B Environ* 235, 103-129.
- Garcia-Segura, S., Brillas, E., 2017. *Journal of Photochemistry and Photobiology C: photochemistry Reviews Applied photoelectrocatalysis on the degradation of organic pollutants in wastewaters. Journal Photochem. Photobiol. C: Photochem. Rev.* 31, 1-35.
- Geraldino, H.C., Freitas, T.K., Manholer, D.D., França, F., Oliveira, J.H., Volnistem, E.A., Lima, A.R., Bertotti, M., Girotto, E.M., Garcia, J.C., 2020. Electrochemical generation of H₂O₂ using gas diffusion electrode improved with rGO intensified with the Fe₃O₄/GO catalyst for degradation of textile wastewater. *J. Water Process Eng.* 36, 101377.
- Guo, H., Gao, N., Yang, Y., Zhang, Y., 2016. Kinetics and transformation pathways on oxidation of fluoroquinolones with thermally activated persulfate. *Chem. Eng. J.* 292, 82-91.
- Hernandez, F., Calisto-Ulloa, N., Gómez-Fuentes, C., Gómez, M., Ferrer, J., González-Rocha, G., Bello-Toledo, H., Botero-Coy, A.M., Boix, C., Ibáñez, M., 2019. Occurrence of antibiotics and bacterial resistance in wastewater and sea water from the Antarctic. *J. Hazard. Mater.* 363, 447-456.
- Jin, X., Zhou, X., Sun, P., Lin, S., Cao, W., Li, Z., Liu, W., 2019. Photocatalytic degradation of norfloxacin using N-doped TiO₂: optimization, mechanism, identification of intermediates and toxicity evaluation. *Chemosphere* 237, 124433.
- Jung, Y.J., Kim, W.G., Yoon, Y., Kang, J.-W., Hong, Y.M., Kim, H.W., 2012. Removal of amoxicillin by UV and UV/H₂O₂ processes. *Sci. Total Environ.* 420, 160-167.

- Khorsandi, H., Teymori, M., Aghapour, A.A., Jafari, S.J., Taghipour, S., Bargeshadi, R., 2019. Photodegradation of ceftriaxone in aqueous solution by using UVC and UVC/H₂O₂ oxidation processes. *Applied Water Science* 9(4), 1-8.
- Kronka, M.S., Fortunato, G.V., Mira, L., dos Santos, A.J., Lanza, M.R., 2023. Using Au NPs anchored on ZrO₂/carbon black toward more efficient H₂O₂ electrogeneration in flow-by reactor for carbaryl removal in real wastewater. *Chem. Eng. J.* 452, 139598.
- Lekkerkerker-Teunissen, K., Benotti, M.J., Snyder, S.A., Van Dijk, H.C., 2012. Transformation of atrazine, carbamazepine, diclofenac and sulfamethoxazole by low and medium pressure UV and UV/H₂O₂ treatment. *Sep. Purif. Technol.* 96, 33-43.
- Li, W., Jain, T., Ishida, K., Liu, H., 2017. A mechanistic understanding of the degradation of trace organic contaminants by UV/hydrogen peroxide, UV/persulfate and UV/free chlorine for water reuse. *Environ. Sci. Water Res. Technol.* 3(1), 128-138.
- Lima, V.B., Goulart, L.A., Rocha, R.S., Steter, J.R., Lanza, M.R., 2020. Degradation of antibiotic ciprofloxacin by different AOP systems using electrochemically generated hydrogen peroxide. *Chemosphere* 247, 125807.
- Ma, Y., Li, M., Wu, M., Li, Z., Liu, X., 2015. Occurrences and regional distributions of 20 antibiotics in water bodies during groundwater recharge. *Sci. Total Environ.* 518, 498-506.
- Martínez-Huitle, C.A., Panizza, M., 2018. Electrochemical oxidation of organic pollutants for wastewater treatment. *Curr. Opin. Electrochem.* 11, 62-71.
- Martínez-Huitle, C.A., Rodrigo, M.A., Sirés, I., Scialdone, O., 2015. Single and coupled electrochemical processes and reactors for the abatement of organic water pollutants: a critical review. *Chem. Ver.* 115(24), 13362-13407.
- Michael, S.G., Michael-Kordatou, I., Nahim-Granados, S., Polo-López, M.I., Rocha, J., Martinez-Piernas, A.B., Fernandez-Ibanez, P., Agüera, A., Manaia, C.M., Fatta-Kassinos, D., 2020. Investigating the impact of UV-C/H₂O₂ and sunlight/H₂O₂ on the removal of antibiotics, antibiotic resistance determinants and toxicity present in urban wastewater. *Chem. Eng. J.* 388, 124383.
- Moreira, F.C., Boaventura, R.A., Brillas, E., Vilar, V.J., 2017. Electrochemical advanced oxidation processes: a review on their application to synthetic and real wastewaters. *Appl. Catal. B: Environ.* 202, 217-261.
- Moreira, J., Lima, V.B., Goulart, L.A., Lanza, M.R., 2019. Electrosynthesis of hydrogen peroxide using modified gas diffusion electrodes (MGDE) for environmental applications: Quinones and azo compounds employed as redox modifiers. *Appl. Catal. B: Environ.* 248, 95-107.
- Oh, W.-D., Dong, Z., Lim, T.-T., 2016. Generation of sulfate radical through heterogeneous catalysis for organic contaminants removal: current development, challenges and prospects. *Appl. Catal. B: Environ.* 194, 169-201.
- Özcan, A., Özcan, A.A., Demirci, Y., 2016. Evaluation of mineralization kinetics and pathway of norfloxacin removal from water by electro-Fenton treatment. *Chem. Eng. J.* 304, 518-526.
- Pan, Z., Wang, K., Wang, Y., Tsiakaras, P., Song, S., 2018. In-situ electrosynthesis of hydrogen peroxide and wastewater treatment application: a novel strategy for graphite felt activation. *Appl. Catal. B: Environ.* 237, 392-400.
- Polianciuc, S.I., Gurzău, A.E., Kiss, B., Ștefan, M.G., Loghin, F., 2020. Antibiotics in the environment: causes and consequences. *Med. Pharm. Rep.* 93(3), 231.

- Rizzo, L., Lofrano, G., Gago, C., Bredneva, T., Iannece, P., Pazos, M., Krasnogorskaya, N., Carotenuto, M., 2018. Antibiotic contaminated water treated by photo driven advanced oxidation processes: ultraviolet/H₂O₂ vs ultraviolet/peracetic acid. *J. Clean. production* 205, 67-75.
- Rosales, E., Pazos, M., Sanroman, M.A., 2012. Advances in the electro-Fenton process for remediation of recalcitrant organic compounds. *Chem. Eng. Technol.* 35(4), 609-617.
- Sánchez-Montes, I., Fuzer Neto, J.R., Silva, B.F., Silva, A.J., Aquino, J.M., Rocha-Filho, R.C., 2018. Evolution of the antibacterial activity and oxidation intermediates during the electrochemical degradation of norfloxacin in a flow cell with a PTFE-doped β -PbO₂ anode: Critical comparison to a BDD anode. *Electrochim. Acta* 284, 260-270.
- Sánchez-Quiles, D., Tovar-Sánchez, A., 2014. Sunscreens as a Source of Hydrogen Peroxide Production in Coastal Waters. *Environ. Sci. Technol.* 48(16), 9037-9042.
- Shankaraiah, G., Poodari, S., Bhagawan, D., Himabindu, V., Vidyavathi, S., 2016. Degradation of antibiotic norfloxacin in aqueous solution using advanced oxidation processes (AOPs)—A comparative study. *Desalination and Water Treatment* 57(57), 27804-27815.
- Silva, T.O., Goulart, L.A., Sánchez-Montes, I., Santos, G.O., Santos, R.B., Colombo, R., Lanza, M.R., 2022. Using a novel gas diffusion electrode based on PL6 carbon modified with benzophenone for efficient H₂O₂ electrogeneration and degradation of ciprofloxacin. *Chem. Eng. J.*, 140697.
- Snowberger, S., Adejumo, H., He, K., Mangalgiri, K.P., Hopanna, M., Soares, A.D., Blaney, L., 2016. Direct photolysis of fluoroquinolone antibiotics at 253.7 nm: specific reaction kinetics and formation of equally potent fluoroquinolone antibiotics. *Environ. Sci Technol.* 50(17), 9533-9542.
- Tamtam, F., Mercier, F., Le Bot, B., Eurin, J., Dinh, Q.T., Clément, M., Chevreuil, M., 2008. Occurrence and fate of antibiotics in the Seine River in various hydrological conditions. *Sci. Total Environ.* 393(1), 84-95.
- Wang, C., Yu, G., Chen, H., Wang, J., 2021. Degradation of norfloxacin by hydroxylamine enhanced fenton system: Kinetics, mechanism and degradation pathway. *Chemosphere* 270, 129408.
- Wang, J., Li, C., Rauf, M., Luo, H., Sun, X., Jiang, Y., 2021. Gas diffusion electrodes for H₂O₂ production and their applications for electrochemical degradation of organic pollutants in water: A review. *Sci. Total Environ.* 759, 143459.
- Wang, X., Jing, J., Zhou, M., Dewil, R., 2022. Recent advances in H₂O₂-based advanced oxidation processes for removal of antibiotics from wastewater. *Chin. Chem. Lett.*
- Ye, Z., Guelfi, D.R., Álvarez, G., Alcaide, F., Brillas, E., Sirés, I., 2019. Enhanced electrocatalytic production of H₂O₂ at Co-based air-diffusion cathodes for the photoelectro-Fenton treatment of bronopol. *Applied Catalysis B: Environmental* 247, 191-199.
- Zhang, W., Bian, Z., Xin, X., Wang, L., Geng, X., Wang, H., 2021. Comparison of visible light driven H₂O₂ and peroxymonosulfate degradation of norfloxacin using Co/g-C₃N₄. *Chemosphere* 262, 127955.
- Zhang, Y., Daniel, G., Lanzalaco, S., Isse, A.A., Facchin, A., Wang, A., Brillas, E., Durante, C., Sirés, I., 2022. H₂O₂ production at gas-diffusion cathodes made from agarose-derived carbons with different textural properties for acebutolol degradation in chloride media. *J. Hazard. Mater.* 423, 127005.

Zhang, Y., Xiao, Y., Zhong, Y., Lim, T.-T., 2019. Comparison of amoxicillin photodegradation in the UV/H₂O₂ and UV/persulfate systems: Reaction kinetics, degradation pathways, and antibacterial activity. *Chem. Eng. J.* 372, 420-428.

Zhou, L.-J., Ying, G.-G., Liu, S., Zhao, J.-L., Yang, B., Chen, Z.-F., Lai, H.-J., 2013. Occurrence and fate of eleven classes of antibiotics in two typical wastewater treatment plants in South China. *Sci. Total Environ.* 452, 365-376.

Zhou, W., Meng, X., Gao, J., Alshwabkeh, A.N., 2019. Hydrogen peroxide generation from O₂ electroreduction for environmental remediation: A state-of-the-art review. *Chemosphere* 225, 588-607.

Supplementary material

An innovative approach to the application of electrochemical processes based on the *in-situ* generation of hydrogen peroxide for water treatment

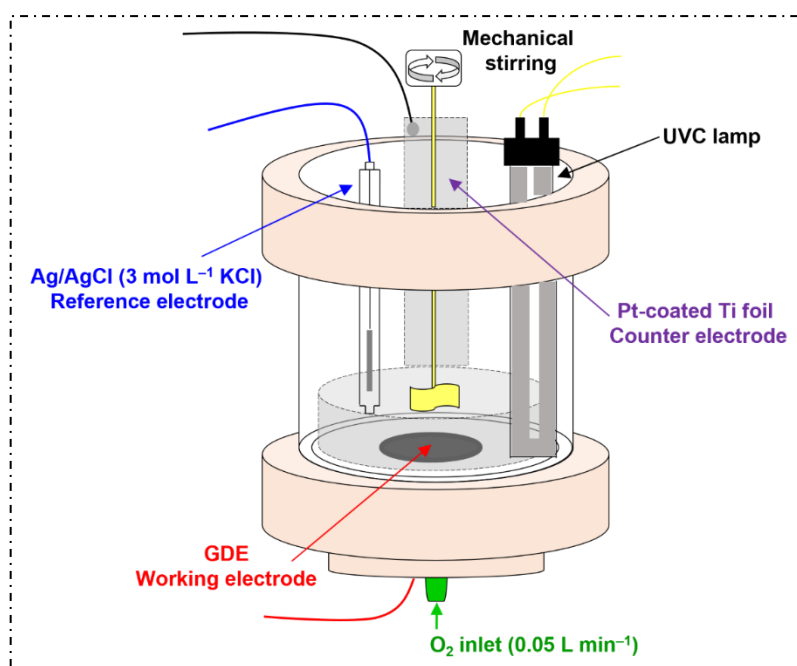


Fig. S1 – Schematic representation of the three-electrode cell used during the electrochemical experiments for H₂O₂ accumulation at different current densities. Conditions: supporting electrolyte = 0.1 mol L⁻¹ K₂SO₄, $j = 10, 25$ and 50 mA cm^{-2} , electrolysis time = 60 min, pH ~7, $V = 250 \text{ mL}$ and $T = 25 \text{ }^\circ\text{C}$.

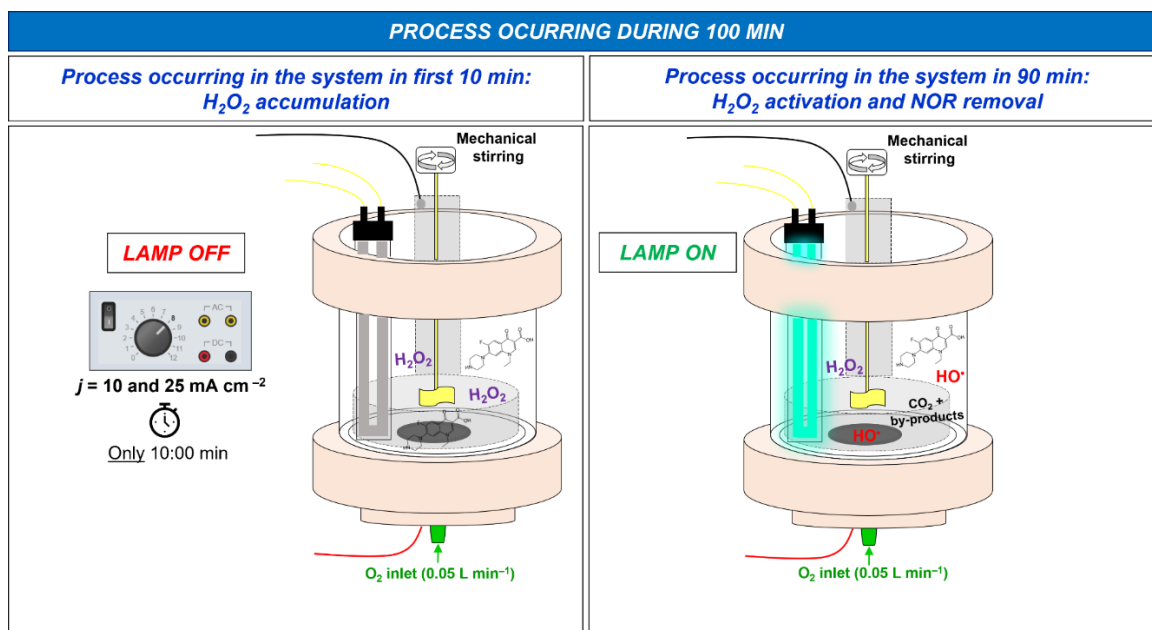


Fig. S2 – Schematic representation of the proposed UVC/ ϕ -H₂O₂ process. First step: H₂O₂ accumulation in solution by applying an electric current for only 10 min – Second step: H₂O₂ activation by UVC light and NOR degradation. Conditions: supporting electrolyte spiked with NOR = 0.1 mol L⁻¹ K₂SO₄ + 60 μmol L⁻¹ NOR, $j = 10$ and 25 mA cm⁻², lamp power = 9 W, pH ~7, $V = 250$ mL and $T = 25$ °C. The electric current supply was interrupted within 10 min, and then the UVC lamp was turned on for 90 min.

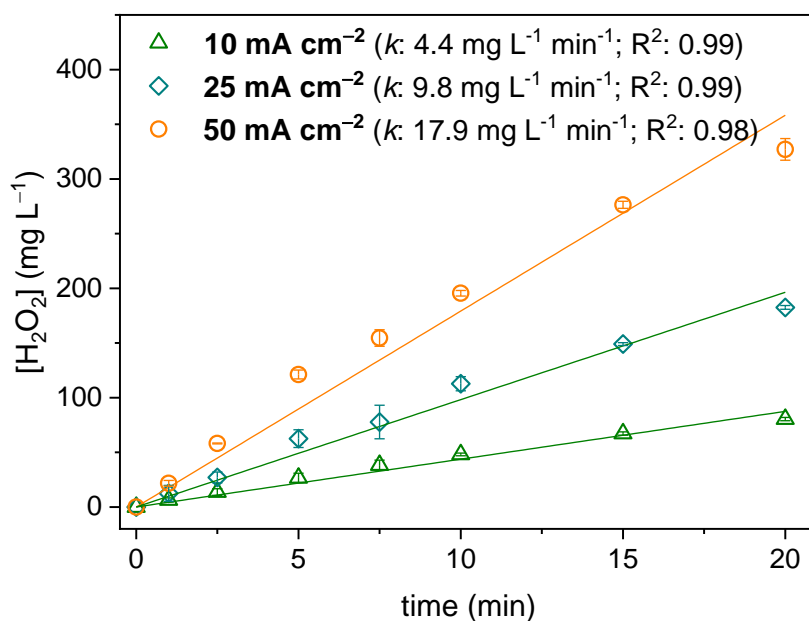


Fig. S3. Zero-order kinetics fitting results for H₂O₂ accumulation at different current densities. Conditions: $j = 10, 25$ and 50 mA cm^{-2} , supporting electrolyte = $0.1 \text{ mol L}^{-1} \text{ K}_2\text{SO}_4$, pH ~ 7 and $T = 25 \text{ }^\circ\text{C}$. The dashed line refers to the concentration of H₂O₂ accumulated in 10 min of electrolysis.

Table S1 – Pseudo-first order kinetic constant (k_{1st}) for NOR removal.

Process	$k_{1st} / 10^{-1} \text{ min}^{-1}$
Only UVC	0.5 ± 0.04 (0.99 ± 0.0)*
UVC/ ϕ -H ₂ O ₂ @ 25 mA cm^{-2}	4.4 ± 0.8 (0.96 ± 0.03)*
UVC/ ϕ -H ₂ O ₂ @ 10 mA cm^{-2}	3.4 ± 0.2 (0.94 ± 0.06)*
UVC/ ϕ -H ₂ O ₂ @ 25 mA cm^{-2}	5.4 ± 0.5 (0.94 ± 0.01)*

*Correlation coefficient (R^2).

Table S2 – Side reactions involved in the UVC/H₂O₂ processes and their kinetic constants (*k*).

Reactions	<i>k</i> / (mol ⁻¹ L s ⁻¹)	Ref.
2HO• → H ₂ O	<i>k</i> = 5.5×10 ⁹	[1]
H ₂ O ₂ + HO• → H ₂ O + HO ₂ • ↔ O ₂ ^{•-} + H ⁺	<i>k</i> = 2.7×10 ⁷	[1]
HO• + O ₂ ^{•-} → HO ⁻ + O ₂	<i>k</i> = 8.0×10 ⁹	[1]
HO• + HO ₂ • → H ₂ O + O ₂	<i>k</i> = 6.0×10 ⁹	[1]

- [1] G. V. Buxton, C.L. Greenstock, W.P. Helman, A.B. Ross, Critical review of rate constants for reactions of hydrated electrons, hydrogen atoms and hydroxyl radicals (•OH/•O) in aqueous solution, J. Phys. Chem. Ref. Data 17 (1988) 513–886. doi:10.1063/1.555805.

Table S3 – Energy consumption per mass (EC_x) removed.

Process	EC _{NOR} (kWh g ⁻¹)	EC _{TOC} (kWh g ⁻¹)
UVC/ <i>c</i> -H ₂ O ₂ @25 mA cm ⁻²	0.39±0.005	7.7±0.27
UVC/ <i>φ</i> -H ₂ O ₂ @10 mA cm ⁻²	0.40±0.001	6.9±0.35
UVC/ <i>φ</i> -H ₂ O ₂ @25 mA cm ⁻²	0.38±0.001	5.7±0.22

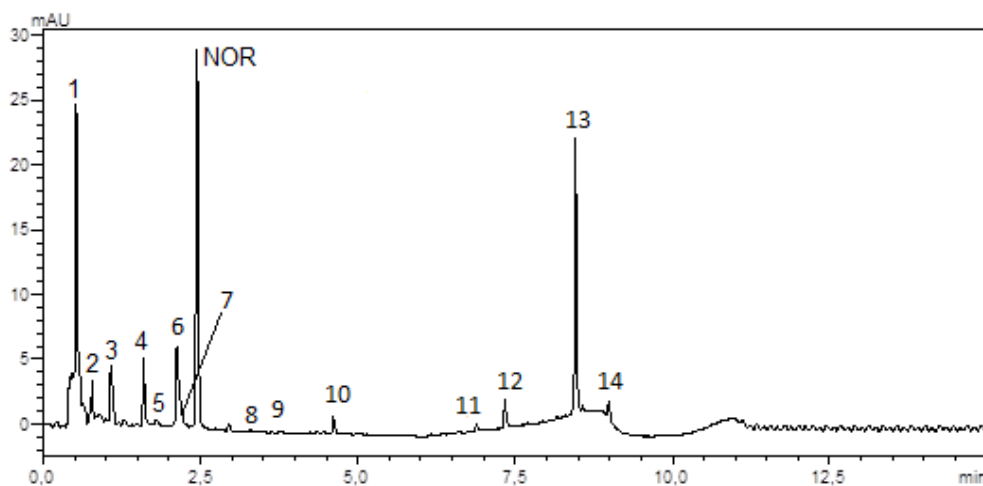


Fig. S4 – Chromatogram of NOR-containing solutions (60 μmol L⁻¹) after treatment using the UVC/*φ*-H₂O₂@25mA cm⁻². The sample corresponds to the time 10 min of treatment. Peak NOR: norfloxacin; Peaks 1-14: NOR by-products.

CONCLUSÃO

Os tópicos que envolvem a eletroprodução de H_2O_2 foram estudados e discutidos ao longo dos 4 capítulos apresentados, desde o material até o estudo de engenharia de sua aplicação real. A tese traz como principal inovação o material PL6C modificado por dispersão física com 2% de BTDA, o material inédito foi utilizado para fabricação do EDG e foi aplicado na eletrogeração de H_2O_2 com o objetivo de tratamento de efluentes.

O Capítulo 1 apresenta os resultados relacionados ao material na reação de redução de oxigênio, quais parâmetros estruturais e químicos interferem para que a reação ocorra pela rota de interesse e resulte na formação do oxidante desejado, podendo concluir que os grupos funcionais presentes na matriz do material é o que apresenta a maior contribuição, o material modificado além de contribuir diretamente para a geração de H_2O_2 também contribui sinergicamente para que os sítios ativos da matriz de carbono fiquem mais evidentes, tornando-o assim ainda mais seletivo, chegando a um valor muito satisfatório de seletividade para H_2O_2 de 97,7%. Após entender como o material participa da RRO de forma conceitual, foi realizado o estudo e a aplicabilidade desse material para a fabricação do EDG.

Para a construção do EDG, é necessário levar em conta a viabilidade do material para essa aplicação, pois é preciso que ele esteja disperso e homogêneo sem perder suas propriedades, já que a forma de produção inclui temperatura, pressão a adição de PTFE para que tanto a solidez quanto a porosidade desejada sejam mantidas. O Capítulo 2 apresenta os dados de eletrogeração de H_2O_2 utilizando a tecnologia EDG, mostrando que o material é capaz de eletrogerar H_2O_2 para a degradação do CIP, nesse caso utilizado como molécula modelo para validar a eficiência do GDE PL6C/BTDA 2%, que atingiu em 20 minutos a degradação total da molécula CIP. Uma vez validado o EDG, procuramos otimizar ao máximo esse processo, buscando realmente tornar essa tecnologia uma aplicação real, ou pelo menos aproximá-la ao máximo possível desse objetivo.

Assim, o Capítulo 3 apresenta estudos de otimização de processos e células eletroquímicas, iniciado com uma nova proposta de EDG (relatada na literatura) onde possibilitou a utilização de menos material, o estudo inicial foi feito em reator flow-by e estudos de layout do sistema foram feitos, como a utilização de membrana para separar os compartimentos catódicos e anódicos, o que melhorou a geração de H_2O_2 . Como o uso de membrana PEM aumenta a eficiência da corrente, surge a proposta de utilizar um reator desenvolvido com a intenção de ser aplicado para a eletrogeração de H_2O_2 com EDG, realizando o projeto e sua fabricação em uma impressora 3D, foi estudado um reator de fluxo

tangencial como prova de conceito para obter uma resposta sobre seu desempenho, foi feito outro reator, escalonado em tamanho, pois o estudo de escalonamento é essencial para tornar a tecnologia o mais próximo possível de aplicações reais e industriais, o reator então se mostrou escalável. Uma vez que o processo, o reator e o material foram otimizados, a última etapa foi a aplicação de todos juntos, onde o material modificado PL6C/BTDA 2% foi aplicado no novo reator usando PEM, de modo que foi possível atingir um valor de eficiência faradaica atual de 99,99%, mostrando como a pesquisa foi eficaz e precisa, atingindo seu objetivo.

Considerando que uma aplicação real leva em conta diferentes situações e formas operacionais, foi realizado um estudo adicional explorando uma nova abordagem para a aplicação dessa tecnologia, em que a geração foi feita *in situ* e eletroquimicamente por um período inicial e, em seguida, nesse mesmo sistema e célula, a ativação do H₂O₂ eletrogerado foi realizada e usada para a degradação da molécula NOR, Buscando explorar ainda mais as possibilidades que o uso dessa tecnologia pode trazer, a aplicação de uma densidade de corrente de 25 mA cm⁻² por 10 minutos foi suficiente para gerar uma quantidade suficiente de H₂O₂ para ser posteriormente ativada pela luz UVC e realizar em 10 minutos a degradação total da NOR.

Conclui-se que a pesquisa realizada e apresentada nesta tese contribui para novas abordagens para a geração eletroquímica *in situ* de peróxido de hidrogênio, contribui para a apresentação de um material inédito e satisfatório para a reação de redução de oxigênio via 2 elétrons, além disso, esta tese traz de forma assertiva um inestimável conhecimento acadêmico científico, que até então, não havia sido explorado.

REFERÊNCIAS BIBLIOGRÁFICAS

- 1 ZHOU, W.; MENG, X.; GAO, J.; ALSHAWABKEH, A. N. Hydrogen peroxide generation from O₂ electroreduction for environmental remediation: A state-of-the-art review. **Chemosphere**, Oxford, v. 225, p. 588-607, 2019. DOI: 10.1016/j.chemosphere.2019.03.042.
- 2 MOHANAN, P.V.; SANGEETHA, V.; SABAREESWARAN, A.; MURALEEDHARAN, V.; JITHIN, K.; VANDANA, U.; VARSHA, S. B. Safety of 0.5% hydrogen peroxide mist used in the disinfection gateway for covid-19. **Environmental Science and Pollution Research**, Berlin, v. 28, n. 47, p. 66602-66612, 2021. DOI: 10.1007/s11356-021-15164-y.
- 3 TREJO, A. C.; CASTAÑEDA, I. D.; RODRÍGUEZ, A. C.; CARMONA, A. V. R.; MERCADO, M. D. P. C.; VALE, L. S.; MONTESERRAT, C.; CASTILLERO, S. B.; CONSUELO, L. C.; SILVIO, M. D. Hydrogen peroxide as an adjuvant therapy for covid-19: a case series of patients and caregivers in the Mexico City metropolitan area. **Evidence-Based Complementary and Alternative Medicine**, New York, v. 2021, p. 12, 2021. DOI: 10.1155/2021/5592042.
- 4 SCHWARTZ, A.; STIEGEL, M.; GREESON, N.; VOGEL, A.; THOMANN, W.; BROWN, M.; SEMPOWSKI, G. D.; ALDERMAN, T. S.; CONDREAY J. P.; BURCH, J.; WOLFE, C.; SMITH, B.; LEWIS, S. Decontamination and reuse of n95 respirators with hydrogen peroxide vapor to address worldwide personal protective equipment shortages during the sars-cov-2 (covid-19) pandemic. **Applied Biosafety**, New York, v. 25, n. 2, p. 67-70, 2020. DOI: 10.1177/1535676020919932.
- 5 DOMENICO, M. B. D. I.; COLLARES, K.; SANTOS, R. B.; LENZ, D. U.; ANTUNES, V. P.; GODINHO, V. W.; CESCA, H.; PONCIANO, T. H. J.; CORAZZA, P. H. Hydrogen peroxide as an auxiliary treatment for covid-19 in Brazil: a randomized double-blind clinical trial. **Epidemiology and Health**, Suwon, v. 43, p. 1-8, 2021. DOI: 10.4178/epih.e2021051.
- 6 BRILLAS, E.; SIRÉS, I.; OTURAN, M. A. Electro-fenton process and related electrochemical technologies based on fenton's reaction chemistry. **American Chemical Society**, Washington, v. 109, n. 12, p. 6570-6631, 2009. DOI: 10.1021/cr900136g.
- 7 BARROS, W. R. P.; ERENO, T.; TAVARES, A. C.; LANZA, M. R. V. In situ electrochemical generation of hydrogen peroxide in alkaline aqueous solution by using an unmodified gas diffusion electrode. **ChemElectroChem**, Weinheim, v. 2, n. 5, p. 714-719, 2015. DOI: 10.1002/celc.201402426.
- 8 HUANG, X.; SONG, M.; ZHANG, J.; SHEN, T.; LUO, G.; WANG, D. Recent advances of electrocatalyst and cell design for hydrogen peroxide production. **Nano-Micro Letters**, Berlin, v. 15, n. 1, p. 86, 2023. DOI:10.1007/s40820-023-01044-2.
- 9 YANG, S.; VERDAGUER-CASADEVALL, A.; ARNARSON, L.; SILVIOLI, L.; ČOLIĆ, V.; FRYDENDAL, R.; ROSSMEISL, J.; CHORKENDORFF, I.; STEPHENS, E. L. Toward the decentralized electrochemical production of h₂o₂: a focus on the catalysis. **ACS Catalysis**, Washington, v. 8, n. 5, p. 4064-4081, 2018. DOI: 10.1021/acscatal.8b00217.
- 10 KJELLANDER, M.; GÖTZ, K.; LILJERUHM, J.; BOMAN, M.; JOHANSSON, G. Steady-state generation of hydrogen peroxide: Kinetics and stability of alcohol oxidase immobilized on nanoporous alumina. **Biotechnology Letters**, Dordrecht, v. 35, n. 4, p. 585-590, 2013. DOI: 10.1007/s10529-012-1110-5.
- 11 BARBOSA, E.; BERGAMINI, F.; MARCOLINO JUNIOR, L. H. A simple, fast, and cost-effective analytical method for monitoring active quinones in a H₂O₂ production process. **Microchemical Journal**, Philadelphia, v. 163, p. 105861, 2021. DOI: 10.1016/j.microc.2020.105861.

- 12 SANTACESARIA, E.; DI SERIO, M.; RUSSO, A.; LEONE, U.; VELOTTI, R. Kinetic and catalytic aspects in the hydrogen peroxide production via anthraquinone. **Chemical Engineering Science**, Brisbane, v. 54, n. 13-14, p. 2799–806, 1999. DOI: 10.1016/S0009-2509(98)00377-7.
- 13 RIEDL, H. J.; PFLELDERER, G. **Production of hydrogen peroxide**. U. S. Patent n° 2,158,525, 16 maio 1939.
- 14 CHEN, Q. Development of an anthraquinone process for the production of hydrogen peroxide in a trickle bed reactor-From bench scale to industrial scale. **Chemical Engineering and Processing Process Intensification**, Amsterdam, v. 47, n. 5, p. 787-792, 2008. DOI: 10.1016/j.cep.2006.12.012.
- 15 CIRIMINNA, R.; ALBANESE, L.; MENEGUZZO, F.; PAGLIARO, M. Hydrogen peroxide: a key chemical for today's sustainable development. **ChemSusChem**, Weinheim, v. 9, n. 24, p. 3374-3381, 2016. DOI: 10.1002/cssc.201600895.
- 16 CHEN, L.; PINTO, A.; ALSHAWABKEH, A. N. Activated carbon as a cathode for water disinfection through the electro-fenton process. **Catalysts, London**, v. 9, n. 7, p. 601, 2019. DOI: 10.3390/catal9070601.
- 17 MUDDMANN, T.; HAUPT, D. R.; SIEVERS, M.; KUNZ, U. Improved operating parameters for hydrogen peroxide-generating gas diffusion electrodes. **Chemie Ingenieur Technik**, Berlin, v. 92, n. 5, p. 505-512, 2020. DOI: 10.1002/cite.201900137.
- 18 GUPTA, A.; GARG, A. Degradation of ciprofloxacin using Fenton's oxidation: Effect of operating parameters, identification of oxidized by-products and toxicity assessment. **Chemosphere**, Oxford, v. 193, p. 1181-1188, 2018. DOI: 10.1016/j.chemosphere.2017.11.046.
- 19 LIMA, V. B.; GOULART, L. A.; ROCHA, R. S.; STETER, J. R.; LANZA, M. R. V. Degradation of antibiotic ciprofloxacin by different AOP systems using electrochemically generated hydrogen peroxide. **Chemosphere**, Oxford, v. 247, p. 125807, 2020. DOI: 10.1016/j.chemosphere.2019.125807.
- 20 SILVA, T. O.; GOULART, L. A.; SÁNCHEZ-MONTES, I.; SANTOS, O. S. G.; SANTOS, B. R.; COLOMBO, R.; LANZA, M. R. V. Using a novel gas diffusion electrode based on PL6 carbon modified with benzophenone for efficient H₂O₂ electrogeneration and degradation of ciprofloxacin. **Chemical Engineering Journal**, Amsterdam, v. 455, p.140697, 2022. DOI: 10.1016/j.cej.2022.140697.
- 21 SÁNCHEZ-MONTES, I.; SANTOS, O. S. G.; SILVA, O. T.; COLOMBO, R. R.; LANZA, R. V. M. An innovative approach to the application of electrochemical processes based on the in-situ generation of H₂O₂ for water treatment. **Journal of Cleaner Production**, London, v. 392, p.136242, 2023. DOI: 10.1016/j.jclepro.2023.136242.
- 22 CARNEIRO, J. F.; ROCHA, R. S.; HAMMER, P.; BERTAZZOLI, R.; LANZA, M. R. V. Hydrogen peroxide electrogeneration in gas diffusion electrode nanostructured with Ta₂O₅. **Applied Catalysis A: general**, Amsterdam, v. 517, p. 161-167, 2016. DOI: 10.1016/j.apcata.2016.03.013
- 23 GE, X.; SUMBOJA, A.; WUU, D.; AN, T.; LI, B.; GOH, F. W. T.; HOR, T.S.A; ZONG, Y.; LIU, Z. Oxygen reduction in alkaline media: from mechanisms to recent advances of catalysts. **ACS Catalysis**, Washington, v. 5, n. 8, p. 4643-4667, 2015. DOI: 10.1021/acscatal.5b00524.
- 24 ARAÚJO, K. S.; ANTONELLI, R.; GAYDECZKA, B.; GRANATO, A. C.; MALPASS, G. R. P. Advanced oxidation processes: a review regarding the fundamentals and applications in wastewater treatment and industrial wastewater. **Revista Ambiente e Água: an interdisciplinary journal of applied science**, Taubate, v. 11, n. 2, p. 387-401, 2016. DOI: doi:10.4136/ambi-agua.1862.

- 25 HEJAZI, S. A.; TAGHIPOUR, F. A novel uv-led hydrogen peroxide electrochemical photoreactor for point-of-use organic contaminant degradation. **Chemosphere**, Oxford, v. 292, p. 133353, 2022. DOI: 10.1016/j.chemosphere.2021.133353.
- 26 MA, R.; LIN, G.; ZHOU, Y.; LIU, Q.; ZHANG, T.; SHAN, G.; YANG, M.; WANG, J. A review of oxygen reduction mechanisms for metal-free carbon-based electrocatalysts. **npj Computational Materials**, London, v. 5, n. 1, p.78, 2019. DOI: 10.1038/s41524-019-0210-3.
- 27 KRONKA, M. S.; FORTUNATO, G. V.; MIRA, L.; SANTOS, A. J.; LANZA, M. R. V. Using Au NPs anchored on ZrO₂/carbon black toward more efficient H₂O₂ electrogeneration in flow-by reactor for carbaryl removal in real wastewater. **Chemical Engineering Journal**, Amsterdam, v. 452, p. 139598, 2023. DOI: 10.1016/j.cej.2022.139598.
- 28 ANTONIN, V. S.; SANTOS, M. C.; GARCIA-SEGURA, S.; BRILLAS, E. Electrochemical incineration of the antibiotic ciprofloxacin in sulfate medium and synthetic urine matrix. **Water Research**, London, v. 83, p. 31-41, 2015. DOI: 10.1016/j.watres.2015.05.066.
- 29 SODRÉ, F. F.; MONTAGNER, C. C.; LOCATELLI, M. A. F.; JARDIM, W. F. Ocorrência de interferentes endócrinos e produtos farmacêuticos em águas superficiais da região de Campinas (SP, Brasil). **Journal of the Brazilian Society of Ecotoxicology**, Rio De Janeiro, v. 2, n. 2, p. 187-196, 2007. DOI: 10.5132/jbse.2007.02.012.
- 30 KIM, M. K.; ZOH, K. D. Occurrence and removals of micropollutants in water environment. **Environmental Engineering Research**, Seoul, v. 21, n. 4, p. 319-332, 2016. DOI: 10.4491/eer.2016.115.
- 31 FROMME, H.; KÜCHLER, T.; OTTO, T.; PILZ, K.; MÜLLER, J.; WENZEL, A. Occurrence of phthalates and bisphenol A and F in the environment. **Water Research**, London, v. 36, n. 6, p. 1429-1438, 2002. DOI: 10.1016/S0043-1354(01)00367-0.
- 32 WESTERHOFF, P.; YOON, Y.; SNYDER, S.; WERT, E. Fate of endocrine-disruptor, pharmaceutical, and personal care product chemicals during simulated drinking water treatment processes. **Environmental Science and Technology**, Washington, v. 39, n. 17, p. 6649-6663, 2005. DOI: 10.1021/es0484799.
- 33 MONNERET, C. What is an endocrine disruptor? **Comptes Rendus - Biologies**, Paris, v. 340, p. 403-405, 2017. DOI: 10.1016/j.crvi.2017.07.004.
- 34 EUROPEAN COMMISSION. **Endocrine disruptors**: questions and answers. Bruxelas, 2018. Disponível em: https://commission.europa.eu/news/endocrine-disruptors-questions-and-answers-2018-11-07_en. Acesso em: 25 jul 2023.
- 35 GHISELLI, G.; JARDIM, W. F. Interferentes endócrinos no ambiente. **Química Nova**, São Paulo, v. 30, n. 3, p. 695-706, 2007. DOI: 10.1590/S0100-40422007000300032.
- 36 BASILE, T.; PETRELLA, A.; PETRELLA, M.; BOGHETICH, G.; PETRUZZELLI, V.; COLASUONNO, S.; PETRUZZELLI, D. Review of endocrine-disrupting-compound removal technologies in water and wastewater treatment plants: An EU perspective. **Industrial and Engineering Chemistry Research**, Washington, v. 50, n. 14, p. 8389-8401, 2011. DOI: 10.1021/ie101919v.
- 37 GOLOVKO, O.; REHRL, A. L.; KÖHLER, S.; AHRENS, L. Organic micropollutants in water and sediment from Lake Mälaren, Sweden. **Chemosphere**, Oxford, v. 258, p. 127293, 2020. DOI: 10.1016/j.chemosphere.2020.127293.

- 38 HONARMAND, M.; NAEIMI, A.; REZAKHANI, M. S.; CHAJI, M. A. Ni/NiO doped chitosan-cellulose based on the wastes of barley and shrimp for degradation of ciprofloxacin antibiotic. **Journal of Materials Research and Technology**, Rio de Janeiro, v. 18, p. 4060-4074, 2022. DOI: 10.1016/j.jmrt.2022.04.046.
- 39 UPADHYAY, S. K.; KUMAR, P.; ARORA, V. Complexes of quinolone drugs norfloxacin and ciprofloxacin with alkaline earth metal perchlorates. **Journal of Structural Chemistry**, Moscow, v. 47, n. 6, p. 1078-1083, 2006. DOI: 10.1007/s10947-006-0428-z.
- 40 CARNEIRO, J. F.; AQUINO, J. M.; SILVA, B. F.; SILVA, A. J.; ROCHA-FILHO, R. C. Comparing the electrochemical degradation of the fluoroquinolone antibiotics norfloxacin and ciprofloxacin using distinct electrolytes and a BDD anode: evolution of main oxidation byproducts and toxicity. **Journal of Environmental Chemical Engineering**, Amsterdam, v. 8, n. 6, p. 104433, 2020. DOI: 10.1016/j.jece.2020.104433.
- 41 WANG, F.; YU, X.; GE, M.; WU, S. One-step synthesis of TiO₂/γ-Fe₂O₃/GO nanocomposites for visible light-driven degradation of ciprofloxacin. **Chemical Engineering Journal**, Amsterdam, v. 384, p. 123381, 2020. DOI: 10.1016/j.cej.2019.123381.
- 42 SAYED, M.; ISMAIL, M.; KHAN, S.; TABASSUM, S.; KHAN, H. M. degradation of ciprofloxacin in water by advanced oxidation process: kinetics study, influencing parameters and degradation pathways. **Environmental Technology, London**, v. 37, n. 5, p. 590-602, 2016. DOI: 10.1080/09593330.2015.1075597.
- 43 ROCHA, R. S.; VALIM, R. B.; TREVELIN, L. C.; STETER, J. R.; CARNEIRO, J. F.; FORTI, J. C.; BERTAZZOLI, R.; LANZA, M. R. V. Electrocatalysis of hydrogen peroxide generation using oxygen-fed gas diffusion electrodes made of carbon black modified with quinone compounds. **Electrocatalysis**, New York, v. 11, n. 3, p. 338-346, 2020. DOI: 10.1007/s12678-020-00591-1.
- 44 BRILLAS, E. A review on the degradation of organic pollutants in waters by UV photoelectro-fenton and solar photoelectro-fenton. **Journal of the Brazilian Chemical Society**, São Paulo, v. 25, p. 393-417, 2014. DOI: 10.5935/0103-5053.20130257.
- 45 GANIYU, S. O.; MARTÍNEZ-HUITLE, C. A.; OTURAN, M. A. Electrochemical advanced oxidation processes for wastewater treatment: Advances in formation and detection of reactive species and mechanisms. **Current Opinion in Electrochemistry**, London, v. 27, p. 100678, 2021. DOI: 10.1016/j.coelec.2020.100678.
- 46 OTURAN, M. A.; AARON, J. J. Advanced oxidation processes in water/wastewater treatment: Principles and applications. A review. **Critical Reviews in Environmental Science and Technology**, Oxford, v. 44, n. 23, p. 2577-2641, 2014. DOI: 10.1080/10643389.2013.829765.
- 47 GLAUNER, T.; KUNZ, F.; ZWIENER, C.; FRIMMEL, F. H. Elimination of swimming pool water disinfection by-products with advanced oxidation processes (AOPs). **Acta Hydrochimica et Hydrobiologica**, Weinheim, v. 33, n. 6, p. 585-594, 2005. DOI: 10.1002/ahch.200400605.
- 48 CUERDA-CORREA, E. M.; ALEXANDRE-FRANCO, M. F.; FERNÁNDEZ-GONZÁLEZ, C. Advanced oxidation processes for the removal of antibiotics from water. An overview. **Water**, Basel, v. 12, n. 1, p. 102, 2019. DOI: 10.3390/w12010102.
- 49 AN, T.; YANG, H.; LI, G.; SONG, W.; COOPER, W. J.; NIE, X. Kinetics and mechanism of advanced oxidation processes (AOPs) in degradation of ciprofloxacin in water. **Applied Catalysis B: environmental**, Amsterdam, v. 94, n. 13-14, p. 288-294, 2010. DOI: 10.1016/j.apcatb.2009.12.002.

- 50 NIDHEESH, P. V.; ZHOU, M.; OTURAN, M. A. An overview on the removal of synthetic dyes from water by electrochemical advanced oxidation processes. **Chemosphere**, Oxford, v. 197, p. 210-227, 2018. DOI: 10.1016/j.chemosphere.2017.12.195.
- 51 LAZAROVA, V.; SAVOYE, P.; JANEX, M. L.; BLATCHLEY, E. R.; POMMEPUY, M. Advanced wastewater disinfection technologies: state of the art and perspectives. **Water Science and Technology**, London, v. 40, n. 4-5, p. 203-213, 1999. DOI: 10.1016/S0273-1223(99)00502-8.
- 52 ASGHAR, A.; RAMAN, A. A. A.; DAUD, W. M. A. W. Advanced oxidation processes for in-situ production of hydrogen peroxide/hydroxyl radical for textile wastewater treatment: a review. **Journal of Cleaner Production**, London, v. 87, p. 826-838, 2015. DOI: 10.1016/j.jclepro.2014.09.010.
- 53 WEI, J.; SHI, L.; WU, X. Electrochemical advanced oxidation process with simultaneous persulfate and hydrogen peroxide on-site generations for high salinity wastewater. **Separation and Purification Technology**, London, v. 310, p. 123147, 2023. DOI: 10.1016/j.seppur.2023.123147.
- 54 BERL, E. **Process for carrying out electrochemical reactions**. U. S. Patent n° 2,000,815 7 de maio de 1931, Germany.
- 55 BERL, E. A new cathodic process for the production of H₂O₂. **Transactions of the Electrochemical Society**, New York, v. 76, n. 1, p. 359, 1939.
- 56 BARHOUMI, N.; OTURAN, N.; AMMAR, S.; GADRI, A.; OTURAN, M. A.; BRILLAS, E. Enhanced degradation of the antibiotic tetracycline by heterogeneous electro-Fenton with pyrite catalysis. **Environmental Chemistry Letters**, Berlin, v. 15, p. 689-693, 2017. DOI: 10.1007/s10311-017-0638-y.
- 57 LI, J.; LI, Y.; XIONG, Z.; YAO, G.; LAI, B. The electrochemical advanced oxidation processes coupling of oxidants for organic pollutants degradation: a mini-review. **Chinese Chemical Letters**, London, v. 30, n. 12, p. 2139-2146, 2019. DOI: 10.1016/j.ccllet.2019.04.057.
- 58 SANTOS, M. S. F.; ALVES, A.; MADEIRA, L. M. Paraquat removal from water by oxidation with Fenton's reagent. **Chemical Engineering Journal**, Amsterdam, v. 175, p. 279-290, 2011. DOI: 10.1016/j.cej.2011.09.106.
- 59 CHAPLIN, B. P. Critical review of electrochemical advanced oxidation processes for water treatment applications. **Environmental Sciences Processes and Impacts**, London, v. 16, n. 6, p. 1182-1203, 2014. DOI: 10.1039/c3em00679d.
- 60 LI, S.; HUANG, T.; DU, P.; LIU, W.; HU, J. Photocatalytic transformation fate and toxicity of ciprofloxacin related to dissociation species: Experimental and theoretical evidences. **Water Research**, London, v. 185, p. 116286, 2020. DOI: 10.1016/j.watres.2020.116286.
- 61 MOREIRA, F. C.; BOAVENTURA, R. A. R.; BRILLAS, E.; VILAR, V. J. P. Electrochemical advanced oxidation processes: A review on their application to synthetic and real wastewaters. **Applied Catalysis B: environmental**, Amsterdam, v. 202, p. 217-261, 2017. DOI: 10.1016/j.apcatb.2016.08.037
- 62 YANG, G. P.; ZHAO, X. K.; SUN, X. J.; LU, X. L. Oxidative degradation of diethyl phthalate by photochemically-enhanced Fenton reaction. **Journal of Hazardous Materials**, Amsterdam, v. 126, n. 1-3, p. 112-118, 2005. DOI: 10.1016/j.jhazmat.2005.06.014.

63 ACOSTA-SANTOYO, G.; LEÓN-FERNÁNDEZ, L. F.; BUSTOS, E.; CAÑIZARES, P.; RODRIGO, M. A.; LLANOS, J. On the production of ozone, hydrogen peroxide and peroxone in pressurized undivided electrochemical cells. **Electrochimica Acta**, Oxford, v. 390, p. 138878, 2021. DOI: 10.1016/j.electacta.2021.138878

64 CHRISTENSEN, P. A.; YONAR, T.; ZAKARIA, K. The electrochemical generation of ozone: a review. **Ozone Science and Engineering**, Oxford, v. 35, n. 3, p. 149-167, 2013. DOI: 10.1080/01919512.2013.761564.

65 ZHAO, X. K.; YANG, G. P.; WANG, Y. J.; GAO, X. C. Photochemical degradation of dimethyl phthalate by Fenton reagent. **Journal of Photochemistry and Photobiology A Chemistry**, London, v. 161, n. 2-3, p. 215-220, 2004. DOI: 10.1016/S1010-6030(03)00344-7.

66 ALEXSANDRO, J.; FORTUNATO, G. V.; KRONKA, M. S.; VERNASQUI, L. G.; FERREIRA, G.; LANZA, M. R. V. Electrochemical oxidation of ciprofloxacin in different aqueous matrices using synthesized boron-doped micro and nano-diamond anodes. **Environmental Research**, New York, v. 204, p. 112027, 2022. DOI: 10.1016/j.envres.2021.112027.

67 XU, B.; GAO, N. Y.; SUN, X. F.; XIA, S. J.; RUI, M.; SIMONNOT, M. O.; CAUSSERAND, C.; ZHAO, J. F. Photochemical degradation of diethyl phthalate with UV/H₂O₂. **Journal of Hazardous Materials**, Amsterdam, v. 139, n. 1, p. 132-139, 2007. DOI: 10.1016/j.jhazmat.2006.06.026.

68 CARNEIRO, J. F.; TREVELIN, L. C.; LIMA, A. S.; MELONI, G. N.; BERTOTTI, M.; HAMMER, P.; BERTAZZOLI, R.; LANZA, M. R. V. Synthesis and characterization of zro₂/c as electrocatalyst for oxygen reduction to H₂O₂. **Electrocatalysis**, New York, v. 8, p. 189-195, 2017. DOI: 10.1007/s12678-017-0355-0.

69 KRONKA, M. S.; SILVA, F. L.; MARTINS, A. S.; ALMEIDA, M. O.; HONÓRIO, K. M.; LANZA, M. R. V. Tailoring the ORR selectivity for H₂O₂ electrogeneration by modification of Printex L6 carbon with 1,4-naphthoquinone: A theoretical, experimental and environmental application study. **Materials Advances**, London, v. 1, n. 5, p. 1318-1329, 2020. DOI: 10.1039/d0ma00290a.

70 YEAGER, E. Electrocatalysts for O₂ reduction. **Electrochimica Acta**, Oxford, v. 29, n. 11, p. 1527-1537, 1984. DOI: 10.1016/0013-4686(84)85006-9.

71 WEI, J.; YUAN, D.; WU, X. Enabling direct H₂O₂ electrosynthesis of 100 % selectivity at 100 mA cm⁻² using a continuous flow sulfite/air fuel cell. **Chemical Engineering Journal**, Amsterdam, v. 455, p. 140695, 2022. DOI: 10.1016/j.cej.2022.140695.

72 WANG, Y.; SHI, R.; SHANG, L.; PENG, L.; CHU, D.; HAN, Z.; WATERHOUSE, G. I. N.; ZHANG, R.; ZHANG, T. Vertical graphene array for efficient electrocatalytic reduction of oxygen to hydrogen peroxide. **Nano Energy**, Amsterdam, v. 96, p. 107046, 2022. DOI: 10.1016/j.nanoen.2022.107046.

73 WANG, X.; OUYANG, C.; DOU, S.; LIU, D.; WANG, S. Oxidized carbon nanotubes as an efficient metal-free electrocatalyst for the oxygen reduction reaction. **Royal Society of Chemistry Advances**, Cambridge, v. 5, n. 52, p. 41901-41904, 2015. DOI: 10.1039/c5ra05172j.

74 ZHU, Q.; PAN, Z.; HU, S.; KIM, J. H. Cathodic hydrogen peroxide electrosynthesis using anthraquinone modified carbon nitride on gas diffusion electrode. **ACS Applied Energy Materials**, Washington, v. 2, n. 11, p. 7972-7979, 2019. DOI: 10.1021/acsaem.9b01445.

- 75 PANGOTRA, D.; CSEPEI, L. I.; ROTH, A.; PONCE, D. E. L. C.; SIEBER, V.; VIEIRA, L. Anodic production of hydrogen peroxide using commercial carbon materials. **Applied Catalysis B: environmental**, Amsterdam, v. 303, p. 120848, 2022. DOI: 10.1016/j.apcatb.2021.120848.
- 76 SOLTANI, R. D. C.; REZAEI, A.; KHATAEE, A. R.; GODINI, H. Electrochemical generation of hydrogen peroxide using carbon black-, carbon nanotube-, and carbon black/carbon nanotube-coated gas-diffusion cathodes: Effect of operational parameters and decolorization study. **Research on Chemical Intermediates**, Dordrecht, v. 39, p. 4277-4286, 2013. DOI: 10.1007/s11164-012-0944-8.
- 77 KRONKA, M. S.; CORDEIRO JUNIOR, P. J. M.; MIRA, L.; SANTOS, A. J.; FORTUNATO, G.V.; LANZA, M.R.V. Sustainable microwave-assisted hydrothermal synthesis of carbon-supported ZrO₂ nanoparticles for H₂O₂ electrogeneration. **Materials Chemistry and Physics**, Amsterdam, v. 267, p. 124575, 2021. DOI: 10.1016/j.matchemphys.2021.124575.
- 78 ROCHA, R. S.; REIS, R. M.; BEATI, A. A. G. F.; LANZA, M. R. V.; SOTOMAYOR, M. D. P. T.; BERTAZZOLI, R. Desenvolvimento e avaliação de eletrodos de difusão gasosa (EDG) para geração de H₂O₂ in situ e sua aplicação na degradação do corante reativo azul 19. **Química Nova**, São Paulo, v. 35, p. 1961-1966, 2012. DOI: 10.1590/S0100-40422012001000014.
- 79 BARROS, W. R. P.; ALVES, S. A.; FRANCO, P. C.; STETER, J. R.; ROCHA, R. S.; LANZA, M. R. V. Electrochemical degradation of tartrazine dye in aqueous solution using a modified gas diffusion electrode. **Journal of The Electrochemical Society**, London, v. 161, n. 9, p. H438-H442, 2014. DOI: 10.1149/2.015409jes.
- 80 FORTUNATO, G. V.; KRONKA, M. S.; SANTOS, A. J.; LEDENDECKER, M.; LANZA, M. R. V. Low Pd loadings onto printex 16: synthesis, characterization and performance towards h₂o₂ generation for electrochemical water treatment technologies. **Chemosphere**, Oxford, v. 259, p. 127523, 2020. DOI: 10.1016/j.chemosphere.2020.127523.
- 81 FUKUZUMI, S.; LEE, Y. M.; NAM, W. Recent progress in production and usage of hydrogen peroxide. **Chinese Journal of Catalysis**, Amsterdam, v. 42, n. 8, p. 1241-1252, 2021. DOI: 10.1016/S1872-2067(20)63767-6.
- 82 SILVA, K. J. S.; SABOGAL-PAZ, L. P. Exploring potentials and constraints of h₂o₂ water disinfection for household settings. **Water, Air, and Soil Pollution**, Amsterdam, v. 232, n. 12, p. 483, 2021. DOI: 10.1007/s11270-021-05434-3.
- 83 TIAN, Y.; DENG, D.; XU, L.; LI, M.; CHEN, H.; WU, Z.; ZHANG, S. Strategies for sustainable production of hydrogen peroxide via oxygen reduction reaction: from catalyst design to device setup. **Nano-Micro Letters**, Berlin, v. 15, n. 15, p. 1-45, 2023. DOI: 10.1007/s40820-023-01067-9.
- 84 YANG, X.; ZENG, Y.; ALNOUSH, W.; HOU, Y.; HIGGINS, D.; WU, G. Tuning two-electron oxygen-reduction pathways for h₂o₂ electrosynthesis via engineering atomically dispersed single metal site catalysts. **Advanced Materials, Weinheim**, v. 34, n. 23, p. 2107954, 2022. DOI: 10.1002/adma.202107954.
- 85 CORDEIRO JUNIOR, P. J. M.; GONÇALVES, R.; GUARALDO, T. T.; DA SILVA, P. A. R.; PEREIRA, E. C.; LANZA, M. R. V. Oxygen reduction reaction: semi-empirical quantum mechanical and electrochemical study of printex 16 carbon black. **Carbon**, New York, v. 156, p. 1-9, 2020. DOI: 10.1016/j.carbon.2019.09.036.
- 86 SCHMIDT, T. J.; PAULUS, U. A.; GASTEIGER, H. A.; ALONSO-VANTE, N.; BEHM, R. J. Oxygen Reduction on ru1. 92mo 0.08seo₄, ru/carbon, and pt/carbon in pure and methanol-containing electrolytes. **Journal of The Electrochemical Society**, London, v. 147, n. 7, p. 2620, 2000. DOI: 10.1149/1.1393579.

- 87 COLÓN-MERCADO, H. R.; POPOV, B. N. Stability of platinum based alloy cathode catalysts in pem fuel cells. **Journal of Power Sources**, Amsterdam, v. 155, n. 2, p. 153-163, 2006. DOI: 10.1016/j.jpowsour.2005.05.011. 2006;155(2):253–63.
- 88 YEAGER, E. Dioxygen electrocatalysis: mechanisms in relation to catalyst structure. **Journal of Molecular Catalysis**, Amsterdam, v. 38, n. 1/2, p. 5-26, 1986. DOI: 10.1016/0304-5102(86)87045-6.
- 89 VISWANATHAN, V.; HANSEN, H. A.; NØRSKOV, J. K. Selective electrochemical generation of hydrogen peroxide from water oxidation. **Journal of Physical Chemistry Letters**, New York, v. 6, n. 21, p. 4224-4228, 2015. DOI: 10.1021/acs.jpcclett.5b02178.
- 90 JIANG, K.; ZHAO, J.; WANG, H. Catalyst design for electrochemical oxygen reduction toward hydrogen peroxide. **Advanced Functional Materials**, Weinheim, v. 30, n. 35, p. 2003321, 2020. DOI: 10.1002/adfm.202003321.
- 91 KULKARNI, A.; SIAHROSTAMI, S.; PATEL, A.; NØRSKOV, J. K. Understanding catalytic activity trends in the oxygen reduction reaction. **Chemical Reviews**, Washington, v. 118, n. 5, p. 2302-2312, 2018. DOI: 10.1021/acs.chemrev.7b00488.
- 92 SAMANTA, C. Direct synthesis of hydrogen peroxide from hydrogen and oxygen: An overview of recent developments in the process. **Applied Catalysis A: general**, Amsterdam, v. 350, n. 2, p. 133-149, 2008. DOI: 10.1016/j.apcata.2008.07.043.
- 93 WANG, F.; HU, S. Studies of electrochemical reduction of dioxygen with rrde. **Electrochimica Acta**, Oxford, v. 52, n. 20, p. 4228-4235, 2006. DOI: 10.1016/j.electacta.2005.11.042.
- 94 KIM, K. J.; KIM, Y. J.; KIM, J. H.; PARK, M. S. The effects of surface modification on carbon felt electrodes for use in vanadium redox flow batteries. **Materials Chemistry and Physics**, Amsterdam, v. 131, n. 1-2, p. 547-553, 2011. DOI: 10.1016/j.matchemphys.2011.10.022.
- 95 CORDEIRO JUNIOR, P. J. M.; KRONKA, M. S.; GOULART, L. A.; VERÍSSIMO, N. C.; MASCARO, L. H.; SANTOS, M. C.; BERTAZZOLI, R.; LANZA, M. R. V. Catalysis of oxygen reduction reaction for H₂O₂ electrogeneration: The impact of different conductive carbon matrices and their physicochemical properties. **Journal of Catalysis**, San Diego, v. 392, p. 56-68, 2020. DOI: 10.1016/j.jcat.2020.09.020.
- 96 MORAES, A.; ASSUMPÇÃO, M. H. M. T.; PAPAI, R.; GAUBEUR, I.; ROCHA, R. S.; REIS, R. M.; CALEGARO, M. L.; LANZA, M. R. V.; SANTOS, M. C. Use of a vanadium nanostructured material for hydrogen peroxide electrogeneration. **Journal of Electroanalytical Chemistry**, Amsterdam, v. 719, p. 127-132, 2014. DOI: 10.1016/j.jelechem.2014.02.009.
- 97 ASSUMPÃO, M. H. M. T.; MORAES, A.; DE SOUZA, R. F. B.; GAUBEUR, I.; OLIVEIRA, R. T. S.; ANTONIN, V. S.; MALPASS, G. R. P.; ROCHA, R. S.; CALEGARO, M. L.; LANZA, M. R. V.; SANTOS, M. C. Low content cerium oxide nanoparticles on carbon for hydrogen peroxide electrosynthesis. **Applied Catalysis A: general**, Amsterdam, v. 411-412, p. 1-6, 2012. DOI: 10.1016/j.apcata.2011.09.030.
- 98 CORDEIRO JUNIOR, P. J. M.; MARTINS, A. S.; PEREIRA, G. B. S.; ROCHA, F. V.; RODRIGO, M. A. R.; LANZA, M. R. V. Bisphenol-S removal via photoelectro-fenton/H₂O₂ process using Co-porphyrin/Printex L6 gas diffusion electrode. **Separation and Purification Technology**, London, v. 285, p. 120299, 2022. DOI: 10.1016/j.seppur.2021.120299.

- 99 BARROS, W. R. P.; WEI, Q.; ZHANG, G.; SUN, S.; LANZA, M. R. V.; TAVARES, A. C. Oxygen reduction to hydrogen peroxide on Fe₃O₄ nanoparticles supported on Printex carbon and Graphene. **Electrochimica Acta**, Oxford, v. 162, p. 263-270, 2015. DOI: 10.1016/j.electacta.2015.02.175.
- 100 MOREIRA, J.; BOCALON, L. V.; GOULART, L. A.; LANZA, M. R. V. Electrosynthesis of hydrogen peroxide using modified gas diffusion electrodes (mgde) for environmental applications: quinones and azo compounds employed as redox modifiers. **Applied Catalysis B: environmental**, Amsterdam, v. 248, p. 95-107, 2019. DOI: 10.1016/j.apcatb.2019.01.071.
- 101 BARROS, W. R. P.; REIS, R. M.; ROCHA, R. S.; LANZA, M. R. V. Electrogeneration of hydrogen peroxide in acidic medium using gas diffusion electrodes modified with cobalt (II) phthalocyanine. **Electrochimica Acta**, Oxford, v. 104, p. 12-18, 2013. DOI: 10.1016/j.electacta.2013.04.079.
- 102 VALIM, R. B.; REIS, R. M.; CASTRO, P. S.; LIMA, A. S.; ROCHA, R. S.; BERTOTTI, M.; LANZA, M. V. R. Electrogeneration of hydrogen peroxide in gas diffusion electrodes modified with tert-butyl-anthraquinone on carbon black support. **Carbon**, New York, v. 61, p. 236-244, 2013. DOI: 10.1016/j.carbon.2013.04.100.
- 103 BLOCK, H.; LEDWITH, A.; TAYLOR, A. R. Polymerization of methyl methacrylate photosensitized by benzophenones. **Polymer**, Guildf, v. 12, n. 4, p. 271-288, 1971. DOI: 10.1016/0032-3861(71)90051-6.
- 104 KYUNG, H. W. A.; HONG, G. S. D. Photocatalytic functional cotton fabrics containing benzophenone chromophoric groups. **Journal of Applied Polymer Science**, New York, v. 106, p. 2661-2667, 2007. DOI: 10.1002/app.26900.
- 105 YEGOROV, A. S.; WOZNIAK, A. I.; IVANOV, V. S.; AVERINA, E. A.; ZHDANOVICH, O. A. Development and optimization of producing 3,3', 4,4'-benzophenonetetracarboxylic dianhydride. **Oriental Journal of Chemistry**, Madhya Pradesh, v. 32, n. 6, p. 3063-3070, 2016. DOI: 10.13005/ojc/320627.
- 106 HOU, A.; SUN, G. Multifunctional finishing of cotton fabrics with 3,3',4,4'- benzophenone tetracarboxylic dianhydride: Reaction mechanism. **Carbohydrate Polymers**, London, v. 95, n. 2, p. 768-772, 2013. DOI: 10.1016/j.carbpol.2013.02.027.
- 107 GIOMO, M.; BUSO, A.; FIER, P.; SANDONÀ, G.; BOYE, B.; FARNIA, G. A small-scale pilot plant using an oxygen-reducing gas-diffusion electrode for hydrogen peroxide electrosynthesis. **Electrochimica Acta**, Oxford, v. 54, n. 2, p. 808-815, 2008. DOI: 10.1016/j.electacta.2008.06.038.
- 108 MORATALLA, Á.; ARAÚJO, D. M.; MOURA, G. O. M. A.; LACASA, E.; CAÑIZARES, P.; RODRIGO, M. A. Pressurized electro-Fenton for the reduction of the environmental impact of antibiotics. **Separation and Purification Technology**, London, v. 276, p. 119398, 2021. DOI: 10.1016/j.seppur.2021.119398 .
- 109 CORDEIRO JUNIOR, P. J. M.; SÁEZ, J. C.; LANZA, M. R. V.; RODRIGO, R. M. A. Electrochemical production of extremely high concentrations of hydrogen peroxide in discontinuous processes. **Separation and Purification Technology**, London, v. 300, p. 121847, 2022. DOI: 10.1016/j.seppur.2022.121847.
- 110 REIS, R. M.; BEATI, A. A. G. F.; ROCHA, R. S.; ASSUMPÇÃO, M. H. M. T.; SANTOS, M. C.; BERTAZZOLI, R.; LANZA, M. R. V. Use of gas diffusion electrode for the in situ generation of hydrogen peroxide in an electrochemical flow-by reactor. **Industrial and Engineering Chemistry Research**, Washington, v. 51, n. 2, p. 649-654, 2012. DOI: 10.1021/ie201317u.

- 111 CORDEIRO JUNIOR, P. J. M.; LOBATO, B. A. J. O. J.; LANZA, M. R. V.; RODRIGO, R. M. A. Highly efficient electrochemical production of hydrogen peroxide using the gde technology. **Industrial and Engineering Chemistry Research**, Washington, v. 61, n. 30, p. 10660-10669, 2022. DOI: 10.1021/acs.iecr.2c01669.
- 112 SHIN, H.; LEE, S.; SUNG, Y. E. Industrial-scale H₂O₂ electrosynthesis in practical electrochemical cell systems. **Current Opinion in Electrochemistry**, London, v. 38, p. 101224, 2023. DOI: 10.1016/j.coelec.2023.101224.
- 113 PEIGHAMBARDOUST, S. J.; ROWSHANZAMIR, S.; AMJADI, M. Review of the proton exchange membranes for fuel cell applications. **International Journal of Hydrogen Energy**, London, v. 35, n. 17, p. 9349-9384, 2010. DOI: 10.1016/j.ijhydene.2010.05.017.
- 114 MONTEIL, H.; PECHAUD, Y.; OTURAN, N.; TRELLU, C.; OTURAN, M. A. Pilot scale continuous reactor for water treatment by electrochemical advanced oxidation processes: Development of a new hydrodynamic/reactive combined model. **Chemical Engineering Journal**, Amsterdam, v. 404, p. 127048, 2021. DOI: 10.1016/j.cej.2020.127048.
- 115 ESSADKI, A. H.; GOURICH, B.; VIAL, C.; DELMAS, H. Residence time distribution measurements in an external-loop airlift reactor: study of the hydrodynamics of the liquid circulation induced by the hydrogen bubbles. **Chemical Engineering Science**, London, v. 66, n. 14, p. 3125-3132, 2011. DOI: 10.1016/j.ces.2011.02.063.
- 116 TOSON, P.; DOSHI, P.; JAJCEVIC, D. Explicit residence time distribution of a generalised cascade of continuous stirred tank reactors for a description of short recirculation time (bypassing). **Processes**, Basel, v. 7, n. 9, p. 1-13, 2019. DOI: 10.3390/pr7090615.
- 117 GUTIERREZ, C. G. C. C.; DIAS, E. F. T. S.; GUT, J. A. W. Residence time distribution in holding tubes using generalized convection model and numerical convolution for non-ideal tracer detection. **Journal of Food Engineering**, London, v. 98, n. 2, p. 248-256, 2010. DOI: 10.1016/j.jfoodeng.2010.01.004.
- 118 ZIER, T.; BOUAFIA, S.; RECHIDI, Y.; CHABANI, M. Hydrodynamics modeling and electrochemical performance of a lab-scale single-channel cell through residence time distribution and kinetic studies. **Desalination and Water Treatment**, New York, v. 279, p. 187-194, 2022. DOI: 10.5004/dwt.2022.29107.
- 119 OH, J.; SALCEDO, D. E.; MEDRIANO, C. A.; KIM, S. Comparison of different disinfection processes in the effective removal of antibiotic-resistant bacteria and genes. **Journal of Environmental Sciences**, Amsterdam, v. 26, n. 6, p. 1238-1242, 2014. DOI: 10.1016/S1001-0742(13)60594-X.
- 120 DOMINGUEZ, C. M.; CHECA-FERNANDEZ, A.; ROMERO, A.; SANTOS, A. Journal of environmental chemical engineering degradation of hchs by thermally activated persulfate in soil system: effect of temperature and oxidant concentration. **Journal of Environmental Chemical Engineering**, Amsterdam, v. 9, n. 4, p. 105668, 2021. DOI: 10.1016/j.jece.2021.105668.
- 121 COSTA, A. J. M.; KRONKA, M. S.; CORDEIRO JUNIOR, P. J. M.; FORTUNATO, G. V.; SANTOS, A. J.; LANZA, M. R. V. Treatment of tebuthiuron in synthetic and real wastewater using electrochemical flow-by reactor. **Journal of Electroanalytical Chemistry**, Amsterdam, v. 882, p. 114978, 2021. DOI: 10.1016/j.jelechem.2021.114978.